Evaluation of the Dosimetric Accuracy of the AAA Algorithm (Analytical Anisotropic Algorithm) of the Eclipse Treatment Planning System

Armando Cristian Camilo Castellanos Jerez

Universidad Nacional de Colombia
Physics Department
Bogotá, Colombia
2016

Evaluation of the Dosimetric Accuracy of the AAA Algorithm (Analytical Anisotropic Algorithm) of the Eclipse Treatment Planning System

Armando Cristian Camilo Castellanos Jerez

Final project presented in partial fulfillment of the requirements for the degree of:
Master of Medical Physics

Director:
Ph.D. María Cristina Plazas
Co-director:
M.Sc. Edwin Rozo Albarracín

Research Group:
Medical Physics

Universidad Nacional de Colombia
Physics Department
Bogotá, Colombia
2016

Dedication

This work, like all the ones I've done, are dedicated to my mother Lucila Jerez, who has been and will be my inspiration engine.

Acknowledgements

I am deeply grateful to a large number of people involved during the learning process and the development of my final master's project. This master's thesis would not have been possible without my director and advisor, PhD. María Cristina Plazas, who has always been a source of guidance as she has assisted me in its completion. A lot of thanks to my co-director M.Sc Edwin Rozo who has dedicated time and provided comments, feedback and encouragement. In addition, I would like to extend thanks to all of those who have helped me in many way to the development of this thesis, such as the technologists of IOCAL at Santa Fe Fundation: Jhonny Pedreros, Eliana Chaljub and Marcela Vargas. I am also thankful to Jaime Castro and Jaime Cabrera for his good comments and company.

I especially want to thank to my girlfriend Diana Álvarez, who has accompanied me during the writing process of this work, advising me and encouraging me to finish the thesis in the best way. I am also thankful to my family that has been a constant support to me throughout my life.

Finally, I want to thank the Hospital Universitario Fundación Santa Fe especially Dr. Andrés Rodríguez, Dra. Zoila Conrrado and Claudia Gracia and all its radiotherapy human team of the IOCAL for having open doors and warmth during the year of hospital practice and development of the final work.

Abstract

This current work evaluates the dosimetric accuracy of version 11.0.31 of the AAA algorithm for calculating the photon dose distributions of the Eclipse treatment planning system respect to the input data. The accuracy of the algorithm was analized for the two photon energy spectrums available on the linear accelerator Clinac iX: 6 MeV and 15 MeV, was calculated.

To perform the evaluation of the AAA algorithm was calculated the percentage differences between its values calculated with the respective measured values taking into account the tolerances and recommendations described in the Task Group report 53. Relative dosimetry was evaluated carefully and it could be observed that a decreasing of this agreement as the depth of the measurement increased, as well as the increase in field size. In the evaluation of the relative dosimetries for both photon energy spectrums, it was found that overall results of percentage agreement was in the inner zone 92.3 % of the points passed the tests, while for the penumbra zone, umbra and build-up the percentage of points which passed the test were 92.4 %, 14.8 % and 100 % respectively.

Absolute dosimetry was analyzed in a homogeneous phantom simulator and additionally, we constructed and characterized imageologically a thorax phantom to analyze the accuracy of the algorithm under conditions of inhomogeneity of the medium.

Keywords: Photon doses distribution, tissue substituted, anthropomorphic phantom, accuracy evaluation of AAA Algorithm.

Resumen

En el presente trabajo se evalúa la exactitud de la versión 11.0.31 del algoritmo AAA encargado del cálculo de las distribuciones de dosis de fotones del sistema de planeación de tratamientos Eclipse respecto a los datos de comisionamiento del acelerador lineal. Se calculó la exactitud del algorimo para los dos espectros de energías de fotones disponibles en el acelerador lineal Clinac iX: de 6 MeV y 15 MeV.
Para realizar la evaluación del algoritmo AAA se calculó la concordancia entre sus valores calculados con las respectivas mediciones teniendo en cuenta las tolerancias y recomendaciones descritas en el Task Group reporte 53. Se evaluaron dosimetrías relativas en las se pudo ver una disminución en dicha concordancia a medida que aumentaba la profundiad de la medición, así mismo con el aumento del tamaño de campo. En la evaluación de las dosimetrías relativas para ambos espectros de energía de fotones se obtuvo como resultado que en la zona inner el 92.3 % de los puntos pasaron la prueb, mientras que para las zona de penumbra, umbra y build-up el porcentaje de puntos que pasaron el test fueron 92.4 %, 14.8 % y 100 %, respectivamente.
Se analizaron las dosimetrías absolutas en una simulador físico homogeneo y adicionalmente, construímos y caracterizamos imagenologicamente un simulador físico de tórax para analizar la exactitud del algoritmo en condiciones de inhomogeneidad del medio.

Palabras clave: Distribución de dosis de fotones, tejido substituto, simulador físico antropomorfico, evaluación exactitud algoritmo AAA.

Table of Contents

List of Figures

List of Tables

1. Introduction

In order to improve the quality of oncological treatments involving ionizing radiation, it is essential to ensure that the equipment and personnel involved in each stage of treatment are in high quality conditions. Managing a highly qualified personnel, it is necessary to carry out quality controls with international standards to the simulation equipment and linear accelerator used for the development of the treatment.

To know that the linear accelerator is operating in optimum conditions, mechanical quality controls were initially developed on a Varian Medical System Clinac iX equipment. It was checked periodically that the results of these mechanical quality controls were within the tolerance range, and then proceed to perform dosimetric quality controls that a medical physicist corresponds to perform and that affect directly radiotherapy treatments.

The dosimetric tests commonly performed in the radiotherapy environment are related to the comparison of relative and absolute dosimetric tests with respect to the so-called "Golden Beam Data"provided by their manufacturers or with acceptance tests. Depending on the technology of each linear accelerator, if you have available techniques IMRT and VMAT, you can also perform quality controls to the treatment plans in which a dosimetric comparison is made between the treatment planned and the delivered doses on an array of detectors, either integrated to the linear accelerator (e.g. Portal Dosimetry).

Something that is not within the usual clinical practices of a medical physicist and is not within the linear accelerator quality control protocols is to determine how accurate is the software of treatment planning which is responsible for calculating the dose distributions. It is expected that year after year, and version after version linear accelerator manufacturers improve their algorithms for calculating dose distributions or treatment planning systems (TPS). However, for some procedures in which there are greater heterogeneities as it is the case of the human thorax the algortithms shows higher limitations. [27].

Due to the biological repercussions on tumour control that are directly on the injury and the probability of complications on surrounding healthy tissue, the accuracy of the algorithm for calculating dose distributions is extremely important. One challenging case of the algorithms is whe tumours are presented in the lung tissue or near it, and for which it was specially evaluated the algorithm in this work, for this reason an anthropomorphic and heterogeneous

thorax phantom was fabricated taking into account the ICRU report 44 recomendations [45].

The Analytical Anisotropic Algorithm (AAA) is responsible for calculating radiation doses distribution with photons and is within the Varian Medical System Treatment Planning System (TPS) commercially called Eclipse. It has been seen thatevery time a new version of TPS is released, that version has significant improvements, and several authors have reported in the literature evaluations to software performance, noting that between the calculated value of the dose that reports the planning system and the value actually delivered there are differences which in some cases could be significant [18,24,27]. Some authors have calculated for certain anatomical regions significant dose variations that exceed the tolerance values described in Task Group report 53 [25].

Due to the multiple tests that are described in the Task Groups 53 and 23 of the AAPM [13, 25] and the international reception that has had by other authors that have performed them for other algorithms and other versions of the AAA algorithm [18,24,26], in the present work were taken as references along with more recent works, with which the performance of the AAA algorithm was compared [18, 24, 27].

It was performed different tests in which the scope of each one was described, and a software was developed which is responsible for the comparison of the relative dosimetries test performed in a homogeneous water phantom, and then performs an analysis to determine the agreement grade of the AAA algorithm in each of the tests respect to the measured values. For the heterogeneity test, an anthropomorphic phantom was designed and absolute dosimetric measurements were performed using an ionization chamber PinPoint.

All the tests were performed under optimum conditions of the equipments: linear accelerator, ionization chambers, electrometers and robotized water tank, however, for some tests the results were not expected or close to those obtained by other authors, which does not mean that the procedure performed is not well-done, but might have been changes in the linear accelerator that affected these input parameters and it may be necessary to perform a recommisioning of the algorithm.

2. Objectives

General Objective

To evaluate the accuracy of the dose calculation of the AAA algorithm of the TPS Eclipse of Varian Medical System for radiotherapy treatments in different clinical conditions and to identify its possible limitations.

Specific Objectives

- To perform a quality control, with their respective protocols, characterizing the factors of the Clinac iX accelerator that take part in the calculation of the dose by the algorithm AAA and this task is the competence of Medical Physicist.
- To determine under what conditions the AAA algorithm presents greater inaccuracies in the calculation of the dose distribution and to evaluate the performance of the algorithm for different tissues.
- To elaborate a protocol based on international recommendations for the evaluation of the dosimetric accuracy of the AAA algorithm in its dose distribution creation.
- To compare the results obtained with those reported by other authors for recent versions of TPS used by other parent companies.

3. Theory

3.1. Radiation Therapy Treatments

The cancer is a disease that affects almost all organs of the body as a result of the genetic damage that occurs in the DNA of its cells, which produces abnormal cells with different proliferation patterns, various degrees of differentiation and oxygenation and a higher or lower radiobiological response. These conditions in some cases represent a major challenge in choosing the right treatment to provide a curative response. In order to achieve the most successful treatment, it has been suggested by the international community that certain steps should be followed. Nowadays, these steps are becoming more widespread in developing countries such as ours and are described below.

3.1.1. Stages in the treatment of radiotherapy

3.1.1.1. Comprehensive clinical evaluation

When a disease is suspected, the greatest amount of information should be collected, taking into account a previous interview with the patient, followed by a general physical and histopathological examinations, and the necessary diagnostic imaging. If a malignant tumour is suspected, it is necessary to perform the most relevant clinical tests in order to avoid false positives or false negatives in the diagnosis.

3.1.1.2. Therapeutic choice

Knowing the type of disease, its location and the stage of the disease, as well as its possible prognosis, the oncologist or an interdisciplinary group of specialists can indicate which treatment plan is appropriate. Within the range of possible treatments are surgery, chemotherapy, immunotherapy and radiotherapy among others, and in some cases, more than one treatment can be administered concomitantly.

Once it has been determined that the treatment to be followed is radiotherapy, it is necessary to know by the radiotherapists more thoroughly the lesion or tumour, and it is required to

obtain a new set of diagnostic images.

3.1.1.3. Determination of clinical volume

There are a variety of diseases of an oncologist nature, but benign tumours, arteriovenous malformations, and spinal cord compressions among others can also be treated with radiation therapy; such treatments have shown good outcomes, and in some cases with less secondary effects than other kind of treatments.

When it has been decided that the optimal treatment is radiotherapy (teletherapy), the radiotherapist oncologist continues with the location and determination of lesion size relating to the surrounding healthy tissue. The realization of this step is based on diagnostic images such as CT, MRI or PET, ultrasound, or the fusion of two of them with a standard set of CT images.

In order to begin with treatment planning, it is necessary to do a simulation of the treatment; it is usually performed on a computerized tomography device known as a simulator in which a set of images are obtained and it has the capacity to reproduce all the conditions of the treatment unit (linear accelerator), the simulator couch is similar to the one that is used during the treatment,and in some cases it is necessary a kind of immobilizer to ensure that the mechanical, geometric and optical conditions are ideally the same.

Once the required images have been obtained, the precise location of the tumour and the surrounding healthy structures have to be clearly identified with a 3D delineation of the volumes involved: the volumes where the tomour is contained with a small margin and the volume of healthy tissue that could receive considerable radiation (organs at risk, OAR). Among the volumes described in the ICRU report 83 [29], five of them should be highlighted:

- Gross Tumour Volume or GTV: It is tumour volume demonstrable in both its dimensions and its location, as well as the volumes where there are metastatic lesions observed by some diagnostic procedure.
- Clinical Target Volume or CTV: It represents the volume of tissue that contains the GTV and additionally an outside margin where there is the possibility that there are tumour cells that cannot be detected by any means of diagnosis.
- Planning Target Volume or PTV: Unlike the previous ones, this volume is a geometric concept that is used to plan the treatment and to evaluate it. It is a margin outside the CTV, as shown in figure **3-1**, and that it is necessary to delineate it, mainly, due

to the possible movements of the tumour and the inaccuracies in the positioning of the patient during the treatment.

- Internal Target Volume ITV: It is defined as the CTV plus a margin due to uncertainties in size, shape and position of the CTV. The ITV is an optional tool to delineate the PTV.

- Organs at risk or OAR: These are the healthy organs or tissues that are close to the tumour and that could receive a considerable amount of radiation doses and suffer morbidity due to the treatment.

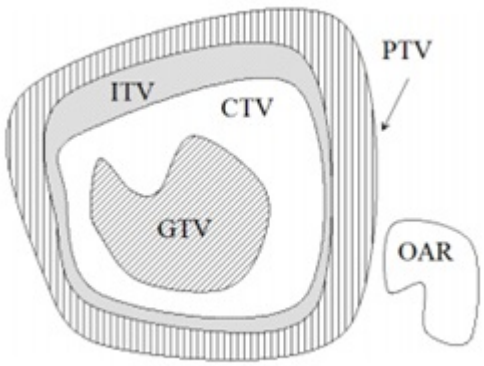

Figure 3-1.: Volumes of clinical interest to irradiate in radiotherapy [36].

3.1.1.4. Treatment planning

By determining the degree of radio sensitivity of tumour cells, size and location, the radiation oncologist and the medical physicist determine which type of particles must be used for the irradiation, their energy, the total dose and the number of fractions in which they are to be delivered [36].

Knowing the prescribed dose and the volumes of interest; the medical physicist performs the last part of the treatment plan, which consists in defining the radiation fields: quantity, size, direction and also which technique to use that is available in the medical service, taking into account which dose distribution could improve the outcomes: the best way to get better results is by delivering the desired dose in a homogeneous way to the tumour and by taking care for the organs at risk. Based on an algorithm of calculation of the distribution of the dose in which relates the aforementioned parameters, it is expected to satisfy the objectives prescribed to have a good tumour control and protect the organs at risk.

3.1.1.5. Performance of treatment

The last stage of the treatment is developed by the technologists specialized in radiotherapy, which can be supervised by the physician or by the medical physicist, so that the patient is well positioned and each therapy is delivered almost in the same setup, especially in procedures that require high precision such as intracranial radiosurgery and hypofractionated treatments.

3.1.2. Radiation therapy techniques

After the discovery by Wilhelm Conrad Röentgen on November 8, 1895 of the artificially generated ionizing radiation and the beginning of the notion of its effects on cell death and genetic damage, its use for the treatment of cancer was begun. The first case that was treated with X-ray was reported in 1896 for breast cancer [17]. Later Marie and Pierre Curie with the discovery of the natural radioactivity, they used the element Radio to treat cancer of cervix and some types of cancer of skin, but until that time treatments were done empirically and with total ignorance of the effectiveness and possibilities of get chronic side effects by using it.
From its beginnings to date, radiotherapy has been significantly modernized, reducing the morbidity associated with ionizing radiation, making it safer and more accurate; it has been divided into two major branches, brachytherapy and teletherapy, showing advantages in some injuries one with respect to each other.

3.1.2.1. Brachytherapy

The word brachytherapy is composed of the union of two Greek words, one of them brachys which means near, and, helps its definition, which it is a treatment that uses natural radioactive sources, that are located as close as possible to the lesion, or even within the tumor. Within the brachytherapy technique are three types: intracavitary, interstitial and intraluminal, all using radioactive sources such as ^{192}Ir, ^{125}I or ^{60}Co among others.

Brachytherapy is especially indicated for tumours that can be easily reached and have small dimensions to avoid affecting the surrounding organs. To obtain the expected results it is necessary to have established protocols, and for this reason there are guidelines of procedures for the brachytherapy treatments widely spread by the AAPM (American Association of Physicist in Medicine)in its ICRU Reports 38, 58 and 89 [23, 29].

3.1.2.2. Teletherapy

In teletherapy, the radioactive source is located at a considerable distance from the patient, in which units of Cobalt 60 and Cesium 137 are used; but in the last decades linear accele-

rators are more used, which do not use radioactive sources, but through physical processes they can emit X-rays, electrons, hadrons and heavy ions. The Cobalt 60 and Cesium 137 units are becoming less widely used and are being replaced by linear accelerators.

The most widely used equipment worldwide is the emitters of X-rays and electrons, whose emissions are controlled and produced artificially. This type of X-rays emitters can be classified into three levels: low energy, orthovoltage and megavoltage equipment. Low energy devices use conventional X-rays tubes that handle peak potential ranging from 50 to 150 kV, because of its low penetration range, these equipment are not indicated for lesions with a depth greater than 5 mm. The medium energy or orthovoltage equipment operates in the range between 150 and 500 kV and due to the energy of the photons is only indicated for injuries up to 3 cm depth. Finally, the megavoltage equipments that are linear accelerators of greater complexity, whose photons of high energy are generated by the deceleration of the electrons that previously have been highly accelerated by a guide of waves, are equipments more and more widespread use, thanks to its depth of penetration. It has been used to treat almost any type of tumour, and has shown important improvements in the accuracy and precision of the procedures since its official appearance in 1937 to date.

The advance in external photon radiation therapy goes from its beginnings with conventional 2D radiotherapy, through three-dimensional conformal radiotherapy (3D-CRT), intensity modulated radiotherapy (IMRT) and finally the arctherapy that will be explained in detail below.

3.1.2.3. Evolution of teletherapy techniques for dose delivery

In the decade of 1920 Coolidge invented an X-ray tube that operated in the range between 200 and 250 kV with which could treat tumors not so superficial and with less damage in the skin. Although it was a breakthrough in radiation therapy by then, it was still very limited, and it was only until 1937 at Bartholomew Hospital in London where a megavolt radiation equipment was used and its advantages in the treatment of deep tumors could be verified. This gave rise to equipment such as betatron for medicine and cobalt 60 units. With these machines, conventional megavoltage radiation therapy began to take its first steps.

With megavoltage radiation therapy equipment, radiotherapy techniques began to develop. Conventional radiotherapy that originated in the 1960s basically uses rectangular fields of radiation, which are defined according to the size of the tumor, and therefore the size of the fields must contain the two-dimensional projection of the tumor plus a margin. The number of fields was scaled from one to four depending on the location and the size of the tumour, if a pair of fields were chosen, they had to be opposites, but if they were four fields, they

should conform a shape of a rectangular box. At the beginning, treatment planning was based on radiographic images, with limited results and high morbidity. To obtain better dose distributions, wedges were introduced and some tissue compensators began to have a more common use, but only with the spreading of CT equipment [44], in which images of axial sections could be seen and thus delimiting the volume of the tumor and organs at risk. The conventional 2D radiotherapy jumped in the 1980s to conventional 3D radiotherapy, improving tumor coverage and so increasing the tumor control.

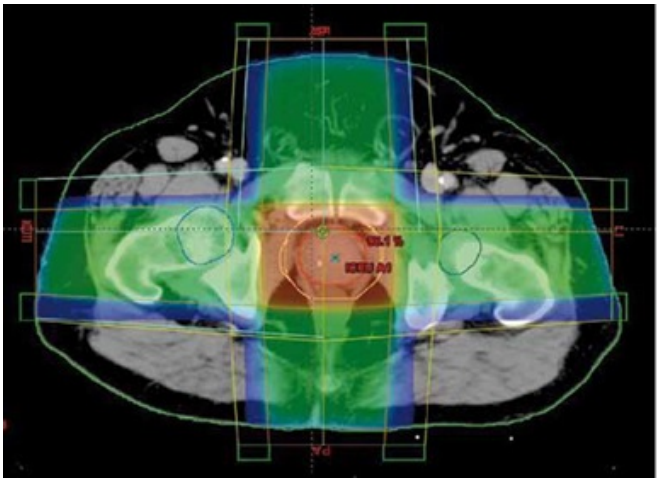

Figure 3-2.: 3D conventional radiotherapy image of prostate cancer [43].

With 3D conventional radiotherapy consisting of a volumetric technique, there were improvements related to coverage in doses of tumour volume [43], as it can be seen in Figure **3-2** the arrangement of the fields and the dose distribution are observed easily in each slice of the CT images set, and for that reason this technique shows a better homogeneous distribution of the doses than 2D radiotherapy. With the advent of CT equipment in the process of radiotherapy treatments, the images obtained were started to be used for computerized calculations of dose distributions.

In order to decrease the dose of the adjacent organs to the tumor volume, the dose conformity was started by molds that had the shape of the tumor in the plane of the projected radiation field, allowing the radiation to pass through it and be attenuated by the edges. These molds have traditionally been made from a mixture of heavy elements called cerrobend and in certain cases could be used simultaneously with wedges or some tissue compensators.

The use of the molds of cerrobend began to give rise to the idea of having three-dimensional conformational radiotherapy, and thanks to the advance in the algorithms for calculating dose distributions and the implementation of multi-leaf collimators MLC in radiotherapy

equipment, it was begun to give better conformity to the dose in the tumor volume. In this technique for each direction of the beam, a view of the shape of the tumour and the organs at risk is obtained through the MLC collimator that is used to cover and protect the healthy tissue, and only irradiate the tumor. This technique was improved by having several shapes of fields for each direction of the gantry and thus modulate the intensity of radiation that reached the tumour and reducing the intensity of radiation to the volumes of healthy organs that overlap the tumour volume.

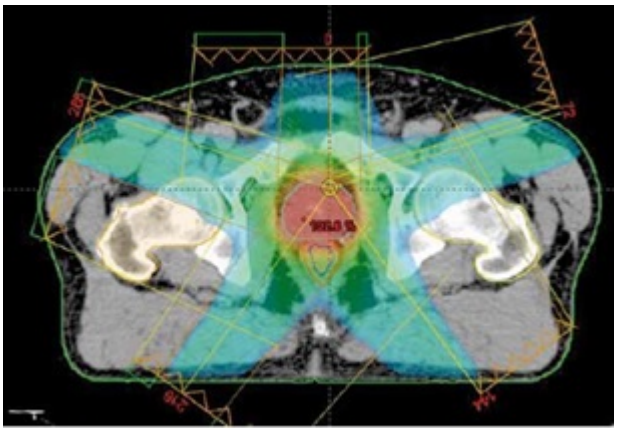

Figure 3-3.: Image of IMRT Technique in a prostate cancer case [43].

Although the use of 3D-CRT radiotherapy is still effective for some types of lesions because it achieves great conformation of the radiation dose, that means this tecnique could cover homogeneously almost all the tumor volume with the prescribed dose in some cases, the radiation intensity modulation (IMRT) emerged to improve the conformation of the hard cases, which is a more advanced form of 3D conformal radiotherapy.
The IMRT technique that started commercially in 1994, was a challenge in the software of calculation of the distribution of the dose since it focuses on the software finds the best dose distribution that needs to deliver to the tumour volume and to restrict the dose to the healthy tissue, this is made by modulating the number of fields and the intensity of the radiation, as it can be seen in Figure **3-3**. Once the number of fields and their directions have been selected, the software develops an inverse optimization planning in which for each field it does a division of smaller zones of the fields called beamlets, which can have different intensities depending on their paths in the patient body, this allows dose falls in a very short distances, and with this it seeks to fulfill the planning objectives that the medical physicist has set.

Within the IMRT there are several techniques to deliver the treatment, among which are the methods: Step and Shoot and Sliding Windows. The Step and Shoot method consists of overlapping field components in different ways, as it is shown in Figure **3-4a**, the linear

accelerator radiates only when the shape of the field is completely formed by the multi-leaf collimator and stop the irradiation when they are in movement. On the other hand, the sliding Windows method has a continuous movement of the multi-leaf while the linear accelerator is radiating, see Figure **3-4b**, each multi-leaf can handle different speeds and the modulation of the intensity will be determined by the time the multi-leaf is in every place [33].

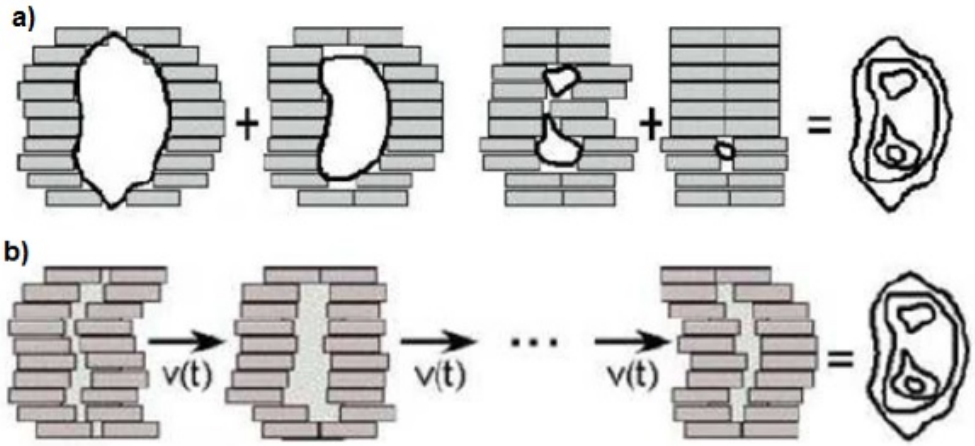

Figure 3-4.: IMRT Techniques: **a)** Step and Shot **b)** Sliding Windows [33].

One of the advances that occurred in IMRT was the delivery of the treatment while the gantry of the linear accelerator rotated (technique called IMAT). Additionally while the gantry rotated with stops every 5 or 10°, the conventional MLC collimators were continuously moved and intensity modulation was generated by overlapping the arcs and the forms adopted by the MLCs.

This technique was initially conducted in a clinical trial by the University of Maryland in 2000, involving 50 patients and in which they concluded that the results were satisfactory in terms of safe dose delivery and linear accelerator eficiency, since it reduced the delivery of the treatments to an average of 7 minutes and a half [19].

From the idea of IMAT came what is now known as VMAT (Volumetric Modulated Arc Therapy) commercially offered by Elekta as PreciseBeam Infinity and by Varian as RapidArc. With this improvement, the times of each treatment were reduced, and fewer monitor units (UM) were delivered to the patient than with conventional IMRT treatments, as it can be seen in Figures **3-5a** and **3-5b**. This technique consists of modulating the intensity in three different ways: one way is by changing the dose rate delivered by the linear accelerator,another way is by moving the multi-leaf (MLC) and finally is by changing the path of the beam by the continuous movement of the gantry [19].

As it was mentioned above, in order to work correctly and the planned dose to be delivered is the one that the patient really receives, it is necessary to perform some quality controls that will be mentioned below. On the other hand, to be sure that all the possible inaccuracies are only due to the algorithm of dose distribution it is necessary that the linear accelerator works properly and is well-calibrated.

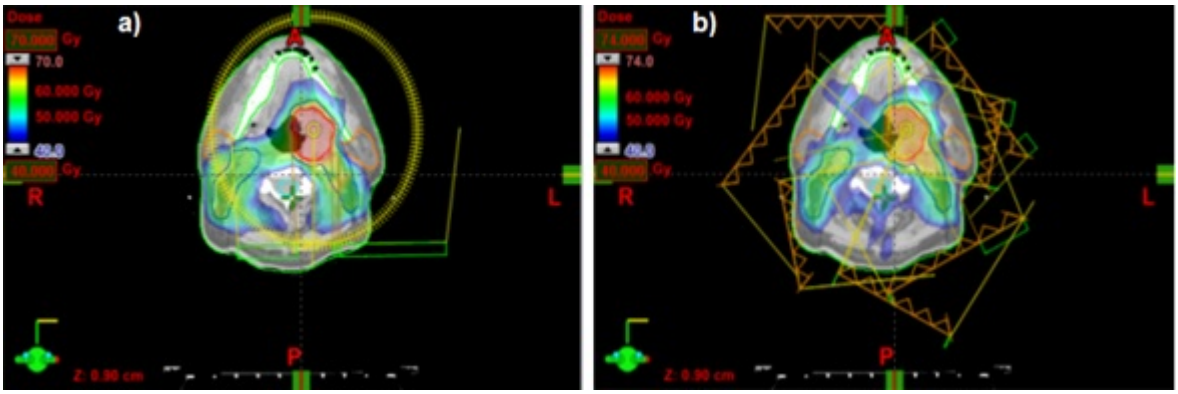

Figure 3-5.: **a)** Distribution of doses with VMAT. **b)**) Distribution of doses with 7 conventional fields of IMRT [19].

3.2. External photon beams: Physical characteristics

There are several parameters by which the photon radiation beams generated in a linear medical accelerator can be characterized. Such characteristics range from how the radiation beam propagates to how it is dispersed and how it affects dose contributions. For this section we will state each of the characteristics that will help us to better understand the dosimetric evaluation of the AAA algorithm.
The main parameters that modify the dosimetric characteristics of the radiation beam are the size of the field of the beam A, the energy of the photons $h\nu$, the source-surface distance SSD, the source-axis distance SAD and beam modifiers.

3.2.1. Collimator Factor CF

Exposure in air X, kerma in air K_{air}, and dose to a small mass of air at a point P of air are made because of each contributions due to the primary beam and scattering [36]. This scattering can come from photons that interacted with both the main collimator and the flattening filter.

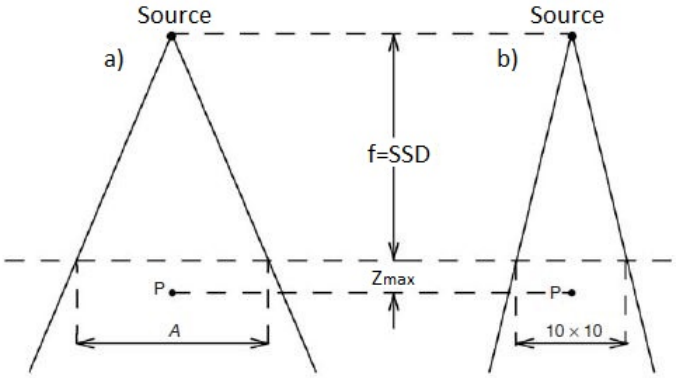

Figure 3-6.: Experimental configuration for measuring the Collimator Factor in air using as a reference field size $A = 10 \times 10$ cm^2 [36].

The collimator factor is defined as the ratio of air exposure X for a field size A to exposure in air for a field size of 10×10 cm^2. Similarly, the kerma in air and the dose in air are related, as it can be seen in the following equation.

$$CF(A, h\nu) = \frac{X(A, h\nu)}{X(10, h\nu)} = \frac{(K_{air}(A, h\nu))_{air}}{(K_{air}(10, h\nu))_{air}} = \frac{D'(A, h\nu)}{D'(10, h\nu)} \tag{3-1}$$

The experimental set-up to measure CF can be observed in figure **3-6**, where using an ionization chamber with its cap, the respective doses $D'(A, h\nu)$ and $D'(10, h\nu)$ can be measured. If the size of field A is very small and measurements are taken at very long distances $SSD + z_{max}$, corrections can be made using the inverse square law.

3.2.2. Peak scatter factor PSF

Peak scatter factor for megavoltage photon beam is defined as the ratio of the total dose and the primary dose at the depth of dose maximum [14]. When a dose is delivered to a small mass of medium D'_P it is measured of absolute dose in air but with sufficient material around the point of interest P to provide sufficient electronic equilibrium (cap of the ionization chamber). D'_P is related to D_P at the maximum dose depth by the equation:

$$PSF(A, h\nu) = \frac{D_P(z_{max}, A, f, h\nu)}{D'_P(A, h\nu)} \tag{3-2}$$

Where D_P is the dose measured in the same point P but in a medium of water or in a phantom. The experimental setup can be seen in figure **3-7**. The ionization chamber should be placed at point P, at a distance $SSD + z_{max}$ for both cases in the air and in the water phantom or its equivalent.

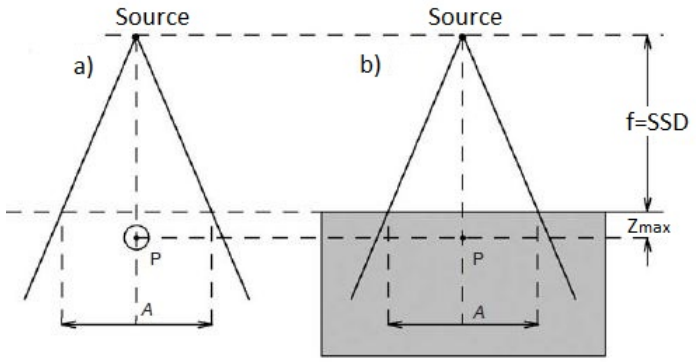

Figure 3-7.: Scheme of the experimental configuration for the dose measuring to calculate the PSF **a)** in air and **b)** in a phantom [36].

Another relevant factor called Scatter Factor or relative PSF relating the dispersion generated by the phantom, which is defined for a field size A and represents the normalized PSF for a field size of 10×10 cm^2, it is stated by the following equation:

$$SF(A, h\nu) = \frac{PSF(A, h\nu)}{PSF(10, h\nu)} \tag{3-3}$$

3.2.3. Total Scatter Factor TSF

Also known as relative dose factor or output factor OF. This factor indicates the scatter from the collimator and the phantom, and depends on the energy of the photons, the size of the radiation field and the distance f=SSD, for a given depth. The output factor is defined as relation between the dose measured at a given point for a field size A and the dose measured at the same point for a field size A $= 10 \times 10$ cm^2 as it can see in next equation:

$$TSF(A, h\nu) = S_{c,p}(A, h\nu) = \frac{D_P(z_{max}, A, f, h\nu)}{D_P(z_{max}, 10, f, h\nu)} \tag{3-4}$$

The geometric configuration for the measurements performed in a water phantom can be seen in Figure **3-8**. In the first configuration that is shown in the figure on the left the field size A is different for the configuration of the figure on the right, where the field size is 10×10 cm^2 as a reference condition.

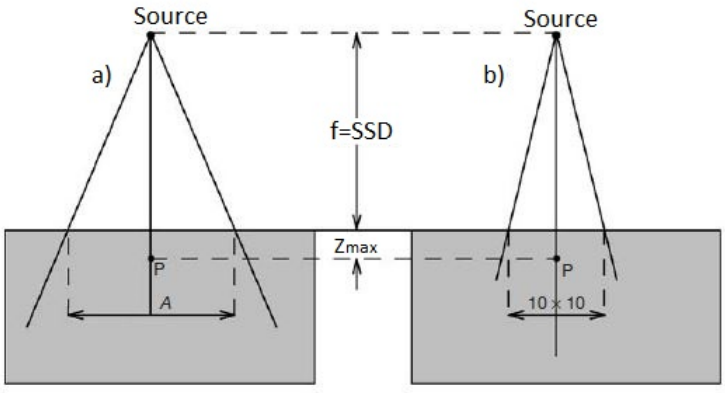

Figure 3-8.: Scheme of the experimental configuration for the absolute dose measuring to obtain the TSF in a water phantom [36].

When using extra collimation systems such as MLC multi-leaf or cerrobend blocks to give the irregular shape of irradiation field B, the total scatter factor TSF approximates the following form:

$$TSF(B, h\nu) = CF(A, h\nu)SF(B, h\nu) \tag{3-5}$$

This equation is a valid approximation when the linear accelerator jaws (first collimator system) forms the radiation field A and the secondary collimation system or MLC shapes the irregular field B.

3.2.4. Percentage depth dose: PDD

The penetration of a photon beam into a homogeneous or heterogeneous medium is of great importance in order to quantify the contributions of the delivered dose. First of all, it is necessary to know the differences in the propagation of the photon beam in air and in a medium such as water or a patient. In the first, its propagation is governed by the inverse square law, while in the second, in addition, this law is governed by processes of attenuation and dispersion [36].

For invasive reasons, the measurement of this parameter (PDD) is done in a water phantom, in which a radiation detector is introduced and radiation beam characteristics such as field size, dose rate and SSD source to surface distance are fixed.

While the linear accelerator is radiating, the detector moves on the central axis from the surface to the desired depth, usually 30 cm depth. In Figure **3-9** one can observe the behavior of a beam of megavoltage photons from the surface until it leaves the phantom or the patient. The normalization of the dose in the PDD graphs are generally at 100 % and placed on the

ordinate axis, while the depth is in millimeters or centimeters on the axis of the abscissa. The region from the surface z=0 to $z = z_{max}$ is known as the dose build-up region.

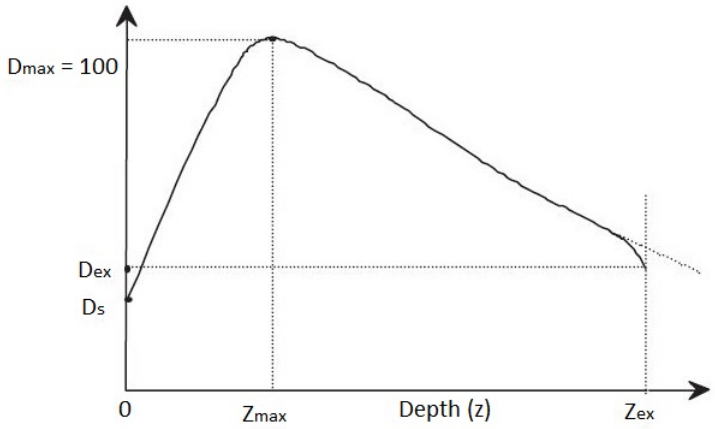

Figure 3-9.: Behavior of the dose deposition in a homogeneous phantom from its entry to its exit z_{ex} [36].

The dose at the surface is much less than the dose delivered in z_{max}. For megavoltage photon beams the dose at the surface depends on the energy of the radiation beam and the size of the field. The higher photon energy, the lower surface dose with respect to its maximum dose. The dose at the surface is due to the next contributions:

- Photons scattered from collimators, flattening filter, beam modifying devices and air.
- Photons backscattered from tissue and patient's prosthesis .
- Electrons produced by the interactions of photons in the air, and with any material crossed different from the patient.

The dose of the aforementioned build-up region is due to the contribution of a large amount of secondary charged particles that are produced by the interaction of the photons with the patient's atoms. The relationship between collision kerma and absorbed dose for megavoltage photons is practically constant because the average energy of the generated electons and their range does not change considerably with depth.

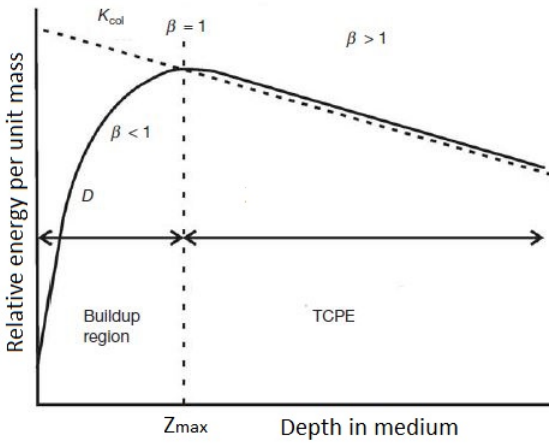

Figure 3-10.: Realistic behavior of the absorbed dose as a function of depth [36]

In the Figure **3-10** β is the relation between absorbe dose and collision kerma $\beta = D/K_{coll}$. The charged particle equilibrium CPE is practically zero at the surface, but it increases with depth, and when z = z_{max} the range of secondary charged particles is approximately equal to or comparable with collision kerma. After z_{max} the collision kerma decreases due to the attenuation of the radiation because of the interaction with the medium resulting in a transient CPE as can be seen in the Figure **3-10**.

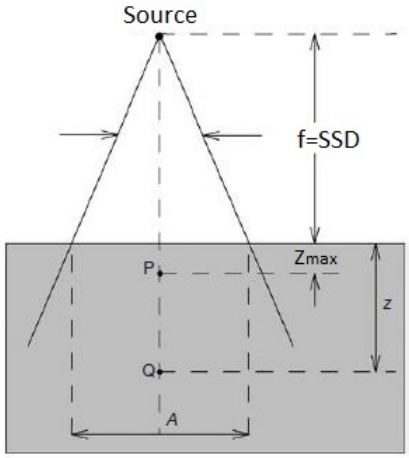

Figure 3-11.: Experimental setup for measuring of PDD [36].

The depth of maximum dose depends on the energy $h\nu$ of the photons and in smaller relation of the size of the field A. The larger energy of photons the larger the depth of maximum dose. The dose distribution at depth is normalized to 100 % the maximum dose and is defined as:

$$PDD(z, A, f, h\nu) = 100\frac{D_Q}{D_P} = 100\frac{\dot{D}_Q}{\dot{D}_P} \tag{3-6}$$

Where D_Q y $\dot{D}_Q$ are the dose and the dose rate in the point Q at depth z as it can see in the Figure **3-11**, that also shows the geometrical configuration for measuring of PDD. The D_P y $\dot{D}_P$ are the dose and the dose rate in the point P at depth z_{max}.

3.2.5. Radiation beam profile

It is the dose distribution measured perpendicular to the central axis of the radiation beam measured at a certain depth within the water phantom. Measurements of the dose profiles are usually done at z_{max} or at 10 cm depth. There are three regions in the radiation profile: inner, penumbra and outer or umbra. In the Figure **3-12** shows the dose distribution in a common profile for a rectangular or square jaw configuration.

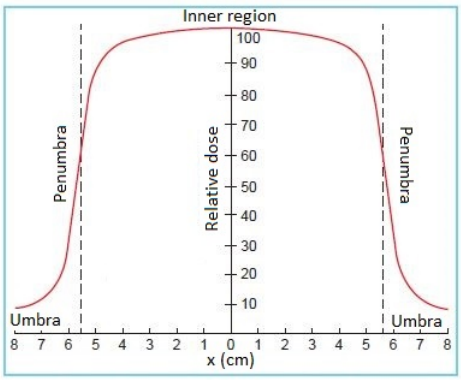

Figure 3-12.: Radiation beam profile [31].

The three regions show in the Figure **3-12** are better explained below:

- The inner region: It represents the central part of the profile, extending from the central axis up to 1-1.5 cm from the edges of the beam [36].
- The penumbra region: It is the edge of the radiation field, region where the dose varies rapidly, ranging from 20 % of the central dose value to 80 %. It depends mainly on the collimators and the size of the source [31].
- The outer or umbra region: This region represents the tails of the radiation profile, which goes after the penumbra, and is mainly due to the radiation transmitted through the collimator and the leakage of the gantry [36].

3.2.5.1. Beam flatness F

The flatness of the beam F is evaluated by determining the maximum dose D_{max} and minimum dose D_{min} values of the dose point in the beam profile within the central 80 % of the

beam width, this pints are within the inner region shows in the Figure **3-12**, and can be calculated by the following relationship [36]:

$$F = 100 \times \frac{D_{max} - D_{min}}{D_{max} + D_{min}} \tag{3-7}$$

The smaller the value obtained from the above equation the greater the beam flatness, for most acceptance tests and quality controls this value is expected to be less than 3 %.

3.2.6. Beam symmetry S

It represents the uniformity of the radiation beam. It usually calculated on a profile obtained at the maximum dose depth [36]. The equation that gives us a quantification of the beam symmetry is given by:

$$S = 100 \times \frac{area_{left} - area_{right}}{area_{left} + area_{right}} \tag{3-8}$$

It is expected to have similar area on the left side of the dose profile from the area on the right, and both areas are measured from middle of the penumbra zone to the center of the profil, in other words, from the dotted vertical line to x= 0 cm s as can be seen in the Figure **3-12**. For the majority of the guidelines the maximum difference would be less than 2 % to be considered a symmetric profile [36].

The importance of perform all the next quality controls is because it is necessary to have the linear accelerator working properly and delivering the prescribed dose without any mechanical or optical inaccuracy, and so the results will depend only on the algorithm AAA.

3.3. Quality Controls in Linear Accelerators

In routine clinical practices that are developed using a linear accelerator, in order to perform a radiotherapy treatments in the better way, it is essential to ensure that all components function properly, and the patients will receive treatment with higher accuracies in positioning and so in dose delivery. For this reason it needs to make mechanical and dosimetric quality controls periodically. Diverse quality controls should be performed by the medical physicist with the respective periodicity: daily, monthly or annualy [32, 37].

3.3.1. Mechanical quality controls

These controls are designed to ensure accuracy in the movements and positions of all parties involved in the linear accelerator, with the purpose to develop treatments which can be carried as initially planned, and its reproducibility is ensured, so it is important to meet the tolerance ranges established by the Task Group 42 report of the AAPM [32].

3.3.1.1. Daily quality controls

The mechanical quality controls that have to be performed every day are three: the laser location, the optical distance indicator (ODI) and collimator size indicator. Depending on the clinical procedure there is a tolerance value that it is recommended to follow [32, 37].

- Laser location

It is a geometric test that can help to place in the right position the patient and the isocenter is in the same place that was chosen in the treatment planning. To assure that all lasers (walls and ceiling lasers) are well-calibrated, it is recommended to follow the next steps:

- First, it is necessary to set up the couch, collimator and gantry at 0°.
- Use a device that has a reference cross, as it is shown in Figure **3-13** place it at the isocenter, align it with the cross-hair and also align each laser with the cross marked on the device just moving the couch in vertical, transversal and longitudinal direction.
- Check that the horizontal lasers in both sides line up with the cross on the device. After, measure the distance between the laser line and the horizontal line of the device and make sure that the measurements agree with the tolerance range, if not, move the lasers controls to achieve the correct values.
- Finally, move the gantry 90° and check if the ceiling laser overlaps with the upper cross of the device, performing the same procedure as in the previous step.

Figure 3-13.: Isocube device [1].

- The optical distance indicator (ODI)

The main purpose of ODI is to be sure that the patient is at the right distance from the radiation source when it is used to set up SSD or an isocentric technique [18]. There are many ways to run a quality control of ODI but the easiest way to check its correct performance

is using a set of front pointer (as it is shown in Figure **3-14**) that indicates the distance between the source and the surface [32, 37]. The steps to follow are described below:

- It is recommended to place the couch and gantry in a fixed position at zero degree and to place over the couch a rectangular phantom with different heights (e.g. solid water layers).
- To put the front pointer tray in the gantry head and then adjust one magnetic front pointer and make sure that mark in the tray line up with front pointer rule.
- For each phantom height, read the value reported in the gantry screen and subsequently compare it with the length of the front pointer and finally, check if the difference agrees with the tolerance range.

Figure 3-14.: Front Pointer device for SSD measurement [5].

- Collimator size indicator

For this test is recommended to use a graph paper with a square of 20×20 cm^2 drawn on the middle of it, and a millimetre ruler. To verify the correct operation of the collimator size indicator, it is recommended to follow the next steps:

- First at all, set up 20×20 cm^2 jaw and set up SSD=100 cm, and then verify that the cross-hair and the light field are aligned on the graph paper.
- Afterwards, to check that the light field edges line up with the marker field outline, if not, move the jaw until fitting it, and read in the gantry screen the jaw values of X1, X2,X3 and X4 and compare with the values of X1=X2=Y1=Y2= 10 cm fixed at beginning.
- To check if the differences agree with the tolerance values. If it is considered to be necessary, perform the previous steps for other jaw sizes [37].

The Table **3-1** shows the tolerances according to TG-142 that must be taken into account when performing daily mechanical quality controls:

Daily		
	Machine-type tolerance	
Procedure	Non-IMRT	IMRT
Laser localization	2 mm	1.5 mm
Distancia indicator ODI	2 mm	2 mm
Collimator size indicator	2 mm	2 mm

Table 3-1.: List of tolerance values for daily mechanical quality controls [32].

3.3.1.2. Monthly quality controls

The AAPM recommends perform the next tests at least once per month to make sure that the mechanical parts of the linear accelerator is working properly and, in addition, it has provided a tolerance table for these tests. All mechanical tests are: symmetric and asymmetric light-radiation field coincidence, symmetric and asymmetric jaw position indicator, cross-hair centering, treatment couch position indicators, localizing lasers, gantry and collimator angle indicator and the last one is to compare distance check device for lasers with front pointer. There are other quality controls (for wedge and compensator) that in some oncological medical centers are still performing, but because of the use of MLC system, those tests will be discontinued soon [32, 37]. .

- Symmetric light field coincidence

This quality control is require to make sure that the field size is mechanically well-calibrated. For this test it is necessary to have a graph paper and a square of 10×10 cm^2 with a cross centered on it, and also a millimeter ruler.

- First, set up gantry and collimator at zero degree, turn off the light in the room, and then, fix jaw setting of 10×10 cm^2 and the SSD=100 cm.
- To project the light field on the graph paper, verify that the light field align with the engraved square on the sheet, if it does not fit, measure the difference, and finally compare to the measured value if it is within the tolerance range.
- If it is possible to repeat with other square jaw setting. For test of the asymmetric light coincidence change the jaw setting in order to have X and Y different values and form a rectangle.

- Symmetric radiation field coincidence

This test is very similar to the previous one but using ionizing radiation instead of light field. It is necessary to have a radiochromic or radiographic film with a square of 10×10

cm^2 drawn on it with a cross in its middle and also marks of gun and target directions. To develop the test it is recommended to follow the steps below:

- First, set up jaw size at 10×10 cm^2 and SSD=100 cm and proceed to irradiate the film with 50 MU.
- After that, measure the square depicted in the film and check if it is symmetric (as is show in the Figure **3-15**) and compare with the square previously drawn it and also with the gantry values. For asymmetric radiation field coincidence, to change jaw setting for different values of X and Y so that forms a rectangle.
- Finally, overlay the radiographic film with graph paper and measure the difference between the light field and the radiation field in order to check if there is a total coincidence or if it is within tolerance range.

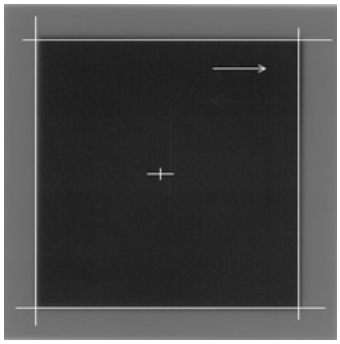

Figure 3-15.: Irradiated radiographic film [37].

- Collimator-gantry angle indicator

The reason for this test is to determine if the gantry and the collimator of the linear accelerator are level and in adequate conditions to impart the medical treatments. For this test it is necessary to have a digital or bubble level and it is recommended to follow the next steps:

- First, put the level on a flat surface of the gantry head when the gantry is in zero degree.
- Then, check that the level readout agrees with the gantry readout and verify if that difference is within the tolerance value. Repeat the same test using a different gantry angles: 0°, 90°, 180° and 270°.
- Finally, with the angle gantry setted up at 90° or 270° rotate the collimator to each of the four cardinal angles: 0°, 90°, 180° and 270°, place the level on a flat place of the collimator and be ensure that the level value agrees with the angle value reported in the screen gantry or within the tolerance range.

- Cross-hair centering

This test is performed to ensure that the central distribution of the dose is delivered in the right place, and that it is independent of the angle of the collimator. For carrying out this test it is necessary to have a calibrated graph paper and a cross drawn on it each 45°. The next steps give a guide to perform this test [37].

- Place a graph paper on the treatment couch at a distance SSD= 100 cm and stick its corners to the table. Then, set up the gantry, collimator and couch at 0° and align the graph paper with the cross-hair.

- Vary symmetric jaw setting and verify that the difference between the cross-hair projected and the cross of the graph paper agrees with the tolerance values.

- Finally, rotate the collimator each 45° and mark the projection of cross-hair on the graph paper and measure the possible disagreement with the previously cross depicted. Measure the difference in millimeters and check if the difference is within the tolerance values.

- Treatment couch position

With the purpose of getting optimal treatment conditions, it is required to perform a quality control to the position of the couch. For that procedure it is necessary to be provided with a millimeter rule, ruler conveyor and a graph paper [37].

- First, the distance of the treatment couch has to be setted at SDD=100 cm, the gantry and collimator have to be set to 0°,and then, draw two orthogonal lines on the graph paper, one in longitudinal direction and the other in transverse direction. and After that, the cross-hair need to be aligned at the center of the graph paper with those lines.

- Straight away, move the couch to the longitudinal directions and stop it in the positions established during commissioning, and compare the value on the graph paper with the console value, if there is a shift, measure it and check if it is within tolerance values.

- Go back to the isocenter position and move the couch laterally and perform the same inspection that was done longitudinally.

- The next step, move the treatment couch so that the horizontal laser lines up with a notch on the couch, move the couch up and down to different positions (the same of the baseline values) and with a rule measure the distances. Ensure the couch readout and measured value agrees and are within the tolerance value.

- Finally, return the couch to the position of isocenter so that the graph paper lines up to the cross-hair, rotate the treatment couch to different values (usually each 45° in both sides), draw the new position of the cross-hair and measure the angle and verify that those values agree with the couch readouts in the floor and in the console screen and also they are within tolerance range or baseline values

- Symmetric and asymmetric jaw position indicator

Using a graph paper, draw a cross-hair on it and around it a equidistant squares of 5×5, 10×10, 15×15, 20×20 and 30×30 cm^2, taking into account that the purpose of this test is to evaluate the symmetry of the values of X1, X2, Y1 and Y2 in each size configuration. The next steps are recommended to follow in order to ease its implementation [37]:

- For the first case, set up in the linear accelerator 5×5 cm^2 field size with a jaw setting X1=2.5 cm, X2=2.5 cm, Y1=2.5 cm, Y2=2.5 cm, and in proportion to the respective configurations perform other field sizes.

- For each square, measure the difference between the square drawn and the field size projected on the graph paper, compare these value with the console value and check if they are within the tolerance values.

- For asymmetric jaw position choose the jaw setting according to the needs of clinical center with different values of X1, X2, Y1 and Y2 in order to create a rectangle and perform the same comparison like those were done in the symmetric configuration.

- Distance check device for lasers compared with front pointer

This test is developed to ensure that the lasers intersect in the isocenter position and for that reason the distance of the front pointer of 100 cm has to be in agreement with the value reported by the ODI. To perform this test is necessary to have a front pointer and a device like Iso-Align phantom (show in the Figure **3-16**) [37].

- First, place Iso-Align phantom at 100 cm using ODI and verify the laser alignment with the cross-hair for the gantry angles of 0°, 90° and 270°, if it is necessary adjust lasers previously. Check the distance to Iso-Align phantom with the front pointer and ensure that all lasers intersect a tip of pointer.

- Check that the difference between the position of the front pointer and each of the lasers is within the tolerance range.

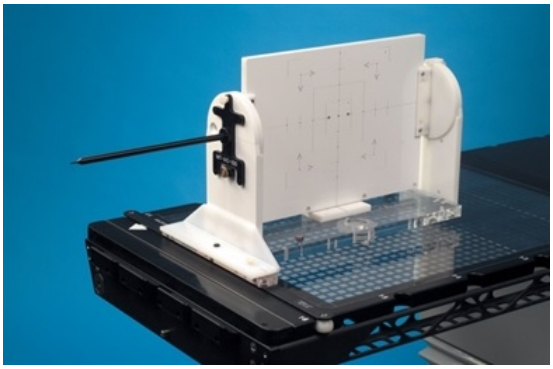

Figure 3-16.: Table pointer device [4].

The Table **3-5** shows the tolerance values according to TG-142 that must be taken into account when performing monthly mechanical quality controls:

Monthly		
	Machine-type tolerance	
Procedure	Non-IMRT	IMRT
Light/radiation field coincidence		2 mm or 1 % on a side
Light/radiation field coincidence (asymmetric)		1 mm or 1 % on a side
Collimator-gantry angle indicator		1°
Treatment couch position	2 mm / 1°	2 mm / 1°
Symmetric and asymmetric jaw position indicator	2 mm / 1 mm	
Distance check device for lasers compared with front pointer	1 mm	

Table 3-2.: List of tolerance values for monthly mechanical quality controls [32].

3.3.1.3. Annually quality controls

The mechanical quality controls that have to be made annually are: gantry and collimator rotation isocenter, couch rotation isocenter, coincidence of radiation and mechanical isocenter, table top sang, table angle, table travel in all directions. Some of these quality controls were described before, and the others are described in detail below [32, 37].

- Collimator rotation isocenter, gantry rotation isocenter and couch rotation isocenter

The isocenter in a linear accelerator is defined by the intersection of three axes: gantry rotation axis, collimator rotation axis and couch rotation axis. For testing the gantry isocenter it could be developed using a rigid rod aligned along the collimator axis [37]. Follow the next steps to perform the quality control in an easy way:

- First, set-up SSD at 100 cm, then place in the head of the gantry the tray and the front pointer of 100 cm, and after that adjust the tip of the rigid rod in the isocenter.

Then, attach to the couch another rigid rod with a small tip in the treatment couch with its tip in the isocenter too, both tips very close but without colliding with each other (as is depicted in Figure **3-17**).

- Immediately, move the couch along its longitudinal axis a few millimeters in order to avoid contact between the tips. Subsequently, move the gantry slowly around the second rod at 90° and 270°. If the gantry axis is in the right place, the points on the two rods should be at the same distance in all positions of the gantry angle or a distance within the tolerance value.
- For testing of the collimator isocenter, place the gantry angle at 0° and move the collimator angle every 45° and inspect that the distance between the tips of the rods remains constant and less than 1 mm, if not, measure the higher distance and compare to the tolerance value.
- The couch rotation isocenter could be tested with the same experimental setup only moving the treatment couch every 45° and measure the distance between the rods and check if the distances for every angle agrees with the tolerance value. The expected result is that the cross-hair image should trace an arc with a radius of less than 1 mm.

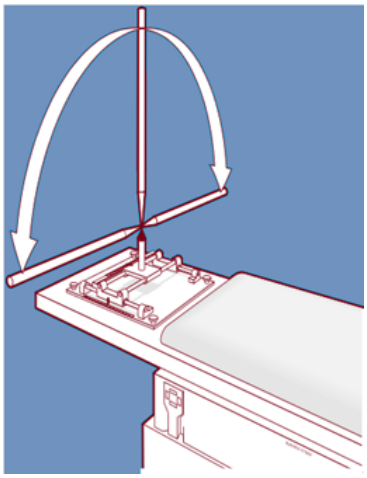

Figure 3-17.: Method of perform the isocenter verification [37].

- Radiation isocenter

For this test it is necessary to have a Virtual Water, a radiographic or radiochromic film or EPID imager. To facilitate its implementation it is advisable to follow the steps below [37]:

- First, place a film between two layers of virtual water at isocenter with adequate build-up for the selected photon energy. Ensure that the film is centered related to central axis of the beam and the gantry angle is at 0°.

- Then, set up the jaw size to create a thin field, e.g. 0.4×20 cm^2, symmetric to the central axis.
- The next step is to irradiate the film using various collimator angles every 15°. This results in a collimator star-shot pattern as it is shown in Figure **3-18** that can also be got by an EPID imager.
- Then repeat all the previous steps but using a new film and varying the treatment couch angle.
- Finally, turn the gantry at 90° ensuring that a new film is at SSD=100 cm and is centered to the central axis laterally. Set up the same jaw size and irradiate the film. Repeat the same procedure with another gantry angles.

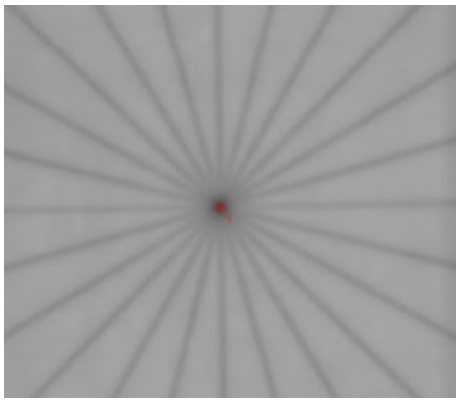

Figure 3-18.: Radiochromic film irradiated [37].

The mechanical and radiation isocenter must coincide with a tolerance of 2 mm from the baseline.

- Tabletop sag

This test is useful to know if the couch remains constant in parameters like height and speed when under the weight of a patient. For this test it is necessary a heavy object with a weighing about 77 kg [37].

- Set up the SDD=100 cm and extend the treatment couch to the maximum longitudinal position towards the gantry.
- Place the heavy object at the head of the couch, enable the ODI or use a front pointer to verify that the displacement of the couch remains almost constant and within the tolerance value.

- Table angle

For this test rotate the treatment couch through the full range and stop every 10° and verify if the value reported in the screen console agree with the mechanical readout [37].

- Table travel maximum range movement in all directions

This test is similar to the previous one, but there are displacements instead of rotate, displacements in lateral, longitudinal and vertical directions, and stopping every 10 cm until its maximum displacement and compare the mechanical measure with the digital measure [37]. The Table **3-3** shows the tolerances according to TG-142 that must be taken into account when performing mechanical quality controls:

Annual		
	Machine-type tolerance	
Procedure	Non-IMRT	IMRT
Collimator/gantri / couch rotation isocenter		±1 mm from baseline
Table top sag		1 mm from baseline
Table angle		1°
Table travel maximum range		±2 mm
Coincidence of radiation and mechanical isocenter	± 2 mm from baseline	

Table 3-3.: List of tolerance values for annual mechanical quality controls [32].

3.3.2. Dosimetric quality controls

In this part is recommended to have the linear accelerator dosimetry well-calibrated in order to make sure high accuracy and reproducibility in the delivering dose for radiotherapy treatments. There are dosimetric quality controls daily, monthly and annuals that are described here only for photon radiation [32, 37].

3.3.2.1. Daily quality controls

The only daily quality control that have to be performed is the X-ray output constancy for all energies, that could help us to know if there is an important change in the dose delivered [32, 37].

- X-ray output constancy

For this test it is necessary to have a dosimeter device like Daily Check or QA Beam Checker Plus [9] (Figure **3-19**). First, place the dosimeter device at a distance recomended by manufacters with a field size (e.g. for Daily Check 16.5×16.5 cm^2) center it with its effective area

and finally irradiate it with 100 MU (Monitor Units: It is the minimum operating unit of a linear accelerator) at least 3 times and verify if the measure values agree with the calibration value (depending on the linear accelerator calibration 100 MU should correspond about to 1 Gy) with a 3 % of tolerance [32, 37].

Figure 3-19.: Constancy daily check device [9]].

3.3.2.2. Monthly quality controls

Every month is necessary to run the next quality controls in order to ensure the correct deliver of treatment dose: X-ray output constancy, backup monitor chamber constancy, typical dose rate output constancy and photon beam profile constancy. The X-ray constancy is running in the same way that was described in the daily dosimetric control [32, 37].

- Backup monitor chamber constancy

Setting up the field size at 10×10 cm^2 and a large number of MU, start to irradiate with the average dose rate that is used in a common treatment, and while the irradiation is on, verify that the values reported by the backup monitor chamber agree with the primary monitor chamber values or the possible differences within the tolerance value [37].

- Typical dose rate output constancy

For this test is necessary to repeat the last test but for different dose rates and verify that the dose rate constancy remains almost the same or is within the tolerance range [37].

- Photon beam profile constancy

Constancy is associated with flatness according to TG 142 but also is recommended to evaluate the symmetry of every profile in both directions. For this test can be developed in a water tank with a robotic system of positioning for the ionization chamber, two ionization chamber with a volume size bigger than 0.120 cm^3 (one for main measure and the other for reference), an electrometer and a software to analyse the results [37]. The recommended steps are described below:

- First, fill the tank with water and align with the cross-hair and also be sure that the tank is well-levelled. Then, put one ionization chamber centered with the lasers in the isocenter point, set-up the SDD=90 cm, place the ionization chamber at 10 cm of depth and verify that all lasers intersect within an effective cross section of the ionization chamber.
- Then, set up the field size of 10×10 cm^2 in the console configuration, and fix the dose rate at average value.
- Finally, configure the system to perform a dose profile and start to irradiate. When the profile is complete, by means the software associated to de hardware, analyze the flatness and symmetry, and compare with the tolerance values if the results are within those ranges.
- Repeat the last steps for 10×10 cm^2 field size and for every energy available in the linear accelerator.

Monthly		
	Machine-type tolerance	
Procedure	Non-IMRT	IMRT
Typical dose rate output constancy	NA	2 %
Photon beam profile constancy		1 %
Backup monitor chamber constancy		

Table 3-4.: List of tolerance values for monthly dosimetric quality controls [32].

3.3.2.3. Annually quality controls

Every year is necessary to perform a complete dosimetry to ensure the stability of the linear accelerator, so that all the X-ray dosimetric quality controls are described here: X-ray flatness change from baseline, X-ray symmetry change from baseline, X-ray output calibration, spot check of field size dependent output factor for X-ray, X-ray beam quality, X-ray monitor unit linearity, X-ray output constancy vs dose rate, X-ray output constancy vs gantry angle, X-ray off-axis factor vs gantry angle and PDD or TMR and OAF constancy [32, 37].

- X-ray flatness and symmetry change from baseline

It is very important to measure the differences in the relative dosimetries of beam profiles with the results obtained in the commissioned process. The set-up for this quality control should be performed in the same conditions of the photon beam profile constancy test, and verify that agrees with the tolerance values for all energies [37].

- Spot check of field size dependent output factor for X-ray

To develop this quality control it is necessary to have a robotized water tank, an ionization chamber, an electrometer and the software for processing data.To facilitate this quality control is recommended to follow the next steps [37]:

- Locate the water tank and the ionization chamber under the reference conditions.
- Acquire at least 3 measurements at the reference point and get an average value.
- Perform the previous step for other field sizes.
- Divide the value obtained in the previous step by the one obtained in the reference point and verify that the field size is dependent of output factors are within expected tolerances relative to the baseline values.
- Repeat all the previous steps for other photon energies available in the linear accelerator.

- X-ray monitor unit linearity

For this quality control it is necessary to have an water tank or solid equivalent water, an ionization chamber and a calibrated electrometer. To facilitate the development of this test it is recommended to consider the following steps [37]:

- Align the water tank and the ionization chamber under the reference conditions.
- Deliver 500 MU at a dose rate of 300 MU/min and store the amount of charge recorded by the electrometer.
- Perform the previous step delivering 300, 200 and 100 MU under the same conditions.
- Graph MU versus measured electric charge and verify its linearity. Additionally verify that the electric charge obtained when irradiated with 300, 200 and 100 MU are a fraction of the electric charge obtained with 500 MU.
- Check that the values obtained are within the tolerance values.
- Perform all of the above steps with other available photon energies.

- X-ray output constancy vs dose rate

With the same configuration of the equipment used and the same reference conditions of the previous test, and setting a delivery of 100 MU, vary the dose rate. Verify that the electric charge measured by the electrometer is the same for all dose rates or within the tolerance range [37].

- X-ray output constancy vs gantry angle

To develop this quality control it is necessary to have an electrometer, a cylindrical ionization chamber with its build-up cap and a support for its location. The following steps help to develop this test [37]:

- Locate and align the ionization chamber on the gantry rotation axis.
- Deliver 100 MU to a specific gantry angle (0°) and record the reading of the electrometer.
- Perform the previous step for other different gantry angles.
- Verify that the reading reported on the electrometer for each gantry angle is the same as for the second step or it is within the tolerance range.

X-ray output calibration, X-ray beam quality and off-axis factor OAF constancy

Through this quality control it is sought to know the constancy in the calibration parameters that were entered to the equipment during its commissioning, and in case of exceeding the tolerance value, make the corresponding adjustments. To develop these measurements it is necessary to have an ionization chamber with a significant sensitive volume, a calibrated electrometer, a robotized water tank and its respective software (e.g. DoseView 3D or MEPHYSTO PTW) [37].

- **X-ray output calibration:** Develop output measurements with the conditions mentioned in the TG-51 (field size 10×10 cm^2, SSD=100 cm and depth=10 cm and 20 cm) or those used during the commissioning stage of the equipment for each of the available photon energies in the linear accelerator [38].
  - Perform an absolute dosimetry for each depth and then make a relation between both measurements: at 10 cm and at 20 cm.
  - Compare these results with the commissioning ones and verify that they are within the tolerance values.
- **X-ray beam quality:** To develop this quality control is possible performing a Percent depth dose PDD_{10}. For this test, perform a relative dosimetry measurement from the surface to a depth of 10 cm using a ionization chamber in a robotized water tank, with a previous setting of the field size of 10×10 cm^2 and a distance SSD = 100 cm. Compare the results with those obtained during the commissioning stage. If it is necessary acquire TMR values, this is possible taking into account the equation that relates with PDD values.

- **Off-axis factor OAF constancy:** For this test it is necessary to set the field size as large as possible, a distance SAD = 100 cm and measure the amount of charge with an ionization chamber at 0, 5, 10 and 15 cm from the central axis. In addition, it is possible to developed this test in air. After that, make the next relation taking into account the definition of OAF::

$$OAF = \frac{rdg_{OAX}}{rdg_{CAX}} \tag{3-9}$$

Where rdg_{OAX} is the electrometer reading performed the measurement with an ionization chamber in a off-axis position, and rdg_{CAX} measurement in central axis [21]. Finally, compare all the results with those obtained during the commissioning stage and make sure that their differences are within the tolerance values.

Annual		
	Machine-type tolerance	
Procedure	Non-IMRT	IMRT
- X-ray flatness change from baseline		1 %
- X-ray symmetry change from baseline		±1 %
- Spot check of Field size dependent		2 % for field size$< 4 \times 4$ cm^2
output factor for X-ray		1 % for field size$\geq 4 \times 4$ cm^2
- X-ray monitor unit linearity	±2 % $\geq$ 5 MU	± 5 %(2-4 MU)
- X-ray output constancy vs dose rate		±2 % from baseline
- X-ray output constancy vs gantry angle		±1 % from baseline
- X-ray output calibration		±1 % (absolute)
- X-ray beam quality		±1 % from baseline
- Off-axis factor OAF constancy		1 mm PDD shift from baseline

Table 3-5.: List of tolerance values for annual dosimetric quality controls [32].

3.4. AAA Photon dose calculation algorithm

The AAA algorithm (Analytical Anisotropic Algorithm) was developed by Drs. Waldemar Ulmer and Wolfgang Kaissl [41], which is a model for calculating dose distributions of 3D pencilbeam convolution-superposition algorithm, that has been integrated by the TPS Eclipse^{TM}. The calculations are initiated with the analytical convolution of the algorithm, that allows to reduce the computation times, followed by corrections of the heterogeneities by the use of 13 photon scatter kernels, these kernels are responsible for creating the dispersions of the primary photons and finally, the calculation of the distribution of dose is obtained by the superposition of the doses from the photons and electron convolutions [41].

The configuration of the AAA model is based on basic physical parameters determined by Monte-Carlo that are adapted to the measured data of the clinical beam. Within the calculations is supported the inclusion of dose modifiers, such as wedges, compensators and MLC

system.

The model of the AAA algorithm has evolved from its origins to completion in a triple gaussian photon kernel model, which has been corrected to improve the speed and accuracy of calculations, as well as corrections for heterogeneities. This algorithm firstly needs to be configured by introducing all the physical parameters that characterize the fluence and energy spectrum of the photons and electrons, and then the calculation of the dose distribution [41].

In order to calculate the dose distribution, the algorithm separates the convolution models for the primary photons, the dispersed photons and the electrons dispersed by the devices that limit the radiation beam. The algorithm divides the beam into small beam segments called beamlets to which the convolution is performed. The final part of the calculation, the algorithm makes a superposition of the calculated doses with the convolution of the photons and electrons for each beamlet [41].

3.4.1. Methods of calculations

The algorithm uses input parameters that are obtained from measurements that characterize the radiation beam and then, they are entered. The measured parameters are obtained in a water-equivalent medium and subsequently during the calculation of the dose distribution are scaled to other mediums.
One parameter that needs the algorithm AAA for its configuration is related to the spectrum of energy, which is initially calculated by Monte Carlo simulation obtaining a Bremsstrahlung spectrum of the electrons when impacting the target [41].

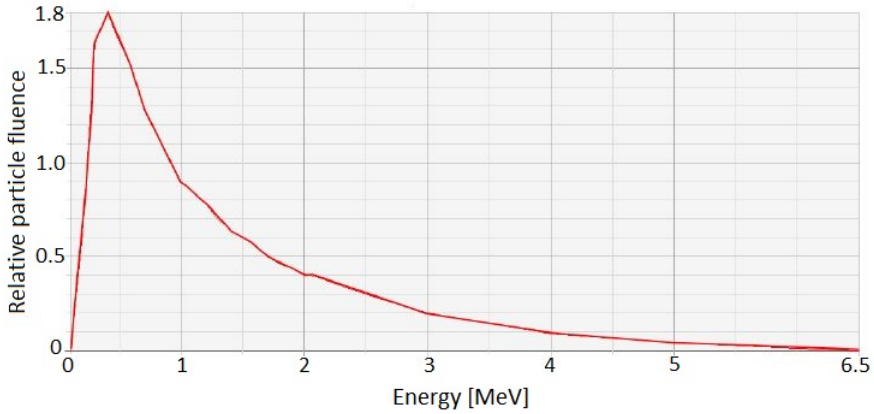

Figure 3-20.: Example of an energy spectrum for a photon beam of 6 MeV [41].

The AAA algorithm needs a parameter that relates the mean energy of the beam and the radius from the central axis to determine the effect of beam hardening due to the flattening

filter in the photon spectrum. The flattening filter is a device in the linear accelerator that is locate after the target and helps to make the dose profile more flat as can be seen in Figure **3-23**. Based on this information, the algorithm calculates the beam energy spectrum at any radial direction. In Figure **3-21** it can see an example of the curve that is obtained when plotting average energy vs radial distance; these data are entered to configure the algorithm [41].

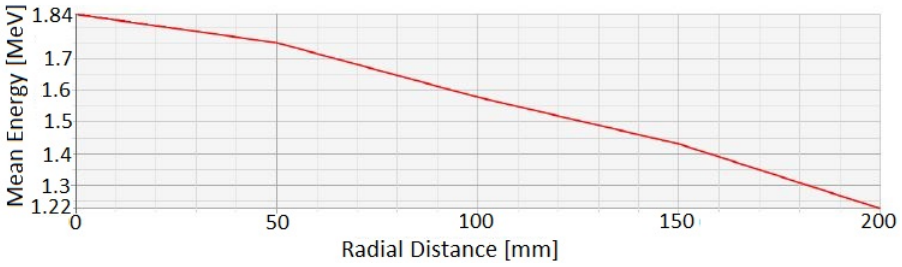

Figure 3-21.: Radial distribution of mean photon energy [41].

The flattening filter also modifies the intensity of the radiation beam by modifying the photon fluence. This fluency is modeled by the algorithm using the intensity profile, which consists of a photon energy fluence as a function of a radial distance from the central axis of the photon beam. In Figure **3-22** an example can be seen of a radiation profile for a photon beam of 6 MeV [41].

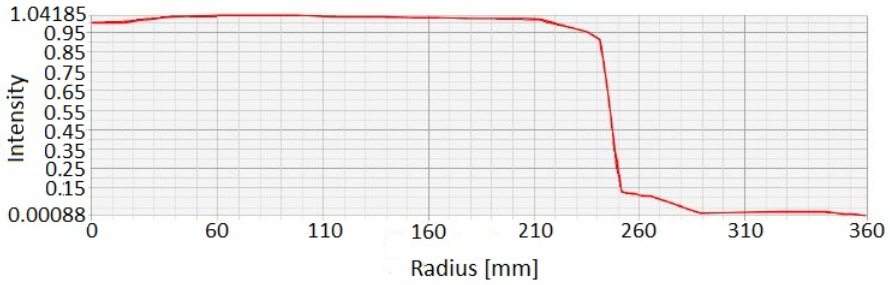

Figure 3-22.: Example of an intensity profile for a photon beam of 6 MeV [41].

To deal with inhomogeneities, the algorithm uses scatter kernels for photons and electrons. The scatter kernels are calculated by means of the Monte Carlo EGSnrc code for a mono-energetic beam, it is irradiated with a polyenergetic beam (Fig. **3-20**), it is necessary for these scatter kernels to adapt to the photon beam, for which a weight is given to each one of the monoenergetic scatter kernels [41].

3.4.2. Clinical Beam Modeling

To model the radiation beam for clinical use, three components must be taken into account in the deposition of the dose: the energy fluence of the primary photons, the fluence of the scattered photons in the flattening filter or the beam limiting devices, and the fluence due to electron contamination.

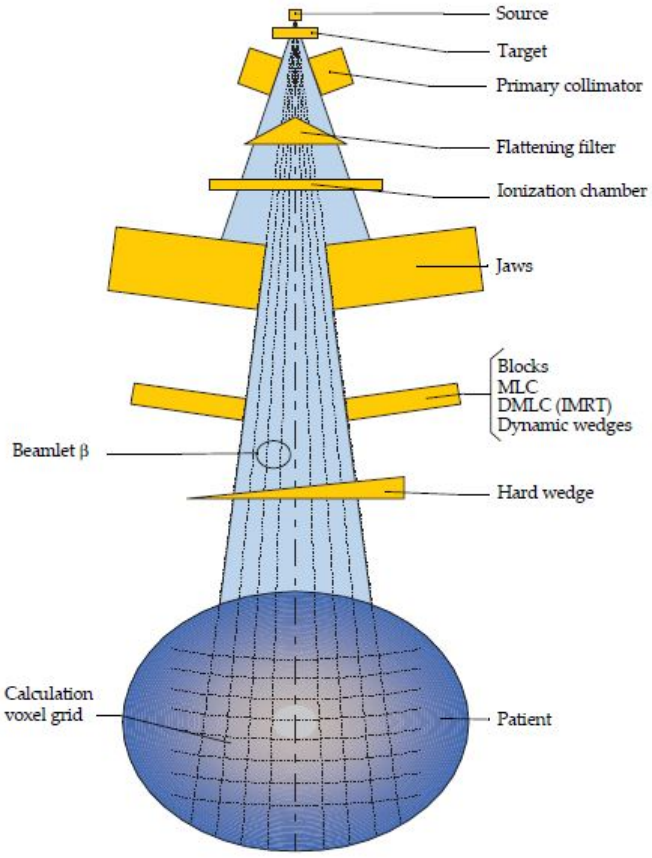

Figure 3-23.: Scheme of the gantry components of a linear accelerator in which the radiation beam interacts [42].

Using EGSnrc code simulates geometric conditions of the linear accelerator and the interactions that these devices have with the beam of radiation in order to have all the characteristics of the calculated beam in agreement with the clinical beam. This code adequately models interactions like the Compton scattering, Bremsstrahlung, photoelectric effect, pair production and annihilation for external beam radiotherapy.

As previously mentioned the beam of radiation is divided into small subbeams called beamlets β, dividing into two separate groups of photons beamleats and electrons beamlets, and assigned an intensity of each beamlet Φ_β [41]. The photon components are due to the pri-

mary beam and those caused by the scattering process of the linear accelerator devices that are between the target and the output of the gantry (extra-focal photons). These extra-focal photons are generated as a result of interaction of the primary radiation with: blocks, MLC, dynamic wedge and jaws, the paths of the radiation (or beamlets) are depicted in Figure **3-23** where it is possible to see the scheme of simulation of the linear accelerator from the target to the patient, between them all the devices of the gantry that could be interacting with primary photons.

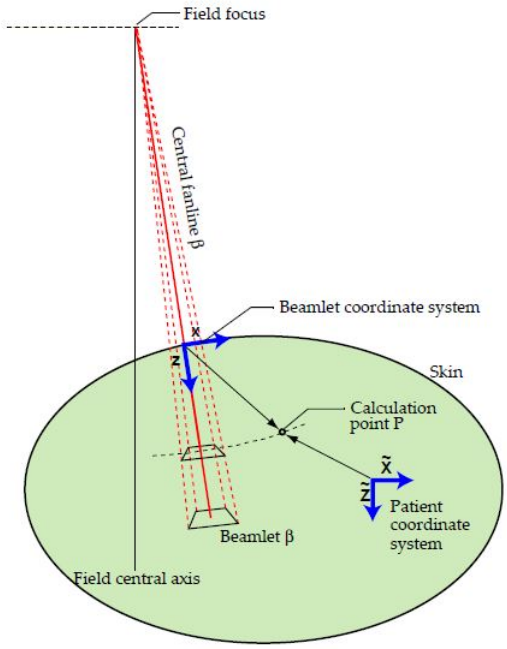

Figure 3-24.: Scheme of the coordinate systems of beamlet and patient [41].

All beam-modifying devices and accessories that influence beam fluence are taken into account by the AAA algorithm. The scattering produced at the head of the linear accelerator (gantry)are taken into account by a convolution of the photon fluence distributions. Extra-focal photons depend on the size and shape of the field of radiation, and this in turn influences the contribution of contaminating electrons [42].

To perform the volumetric calculation of the dose distribution, the patient's body is divided into a 3D matrix of small volumes called voxels. The calculation of the dose distribution is performed for each voxel taking into account the electron density of the tissue. The electron density ρ_e is obtained indirectly by means of a set of CT images and the Hounsfield units associated with each tissue. This calculation of 3D dose distribution is computed in its first part by two separate convolutions: one for primary photons and other for extra-focal photons and contaminating electrons; and in its final part by superpositioning of the contributions

of each beamlet [42].

The algorithm chooses two coordinate systems: one for the patient and the other for beamlet β. The coordinate system for the dose calculation point P is associated with the coordinates of the patient. In the figure **3-24** the relation of the two coordinate systems can be observed. Each beamlet has a cross-section corresponding to the resolution of the calculation voxel and that cross-section is taken into account for the calculation of the dose [41].

The final calculation of the dose at a point P in the patient with cordenades ($\tilde{\mathrm{X}}$, $\tilde{\mathrm{Y}}$, $\tilde{\mathrm{Z}}$) is determined by the sum of the contributions of each beamlet with cordenades (x,y,z) by computing of superposition [41].

3.4.2.1. Photon dose calculation

For the calculation of the dose at an arbitrary point P, the algorithm uses an energy deposition density function $I_\beta(z,\rho)$, that also denotes the area integral of the deposited energy over a sphere surface of the pencil beam at a depth z, and ρ is the electron density of each voxel; and a function representing the scatter kernel $K_\beta(x,y,z,\rho)$ that defines the lateral dose scattering [41], where x and **y** represent lateral coordinates, and **z** the depth that is measured from the intersection point of the central axis of the beamlet and the skin [42]; both functions are individually defined for each beamlet. The final calculation for an arbitrary beamlet is calculated by the following convolution:

$$D_{\beta,ph}(\widetilde{X},\widetilde{Y},\widetilde{Z}) = \Phi_\beta \times I_\beta(z,\rho) \times K_\beta(x,y,z;\rho) \tag{3-10}$$

In this convolution, the point P($\tilde{\mathrm{X}}$, $\tilde{\mathrm{Y}}$, $\tilde{\mathrm{Z}}$) where the dose is calculated is represented by (x,y,z) that is relative to the origin of the coordinate system of the beamlet. In adition, Φ_β is the photon fluence associated with a cross section of each beamlet β and the energy deposition density function $I_\beta(z,\rho)$ denotes the integral area of the dose over the entire transverse plane of the pencil beam at depth z [41].
$I_\beta(z,\rho)$ is a polyenergetic function that contains different photon energies and is constructed by the superposition of monoenergetic energy deposition density functions. This function also denotes the area integral of the deposited energy over the sphere surface of the pencil beam at depth z. This function is described as:

$$I_\beta(z,\rho) = \iint h_\beta(t,v,z)dt\,dv \tag{3-11}$$

where h_β is the polyenergetic pencil beam kernel that is calculated from Monte Carlo simulations. The function $I_\beta(z,\rho) = I_\beta(z')\frac{\rho(0,0,z)}{\rho_{water}}$ takes into account the heterogeneity of the medium by radiological scaling [41]. This scaling defines the radiological depth z' as:

$$z' = \int_0^z \frac{\rho(t)}{\rho_{water}}\,dt \tag{3-12}$$

The other photon scatter kernel function is composed of the weighted sum of four Gaussian functions, and also this function takes into account differences of electron densities, and it is shown in the following equation [41]:

$$K_\beta(x,y,z) = \frac{\rho(x,y,z)}{\rho_{water}} \sum_{k=0}^{5} c_k(z') \frac{1}{\sqrt{x^2+y^2}} e^{(-\mu_k r_d(x,y,z))} \tag{3-13}$$

Where μ_k is a decay constant that characterizes the Gaussian kernels, and c_k weigh each of the four Gaussian kernels and ensure the unity normalization of the total kernel energy and finally, $r_d(x,y,z$ is the radiological distance from kernel origin *(0,0,z)* to *((x,y,z)*. Each of the parameters that the K_β function used are determined by the scatter kernel and the photon beam spectrum. For the contribution of the dose due to extra-focal photons, the algorithm performs a similar calculation to the primary photons with the exception of their spectral composition and the position and size of the focal spot (secundary sources), and also it performs all the calculations about the interactions with the scatter kernels in all directions to perform anisotropic modeling [41].
Due to the abrupt changes that occur in the edges of two different tissues, the equation (3-13) would overestimate the dispersion conditions and this is because of the differents electron densities, so to avoid this situation, the energy distribution in the z-direction is moved depeer through the use of a one-dimensional scatter kernel, and then this motion is pre-compensated by applying an inverse transformation to the h_β function [41]. The one-dimensional scatter kernel can be written as:

$$K_z(z) = \sum_{i=1}^{2} c_i \frac{1}{\mu_i} e^{-\mu_i z} \tag{3-14}$$

where c_i and μ_i are determined using optimization methods, and in presence of heterogeneities the last equation is scaled as follows:

$$K_z(z) = \frac{\rho(z)}{\rho_{water}} \sum_{i=1}^{2} c_i \frac{1}{\mu_i} e^{-\mu_i z'} \tag{3-15}$$

The pre-compensation to the poly-energy pencil beam kernel h_β mentioned above will be performed as follows:

$$h_\beta^{'}(x,y,z) = h_\beta(x,y,z) \otimes inv(k_z(z)) \tag{3-16}$$

Where $inv(k_z(z))$ is the deconvolution that makes modifications over a pencil beam in order to perform corrections for heterogeneities. If the medium is homogeneous, the algorithm does not affect the calculation [41].

Regarding to the contaminating electrons that are produced mainly by the primary beam interactions with some components of the gantry like the flattening filter, the ionization

chambers, the collimators, the air and any device that is between the source and the body of the patient, it is neccesary to perform other convolution and the AAA algorithm calculates its contributions to the dose distribution for an arbitrary beamlet due to contaminating electrons [41].

$$D_{cont,\beta}(\widetilde{X},\widetilde{Y},\widetilde{Z}) = \Phi_{cont,\beta} \times I_{cont,\beta}(z,\rho) \times K_{cont,\beta}(x,y,z,\rho) \tag{3-17}$$

The scatter kernel for contaminating electrons is modeled by a Gaussian distribution function as follows:

$$K_{cont,\beta}(x,y,z,\rho) = \frac{1}{2\pi\sigma^2_{cont}(z)} exp\left(-\frac{x^2+y^2}{2\sigma^2_{cont}(z)}\right) \tag{3-18}$$

Where σ_{cont} is a constant derived from the measured data. This scatter kernel is used in the same way that the other scatter kernels were used with the primary beam. The calculation of the final dose for a given point within the patient's body consists of the superposition of all separate dose contributions: due to the photons of the primary beam $D_{ph1,\beta}$, the extra-focal photons $D_{ph2,\beta}$ and as a result of the contaminating electrons $D_{cont,\beta}$ from all individual beamlets [41]:

$$D_(\widetilde{X},\widetilde{Y},\widetilde{Z}) = \sum_{\beta}(D_{ph1,\beta}(\widetilde{X},\widetilde{Y},\widetilde{Z}) + D_{ph2,\beta}(\widetilde{X},\widetilde{Y},\widetilde{Z}) + D_{cont,\beta}(\widetilde{X},\widetilde{Y},\widetilde{Z})) \tag{3-19}$$

All the convolutions that appear in the superposition can be performed analytically, but by the form of the Gaussian scatter kernels and the respective fluences, they can be treated as uniform across the cross-sections of the beamlets [42].

4. Materials and Methods

For this part of the work the elements necessary for routine dosimetries have been used in the clinical part and are described below, with each detail. Additionally, an anthropomorphic and heterogeneous phantom was constructed in order to carry out a more complete evaluation of the AAA algorithm. In the second part of this section, the explanation of the methodology used for the evaluation of the dosimetric accuracy of the AAA algorithm is performed.

4.1. Materials

4.1.1. Linear accelerator Clinac iX

A Clinal iX lineal accelerator manufactured by the Varian Medical System was used, with available photon energy of 6 MeV and 15 MeV, for which the licenses of 3DCRT, IMRT and VMAT are enabled. The equipment has a MLC millenium 120 multi-leaf collimation system.

Figure 4-1.: Linear accelerator Clinac iX by Varian [2].

4.1.2. Water tank MP3-M

The PTW MP3-M tank has a robotic positioning system for detectors with a pitch of one tenth of a millimeter in all three Cartesian directions and a maximum speed of 50 mm / s. The manipulation of the movements of the robotic system can be done from a digital control connected to the tank or by a long distance connection by means of a cable connected to the

computer that owns the software MEPHYSTO, in which the movements can be configured to it.

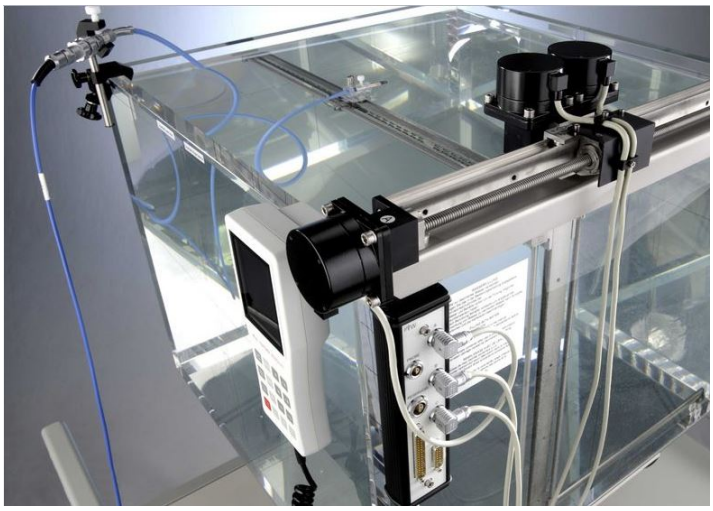

Figure 4-2.: Water tank MP3-M used for the dosimetries [8].

The dimensions of the tank are $50 \times 50 \times 40{,}8$ cm^3 and it has an automatic filling system and height adjustment of the tank controlled by a support called Scanlift.

4.1.3. Ionizing chamber Semiflex 31010

For the dosimetries, two PTW Semiflex 31010 ionization chambers were used due to their impermeability and their volume, and also because of the experience that other authors have had evaluating diverse algorithms of dose distribution with ionization chambers with similar volumes [18, 27]. Its effective volume of ionization is 0.125 cm^3 and this kind of ionization chambers are designed for field sizes like all we used in this work.

Figure 4-3.: Ionization chamber Semiflex of PTW used for clinical dosimetry [3].

One of the ionization chambers is used as reference and the other (the calibrated ionization chamber) for performing the measurements. For 3D dosimetry measurements in water phantoms, the ionization chamber is ideal since its volume is almost spherical which leads to have a flat angular response over an angle of ±180° and a uniform spatial resolution.
Its nominal power range for photons is from 140 keV to 50 MeV, this property and others are listed in the table below.

Property	Characteristics
Volume	0.125 cm^3
Range of nominal photon energy	140 keV-50 MeV
Operating voltage	±100-±400 V
Leakage current	$\leq \pm 4$ fA
Nominal response	3.3 nC/Gy

Table 4-1.: Properties of the ionization chamber Semiflex 31010 for photons [6].

Repeatability tests were performed to observe the stability of the ionization chamber, measurements were taken under absolute dosimetry conditions: field size 10×10 cm^2, SSD = 100 cm and 10 cm depth, and analysis was performed for the two photon energies available from the linear accelerator.
For this characterization, 30 measurements of electric charge were carried out under the conditions mentioned above, the results can be seen in Table **4-2**.

Energy photon spectrum [MeV]	Mean electric charge [nC]	Standar Deviation [nC]
6	1.95	$1{,}28 \times 10^{-3}$
15	2.24	$1{,}02 \times 10^{-3}$

Table 4-2.: Results of the Semiflex 31010 ionization chamber stability test.

From the analysis of Table **4-2** with respect to its standard deviation it can be said that the ionization chamber is quite stable between one measure and another one, and the variation between one measure and another are not significant.

4.1.4. Ionizing chamber PinPoint 31014

This ionization chamber was used to measure the absolute doses in the heterogeneous phantom. It is suitable to perform dosimetry in small spaces and radiation fields due to its

dimensions, its internal diameter is 2.0 mm and just like the Semiflex chamber has a flat angular response because its volume is almost spherical.

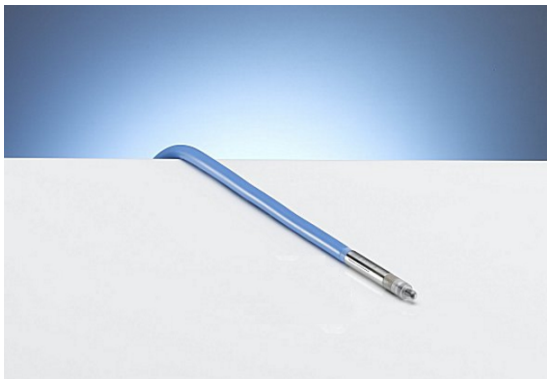

Figure 4-4.: Ionazing chamber PinPoint of PTW [3]

Some of its main characteristics are listed below:

Property	Characteristics
Sensitive volume	0.015 cm^3
Range of nominal photon energy	140 keV-50 MeV
Operating voltage	±100-±400 V
Leakage current	$\leq \pm 4$ fA
Nominal response	0.004 nC/cGy

Table 4-3.: Properties of the ionization chamber PinPoint for photons [7].

4.1.5. Electrometer PTW UNIDOS E T10010

In order to perform the readings in absolute dosimetry, it is necessary to have an electrometer connected to the ionization chamber used to perform the collection and count of charges. For this measurements it was used the PTW electrometer with reference UNIT E T10010 operating in the range of 0 to ± 400 V and having a high resolution of the order of few fA [11].

Figure 4-5.: Electrometer PTW UNIDOS E T10010 [11].

4.1.6. Electrometer PTW TANDEM

To carry out the relative dosimetry readings, a dual-channel TANDEM reference PTW electrometer was used, one channel for the reference ionization chamber and another for the measurement chamber. This electrometer has a resolution of 10 fA and has an operating range of 0 to 400 V, with a 50 V step, with reversible polarity. The minimum response time is 10 ms and it can be controlled using the MEPHYSTO software [10].

Figure 4-6.: Electrometer PTW TAMDEM [10].

4.1.7. Creation and characterization of anthropomorphic thorax phantom

The main purpose for creating an anthropomorphic phantom was to evaluate more rigorously the AAA algorithm; for getting this aim, an anthropomorphic and inhomogeneous phantom was developed for a human thorax. For creating an heterogeneous phantom it is necessary to take into account the electronic density of every tissue body to relate to the materials of the equivalent tissues. The fabrication of the anthropomorphic phantom was based on ICRU Report 44 [45] and three different materials were used which are described in detail below.

This kind of phantom has to have the same shape and dimension that a human body has. For this study, a male thorax phantom was created with the similar characteristics of a male human thorax such as mass density, position of the organs and radiation interactions. For homogeneous or heterogeneous phantoms it is required to have similar electron density in order to get the equivalent radiation-tissue interactions; therefore it is necessary to choose the appropriate materials.

4.1.7.1. Phantom materials

In a clinical treatment, the interactions between radiation and tissue produce different absorption and scattering for each organ because their electron and mass densities are different and, in addition, these interactions modify the absorbed dose in the tumour. For that reason, it is necessary to take into account all these interactions. There are many reports that have been published giving enough information about the material that can substitute human tissue, beginning with water for homogeneous phantoms and introducing more materials that could be equivalent in heterogeneous phantoms [20, 45].

Besides, the human shape and dimension must be considered for analysing more accurately all the aforementioned interactions. There are many different phantoms that are commercially available, from whole body anthropomorphic phantoms to phantoms that represent only a body section like head or thorax.

Depending on the kind of ionizing particle and their energies, the interactions properties changes, and accordingly to electron density of the tissue and these interaction, the body tissue substitute must be suitably chosen. All these aspects should be taken into account in order to evaluate how suitable they are for the manufacture of the heterogeneous phantom. In this work the interactions of the ionizing particles with the phantom only involved photons with a spectrum of energies of 6 MeV and 15 MeV, such spectrums like one depicted in Figure **3-20**.

Due to a high energy interval of photons all the interactions must be considered with its attenuation coefficients such as photoelectric absorption, Compton scattering, coherent scattering and pair production. These coefficients have to be similar between body tissues and substituted materials. For photon energy greater than 10 MeV the production of neutrons is present when it interacts with the substitute tissue and, due to the atomic number Z, one of the four possible interactions will predominate over the others, therefore it is necessary to know the atomic composition of each material and the body tissue [30].

Sample	Elemental composition (percentage by mass)				
	H	C	N	O	Others
24 Adults (20-74 years)	3.4	15.5	4.2	43.5	10.3 P, 22.5 Ca, 0.1 Na, 0.2 Mg
10 Children (6-13 years)	3.9	15.8	4.4	45.0	9.8 P, 20.9 Ca, 0.2 Mg
4 Children (2-5 years)	4.0	15.7	4.5	45.4	10.1 P, 20.1 Ca, 0.2 Mg

Table 4-4.: Elemental composition of cortical bone [45].

4.1.7.2. Elemental composition of human tissue

All the bodies are different between one and other person, even with the same age, sex and race, and even more their elemental compositions of each tissue. The elemental composition of a person varies between the childhood and the adulthood considerably. It has been known that the levels of some elements like calcium decrease with the age in the adulthood, for this reason it is necessary to have a mean elemental composition for a human body when it looks for materials and quantities to build an heterogeneous phantom. Different concentrations have been reported in analyses samples of soft tissue, skeletal muscle and adipose tissue of human specimens with the same age and the same gender. According to ICRP (1975), a review report shows that water content in adipose tissue can vary from 10.9 to 21 % [45] which supports adipose tissue quantities like water and lipid can vary significantly [45].

The cortical bone is composed in greater amounts (between 99.4 % and 99.8 %) by hydrogen, carbon, nitrogen, oxygen, calcium and phosphorus; and in smaller amounts (less than 0.6 %) it is composed by sodium, magnesium and sulphur. However, the amounts of these elements depend on each person's age according to sample analysed by Woodard, 1984 (see Table **4-4**). In order to choose a substitute material of the bone for the elaboration of the phantom it is necessary to consider the elemental composition [45].

The composition reported by various authors could include errors because of missing elements or additional elements in their counts. In ICRU report 44 it was adopted a correction method introduced by Woodard (1984) [45]. There is a close relationship between the elements which compose a tissue and their amounts with the electron density. The recommendations made by ICRU report 44 [45] about the elemental composition and electron and mass densities are listed in Table **4-5** for the main organs and tissue.

The same ICRU Report [45] listed others tissues with its elemental composition. For the purpose of this study the properties of tissues that are necessary to consider for creating the

Sample	Elemental composition (percentage by mass)					ρ [kg/m^3]	n_0 [m^{-3} $\times 10^{26}$]
	H	C	N	O	Others		
Adipose tissue	11.4	59.8	0.7	27.8	0.1 Na, 0.1 S, 0.1 Cl	950	3180
Blood	10.2	11.0	3.3	74.5	0.1 Na, 0.1 P, 0.2 S, 0.3 Cl, 0.2 K, 0.1 Fe	1060	3510
Breast	10.6	33.2	3.0	57.2	0.1 Na, 0.1 P, 0.2 S, 0.1 Cl	1020	3390
GI tract	10.6	11.5	2.2	75.1	0.1 Na, 0.1 P, 0.2 S, 0.2 Cl, 0.1 K	1030	3420
Heart (blood filled)	10.3	12.1	3.2	73.4	0.1 Na, 0.1 P, 0.2 S, 0.3 Cl, 0.2 K, 0.1 Fe	1060	3510
Kidney	10.3	12.1	3.0	72.4	0.2 Na, 0.2 P, 0.2 S, 0.2 Cl, 0.2 K, 0.1 Ca	1050	3480
Liver	10.0	13.0	3.0	74.9	0.2 Na, 0.3 P, 0.3 S, 0.2 Cl, 0.3 K	1060	3510
Lung	10.3	10.5	3.1	74.9	0.2 Na, 0.2 P, 0.3 S, 0.3 Cl, 0.2 K	Deflated: 1050 Inflated: 2060	3480 862
Muscle (skeletal)	10.2	14.3	3.4	71.0	0.1 Na, 0.2 P, 0.3 S, 0.1 Cl, 0.4 K	1050	3480
Pancreas	10.6	16.9	2.2	69.4	0.2 Na, 0.2 P, 0.1 S, 0.2 Cl, 0.2 K	1040	3460
Skeleton- cortical bone	3.4	15.5	4.2	43.5	0.1 Na, 0.2 Mg, 10.3 P, 0.3 S, 22.5 Ca	1920	5950
Skeleton-Spongiosa	8.5	40.4	2.8	36.7	0.1 Na, 0.1 Mg, 3.4 P, 0.2 S 0.2 Cl, 0.1 K, 7.4 Ca, 0.1 Fe	1180	3480
Skin	10.0	20.4	4.2	64.5	0.2 Na, 0.1 P, 0.2 S, 0.3 Cl, 0.1 K	1090	3510

Table 4-5.: The recommended elemental composition, ρ and n_0 of some body tissue [45].

thorax phantom are shown in Table **4-5**. Because of the characterization of the phantom was imageologically performed, taking into account the CT images that were taken of the phantom. In Table **4-6** are shown different tissues of the thorax with its respective Hounsfield Units (HU) that will be related them with those of its substituted materials later.

Human tissue	HU
Soft tissue or muscle	10-100
Lung [39]	-750
Spine or bone	700-3000

Table 4-6.: Hounsfield units (HU) for main human thorax tissues [12].

4.1.7.3. Tissues substitute for thorax phantom

There are many materials for substituted tissues that can be suitable to create anthropomorphic and heterogeneous phantoms, but this study focused on those materials which were used in creation of thorax phantom: paraffin wax, cork, PVC and bee's wax [16, 22, 40].

Paraffin wax whose general formula is C_nH_{2n+1},$n > 15$, can substitute soft tissue or muscle because of its elemental composition and properties like its lightness and its malleability with the heat [45]. The mass attenuation coefficient and mass energy-absorption coefficient that are related to the contribution of photoelectric effect, Compton effect, pair production and Rayleigh scattering for this material and muscle and its relation are shown in Figure **4-7**.

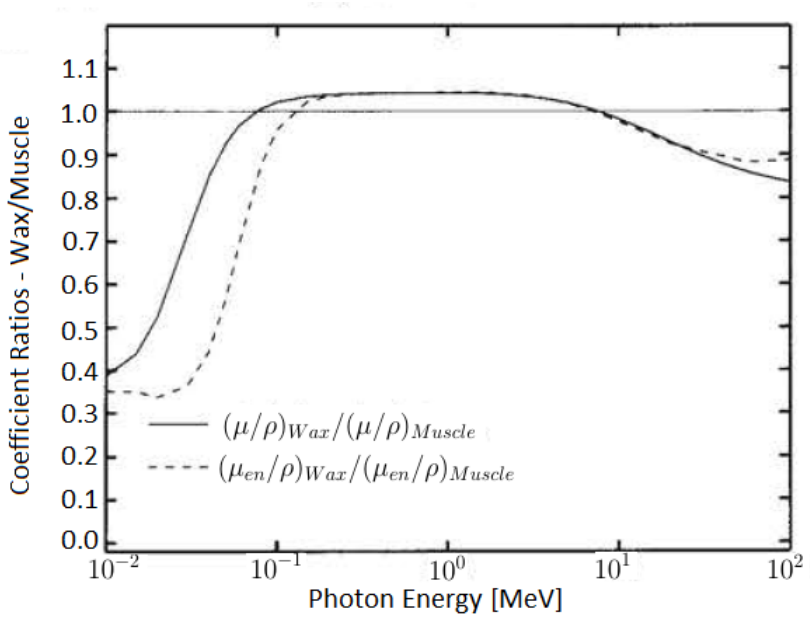

Figure 4-7.: Graph of coefficient ratios vs. photon energies [45].

The behavior of the graph of the paraffin wax and the muscle are similar for the photon energies in the range of a few keV up to 10 MeV where there is a ratio of photon interaction coefficients (μ/ρ and μ_{en}/ρ) as a function of photon energies as can be seen in Figure **4-8**; the adjustment of both coefficients μ/ρ (solid line) and μ_{en}/ρ(dotted line) is almost a 100 % for that energy range. Having in mind the previous graph it can infer that the paraffin wax is suitable as a substituted tissue like muscle for photon energies up to 10 MeV, above this value the concordance is between 85 and 95 %.

In the same report [45], they present a graph about the percentage difference in calculate depth-dose for the muscle substitute of paraffin wax for different photon energies and as it can see in Figure **4-8**, for a high photon energy of 10 MeV the percentage difference after 5 cm of depth is very low, and before 5 cm they explain that difference is due to Monte-Carlo uncertainties.

There are other substituted materials that can be used instead of paraffin wax that are provided in the next table and it has information about their elemental composition, mass and electron densities.

According to the results reported in their calculations [45], it can be concluded that the paraffin wax is a good substitute material for muscle and soft tissue. If it takes into account its

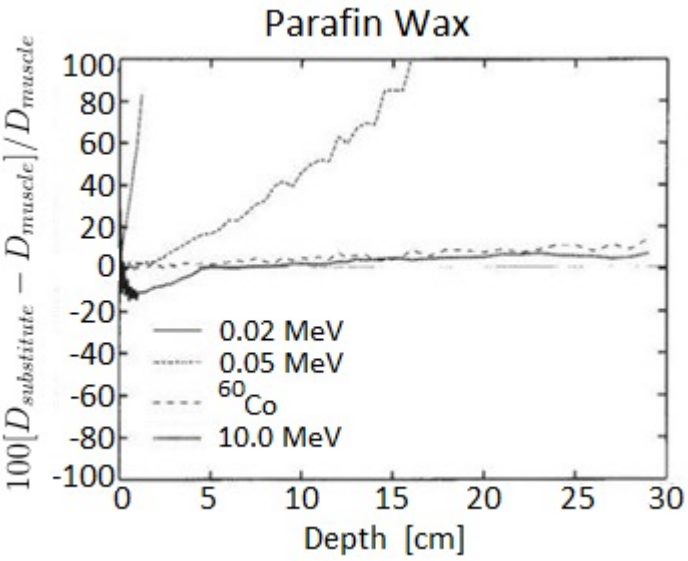

Figure 4-8.: Percentage difference in calculated depth-dose for the muscle substitute of paraffin wax [45].

Tissue substitute	Elemental composition (percentage by mass)					ρ [kg/m^3]	n_0 [m^{-3} $\times$ 10^{26}]
	H	C	N	O	Others		
Acrilic	10.1	60.0	-	32.0		1170	3800
Alderson muscle	8.9	66.8	3.1	21.1	0.1 Sb	1000	3270
Paraffin wax	15.0	85.0	-	-	-	930	3210
Polyethylene	14.4	85.6	-	-	-	920	3160
Polyestyrene	7.7	92.3	-	-	-	1050	3400

Table 4-7.: The recommended elemental composition, ρ and n_0 of some equivalent human soft tissue [45].

electron and mass densities and the energy photon range chosen and taking into consideration the recommendation of Hasanzadeh et al. [28], in which they explained why paraffin wax is the best substitute for soft tissue in the phantom manufacture from the dosimetric point of view in the range of the photon energy from 20 keV to 20 MeV [28]. The bee's wax is also a good material to replace soft tissue and it has similar properties as paraffin wax does [40]. The PVC or polyvinyl-chloride $(C_2H_3Cl)_n$ is a thermoplastic material and it can be used to substitute bones in creation of phantoms for radiotherapy. Due to their characteristics the PVC could replace cortical bones and in some cases, this material also works for other types of bones depending on their dimensions. Table **4-9** shows characteristics of PVC and other materials that can be substituted many kinds of bones.

Tissue substitute	Elemental composition (percentage by mass)					ρ [kg/m^3]	n_0 [m^{-3} $\times$ 10^{26}]
	H	C	N	O	Others		
P.V.C.	4.8	38.5	-	-	56.7 Cl	1350	4160
P.T.F.E	-	24.0	-	-	76.0 F	2100	6070
B100	6.6	53.7	2.2	3.2	16.7 F, 17.7 Ca	1450	4610
Plaster of Paris	2.3	-	-	55.8	18.6 S, 23.2 Ca	2320	7140
SB5	2.6	30.6	1.0	38.9	0.1 Cl, 26.8 Ca	1870	5570

Table 4-8.: The recommended elemental composition, ρ and n_0 of some substituted material of bone tissue [45].

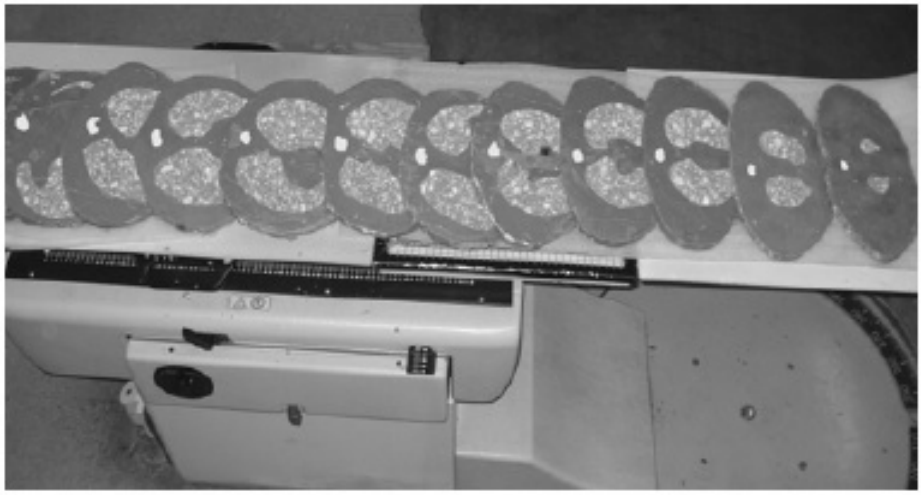

Figure 4-9.: Fabrication of thorax phantom [40].

The material that better substituted lung tissue is cork because of its mass density (0.26 g/cm^3) and other properties [20, 45]. Different authors have chosen this material for the design of various thorax phantoms for radiotherapy with really good results. Depending on the respiratory phase the mass density of the lungs changes but, for inspiration phase a suitable material is cork in terms of electron and mass density, and also because of its ease in the design of lungs.

Senthilkumar made a thorax phantom using cork as a substitute material for lungs [40], as can be seen in Figure **4-9**, the thorax phantom was fabricated slice by slice. To evaluate this phantom, different techniques of irradiation were used with photons of a cobalt unit [40]. They found a good concordance of the results between the calculated dose by Plato TPS and the absorbed dose of TLD (LiF) as it can see in the Figure **4-11**, the brown line and black line have a similar behaviour of absorbed dose in all the points measured.

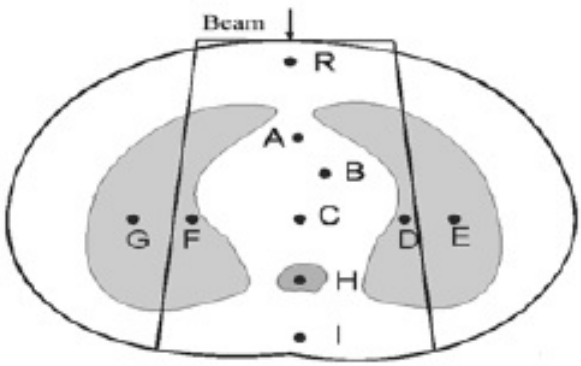

Figure 4-10.: Axial distribution of TLD for dose measurements in differents points labeled by letters [40].

It was concluded that despite of the heterogeneous region of the thorax its study reveals good results between calculations and measurements and for its algorithm of dose distribution calculation they recommend some corrections for heterogeneities in every TPS [40].

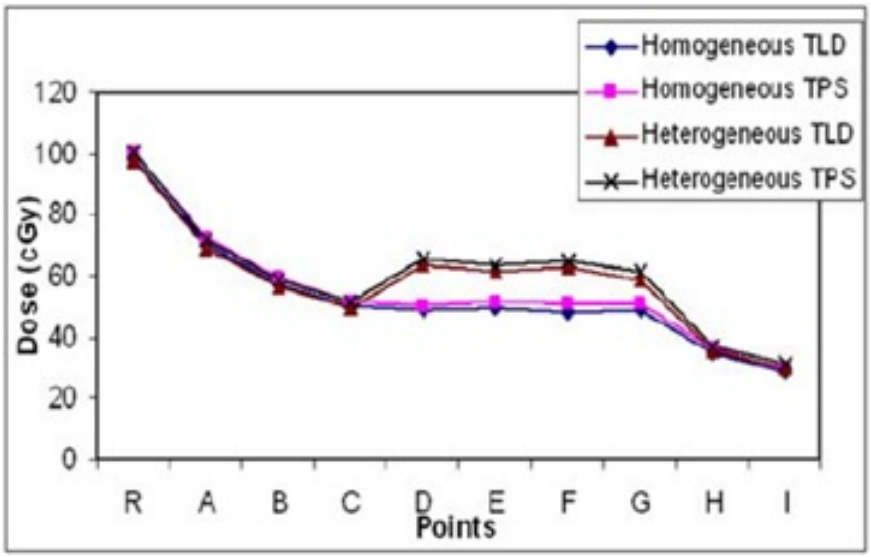

Figure 4-11.: Result of absolute dosimetries in the heterogeneous phantom [40].

4.1.7.4. Hounsfield units and electron density

In a treatment planning it is necessary to know the shape, dimensions and composition of the region of treatment and its surrounding volume, for these reasons, it is required an image of CT. Images of CT represent the spatial distribution of photon attenuation coefficient. These kinds of images have implicitly in each pixel a Hounsfield unit. The scaled Hounsfield number is defined by [31]:

$$HU = 1000 \times \frac{\mu_{tissue} - \mu_{water}}{\mu_{water}} \tag{4-1}$$

where μ is the linear attenuation coefficient of a material and μ_w is the same coefficient but in water. This coefficient can be written:

$$\mu = \rho N_A \sum_{i=1}^{n} \frac{w_i}{A_i} \sigma_i(E) \tag{4-2}$$

where ρ is the physical density, N_A is Avogadro's number, A_i is the atomic weight of the ith element, w_i is its proportion by weight and σ_i the total cross section. In addition, σ_i is the sum of cross-sections of photoelectric effect σ^{ph}, coherent scattering σ^{coh} and incoherent scattering σ^{incoh}. The Equation 4-2 shows the relationship between electron density and the linear attenuation coefficient that are related to the Hounsfield units.
The Hounsfield units or CT numbers for different tissue substitutes are listed in Table **4-9** and also contains information like mass density ρ and relative electron density ρ_e.

Tissue Substituted	ρ [g/cm^3]	ρ_e [$\times 10^{23}$ e^-/g]	HU
Water [45]	1	3.34	0
Paraffin wax [22, 45]	0.93	3.21	-163
PVC [12]	1.35	4.16	800-1700
Cork [20]	0.26	3.25	-950 to -750

Table 4-9.: The recommended elemental composition, ρ and n_0 and HU of some substituted material of body tissue.

Tables **4-6** and **4-9** show the equivalence in Hounsfield Units for human tissues and substituted tissues, which gives us bibliographic support for the manufacture of phantom.

4.1.7.5. Manufacture of thorax phantom

The thorax region is known for its high level of inhomogeneities and it is a challenge for all the algorithms of dose calculation in reproducing the interaction of ionizing radiation with the tissue of this region. Taking into account the characteristics mentioned above for substituted tissue we developed a thorax phantom using a mold with shape and dimensions of a normal Colombian adult male thorax. In order for a equivalent phantom to have similar interactions,

the phantom materials had been chosen because of their characteristics comparable to the real tissues: paraffin wax for muscle and soft tissue, cork for the lungs and PVC for the spine.

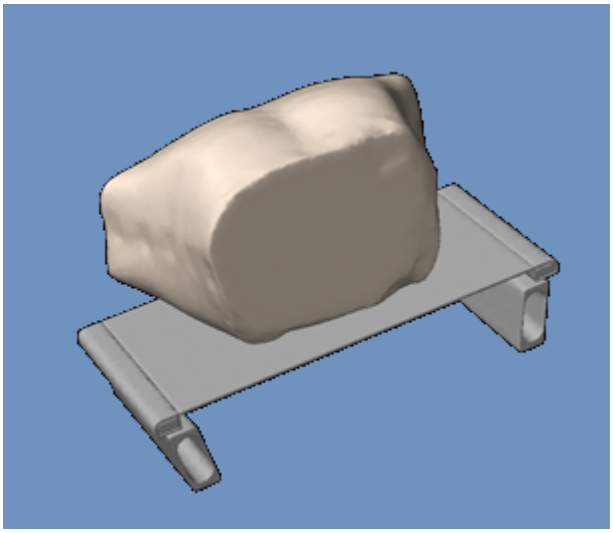

Figure 4-12.: Image of the phantom reconstructed.

Figure **4-13** shows a CT image of the phantom where it can be clearly noticed the muscles and soft tissue in gray, the lungs in black and the spine in white.

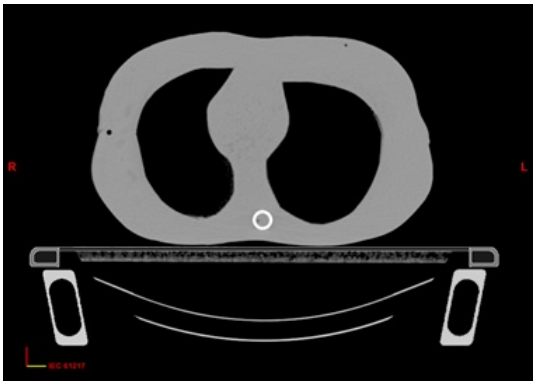

Figure 4-13.: CT image taken in central axis of the thorax phantom.

All the substituted tissues were also chosen based on the aforementioned information of the ICRU 44 and the article related to the thorax phantom made by Senthilkumar. On the other hand, a CT image was acquired in order to characterize every material as can be seen in Figure **4-13** (each slice of the thorax phantom was taken every 3 mm).

The substituted materials for fabrication of the thorax phantom of the current research were analyzed considering the HU numbers and, the properties of electron and mass density

reported by other authors. Using a tool of Eclipse called Image Browser the HU number of each pixel of the CT image was measured. The calculation of HU number was made in the whole slice of the central axial region. The whole spectrum in terms of HU numbers for the entire central slice of phantom is depicted in Figure **4-14**, which shows a large numbers of pixels with its respective HU number and, where the HU are equal to 800, the region around it has a few numbers of pixels because of the small size of the PVC area. For that reason, only some pixels are analyzed for this substituted tissue.

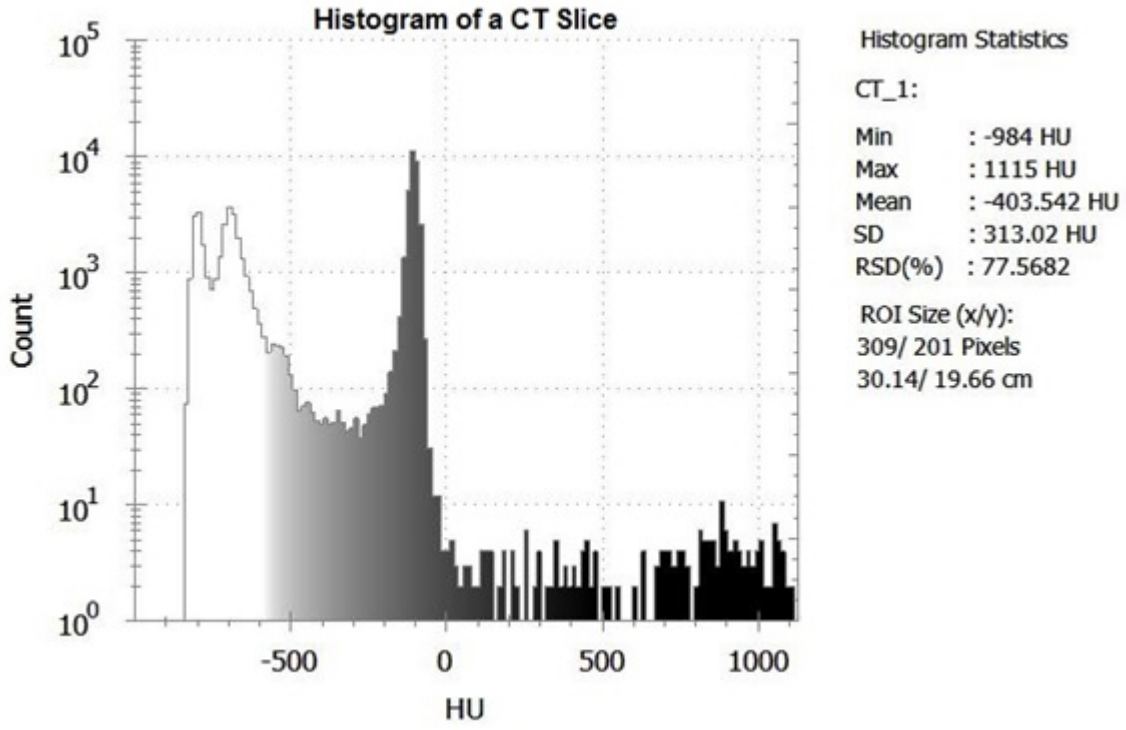

Figure 4-14.: Histogram of the central CT slice of the thorax phantom.

The mean of the HU for this material is -111.5 with standard deviation of 14.8 which is given in a histogram by the same software, setting up a ROI of 45 pixels. Considering the results of the fabrication of the phantom made by Senthilkumar where he chose bee's wax as a substituted material for the muscle and soft tissue which have a similar range of HU numbers than paraffin wax and taking into account the recommendations of ICRU report 44 about paraffin wax [45].

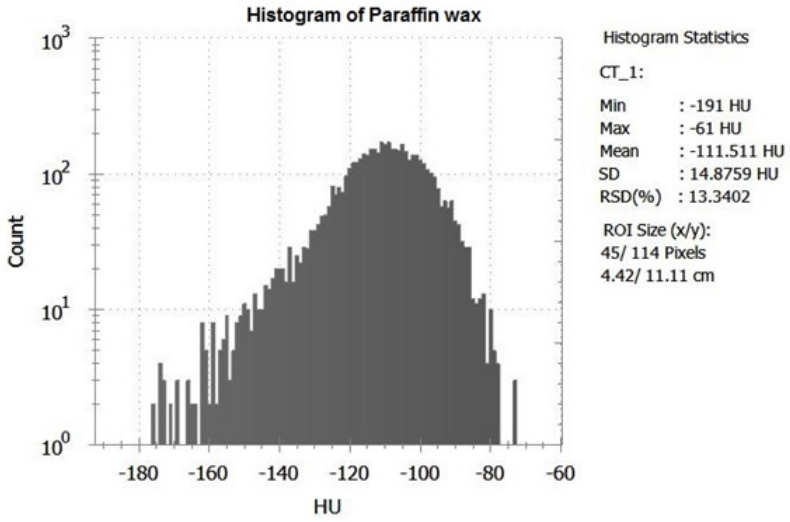

Figure 4-15.: Histogram of the paraffin wax.

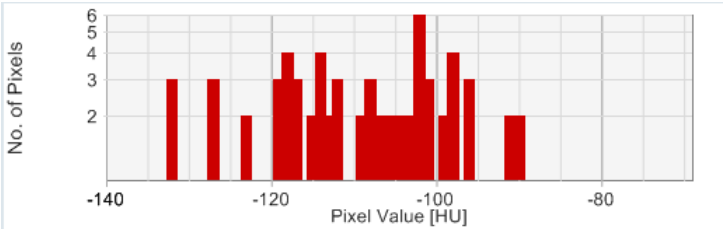

Figure 4-16.: Histogram of the bee's wax.

A CT scan was done on a sample of bee's wax and analyzed with Image Browser program to know their HU numbers for each pixel, a mean HU value of -108.4 was obtained with a standard deviation of 13.28, the histogram of bee's wax can be seen in figure **4-16**.

Carrying out the same analysis for cork as substituted material of lung tissue, it is obtained a mean value and a range of HU numbers of the inflated lung tissue similar to a human lung tissue as it is reported in literature [20, 45]. In the histogram of Figure **4-17** is shown the distribution of HU numbers for a ROI taken from the cork area. The mean HU number for cork is -789.9 with a standard deviation of 16.9; these results are within the range reported for lung in inhalation phase.

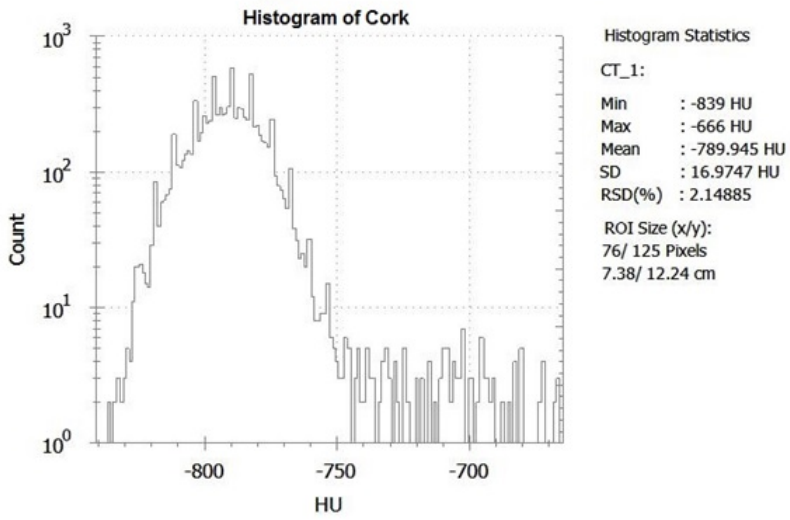

Figure 4-17.: Histogram of the cork.

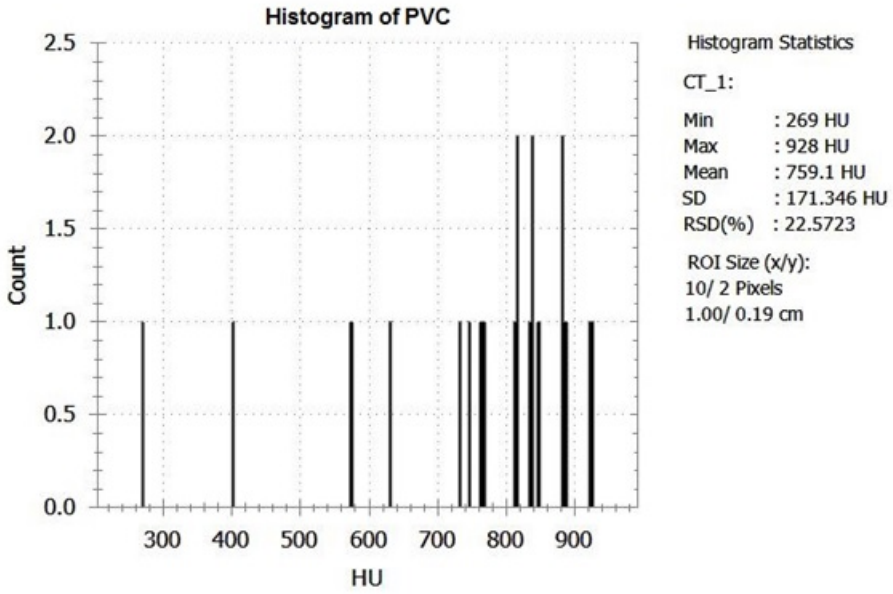

Figure 4-18.: Histogram of the PVC of the phantom.

Finally, for the PVC as a substituted material of spine was obtained another histogram; the result of the mean HU number was 759.1 with standard deviation of 171.36; the ROI was taken in the PVC zone within central axis of irradiation, the number of pixels in the histogram is low because of the PVC size in the CT slice. In addition, something that it could worry about is the amount of counts in the histograma, so another histograms were obtained in other slices and similar histogram were gotten and the mean HU number are similar in

all the histograms, for this reason only one histogram in the central area was chosen. This result agrees with values reported in literature by other authors [40]. Teflon and PVC are suitable as a substituted material for trabecular bones. The histogram of the PVC sample is depicted in Figure **4-18**.
Table **4-10** shows the results of the imaging analysis of each substitute material used to make the phantom of the present work.

Tissue Substituted	Mean HU
Paraffin wax	-111.5
Bee's wax	-108.4
PVC	759.1
Cork	-789.9

Table 4-10.: Result of the measurement of Hounsfield units (HU) for materials used in the manufacture of the phantom.

As we can see in Table **4-10**, the results obtained are close to those obtained by other authors and reported in Table **4-9**.

4.2. Methods

The present section show the way to evaluate the accuracy of the AAA algorithm and for this purpose a dosimetric tests based on Task Group Report 53 were established. The methodology used to develop this work is represented in the diagram depicted in Figure**4-19**.

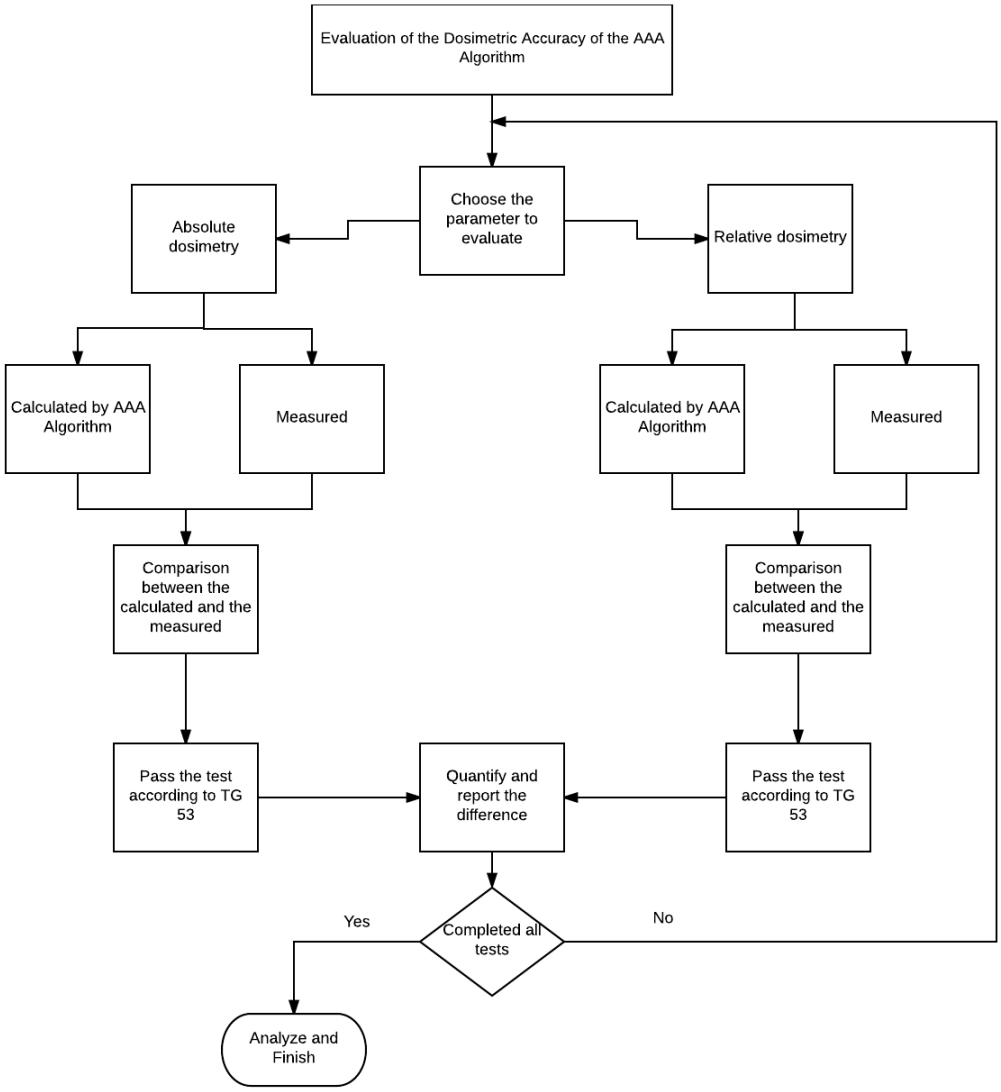

Figure 4-19.: Diagram of methodology for the dosimetric evaluation used in the present work.

Using the Eclipse treatment planning system, the planning of each test was carried out and simultaneously each one of them was realized experimentally. For both photon energy spec-

trums: 6 MeV and 15 MeV all the test were performed, and it is necessary to mention that when it will refer to photon energy spectrum of 6 MeV we are talking about that the kinetic energy of the electrons is about 6 MeV and after these electrons interact with the target, as a result a photon energy spectrum is obtained with a large distribution of photon energies including some amount of photons with energy of 6 MeV as we can see in Figure **3-20** but no a monoenergetic beam of photons of 6 MeV. Furthermore, the same situation occurs with the photon energy spectrum of 15 MeV.

By using this aforementioned software a water phantom was designed with the dimensions of the previously mentioned MP3-M water tank, and all the characteristics in the experimental set-up were taking into account, and finally, the planning of the irradiation was done. An example of one of all the cases performed is shown in Figure **4-20** where can be seen one of the planned cases with its simulated homogeneous phantom. For this specific planned case in its upper part one can see the shape of the MLC system and inside in the simulated tank the dose distribution calculated by AAA algorithm.

The methodology described here can be used as a protocol to perform the dosimetric accuracy assessment of any calculating dose distributions algorithm. A set of tests recommended in Task Group report 53 was adjusted according to the needs of the clinical center. Each test is aimed at evaluating some aspect of the AAA algorithm, in Table **4-11** one can observe each of the tests and below its explanations in detail and the scope of each one.

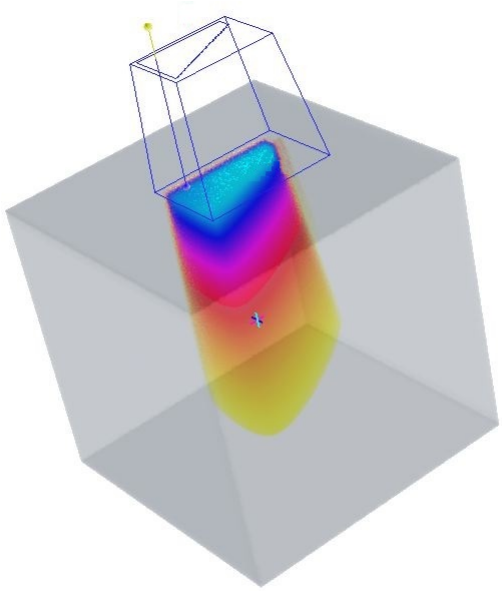

Figure 4-20.: Water phantom designed with the TPS Eclipse for all the planned cases.

4.2.1. Relative dosimetry

One part of all the tests to be developed is the relative dosimetry (as one can see on right in Figure **4-19**), which helps to observe how the dose distributions behave according to certain variations of the radiation field. Variations such as field sizes, gantry angle, SSD (surface-source distance) and others are taken into account when the AAA algorithm is evaluated. The relative dosimetric tests are basically radiation profiles and PDDs.
For the analysis of the regions of the radiation beam that were evaluated, the criterion of Venselaar was taken into account in which it can divide the beam into the regions that are listed below and illustrated in Figure **4-21** [25].

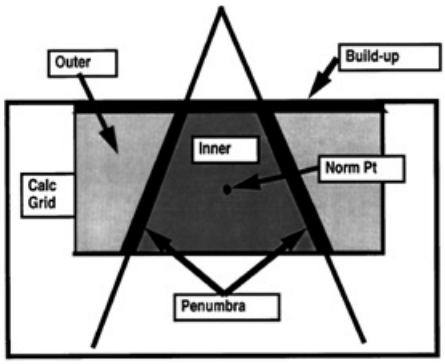

Figure 4-21.: Parts of the radiation beam [25].

- **Inner region**
- **Penumbra region**
- **Outer region**
- **Build-up region**

The inner, penumbra and outer (umbra) regions were described in detail before in theory section. The last region (Build-up) is the zone in the PDD that goes from the surface to the point of maximum dose.
Dosimetric profiles were obtained at different depths and PDDs for each of the tests, both those calculated by the TPS and those measured. Then, they were compared point by point, having a tolerance difference for each of the tests according to the given table by the TG Report 53 [25].

All measurements of dose profiles previously mentioned were performed at 4 different depths, for the photon energy spectrum of 6 MeV fixed depths of 1.2, 4, 10 and 20 cm, and for the

energy spectrum of 15 MeV of 3.2, 6, 10 and 20 cm. The differences in the two first depths in both energy spectrums are because of the capability of each energy distributions in penetrating in the water phantom. A total of 200 profiles and 26 PDD were performed for each energies spectrum configuration. Moreover, the ionization chamber with which the measurements were performed has been characterized to establish its stability, and thus avoiding obtaining more measurements.

Each of the relative and absolute dosimetric tests that were performed using a homogeneous water phantom, and the objective to be evaluated in the AAA algorithm by which they were developed, are listed in Table **4-11**.

Test	Description	SSD [cm]	Gantry angle	Field size [cm^2]
1	Open square fields	100	0	5^2, 10^2, 25^2
2	Extended SSD square fields	125	0	8^2, 20^2
3	Rectangular fields	100	0	5×25, 25×5
4	Open with 45-degree collimator	100	0	20^2
5	Isocentric 10×10 cm^2 at surface	6 MeV[a]: 90	0	11.1^2
		15 MeV[b]: 80	0	12.5^2
6	Oblique incidence	100	305, 330	10^2
7	Asymmetric half-beam	100	0	10 : 0
8	Multileaf collimator (MLC)	100	0	Triangle (Fig. **5-52**)

[a]Photon energy spectrum due to interactions of 6 MeV electrons
[b]Photon energy spectrum due to interactions of 15 MeV electrons

Table 4-11.: Summary of dosimetric test case recommended by TG report 53 [25].

For each of the measurements made for each region the Task Group report 53 [25] gives a tolerance table:

Test	Description	inner (%)	Penumbra (mm)	Outer (%)	Buildup (%)	TSF (%)
1	Open square fields	1.5	2	2	20	0.5
2	Extended SSD square fields	1.5	2	2	40	1
3	Rectangular fields	2	2	2	20	0.5
4	Open with 45-degree collimator	5	3	3	50	2
5	Isocentric 10×10 cm^2 at surface	1.5	2	2	20	0.5
6	Oblique incidence	3	2	5	40	1
7	Asymmetric half-beam	3	2	3	20	1
8	Multileaf collimator (MLC)	3	3	5	20	1

Table 4-12.: Tolerances used in the validation of the Analytical Anisotropic Algorithm recommended by TG report 53.

In order to evaluate the following tests, taking into account their respective configurations, the dose profiles were acquired for each energy spectrum of the photons and for each of the depths and in the cross-plane and in-plane directions. Otherwise, the PDDs were also acquired for each of the tests and field size or different gantry angle. The ionization chamber used was configured for the acquisition of the measurements per point between 1 and 3 mm, this because the calculation matrix of the algorithm AAA gives results every 0.25 mm and it is necessary to have the highest number of points to compare.

After performing the respective measurements, it proceeded to compare each measured profile with that calculated by the AAA algorithm. For this procedure it was created a software in RStudio, which performed an interpolation to ensure that each point to be compared had its counterpart. After this, the program performs the point-to-point comparison, and gives a result of the number of points passing the test for each profile, taking into account the different tolerances for the test in evaluation, and for each region of the profile.

Next, it will show the procedure performed for a specific case, for one of the tests that was selected a single field size, the profiles obtained in both directions were compared, but for the next example only in cross-plane and at four depths; in the same way each of the profiles of each case and each photon energy spectrum were analyzed taking into account the differences in the tolerances.

4.2.1.1. Model case

The model case is part of the test 1, for the photon energy spectrum of 6 MeV, for a square field of 10×10 cm^2 for each depth and only for the cross-plane direction. The point-to-point analysis was performed, and a total of 1742 points were analyzed and compared for this model, as we can see in Figure **4-22**,the measured profile (red crosses) was compared with the profile calculated by the AAA algorithm (solid black line).

For each point in the inner region, a comparison of the dose values between the measured and the calculated is performed, if the difference percentage is less than 1.5 %, it can established the test is approved. In the penumbra region, for each dose value is calculated the difference in the distance between the calculated and the measured points, and this difference should be less than 2 mm. For the outer region the dose difference for each position should not exceed 2 %.

In Figure **4-23** it can see all the profiles for this model case for each depth. Furthermore, they were compared: the measured profiles with those calculated ones in the cross-plane direction for the depths of 12 mm (black line), 40 mm (red line), 100 mm (blue line) and 200 mm (green line). The results of these comparison can be observed in Table **4-13**.

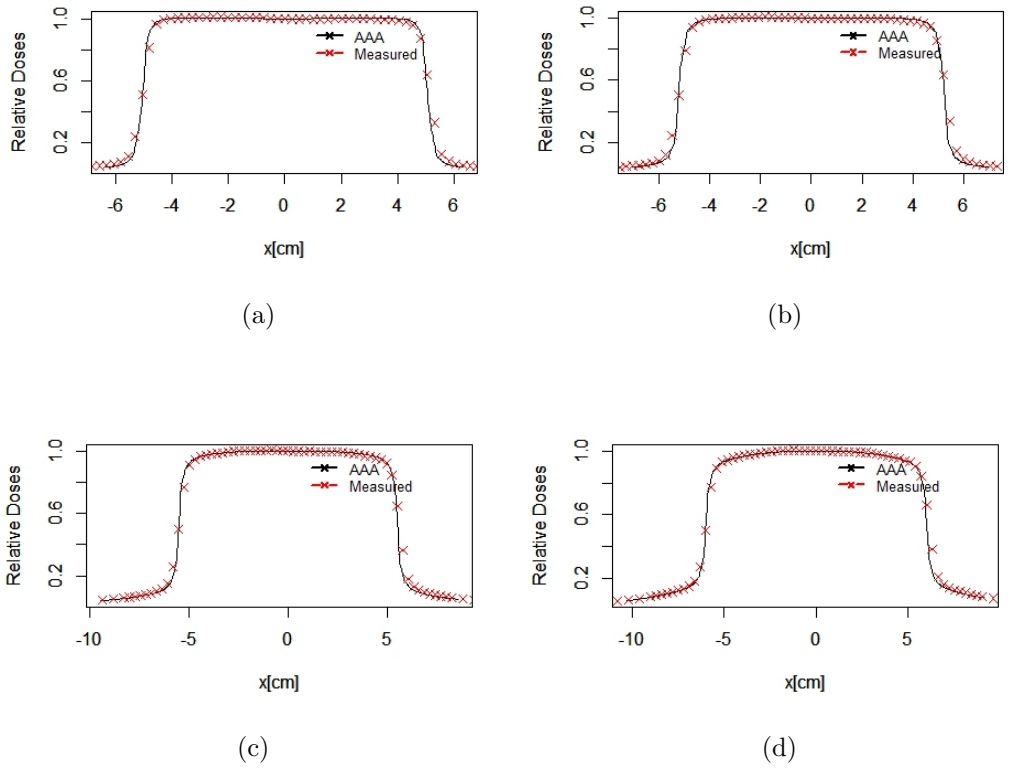

Figure 4-22.: Comparison between measure and calculated profiles for the model case in the cross-plane at a) 12 mm depth b) 40 mm depth c) 100 mm depth and d) 200 mm depth.

Depth	Inner		Penumbra		Outer	
[mm]	Pass	Fail	Pass	Fail	Pass	Fail
12	335	6	30	0	2	12
40	338	11	30	0	2	27
100	347	0	28	8	2	101
200	266	39	41	14	15	88

Table 4-13.: Number of points tested for test 1 in cross-plane direction TG report 53 for each depth

All the 1742 points that were compared from the four profiles are shown in Table **4-13**. Additionally, it shows the distribution of the results for each depth according to the area of the dose profile. For the inner zone it can see that 1286 of the 1342 points passed the test 1, this represents 96.5 % of the

points in this zone; for the penumbra zone 92.8 % of the 151 points pass the test. Finally, for the outer zone only 8.4 % of the 249 point pass the test. The following relation was used to compare all the points and to obtain the percentage differences in the outer, inner and build-up zones:

$$\%\ Difference = \frac{D_{meas} - D_{calc}}{D_{meas}} \times 100 \tag{4-3}$$

where D_{calc} is the relative dose calculated by AAA algorithm and D_{meas} is the relative dose measured.

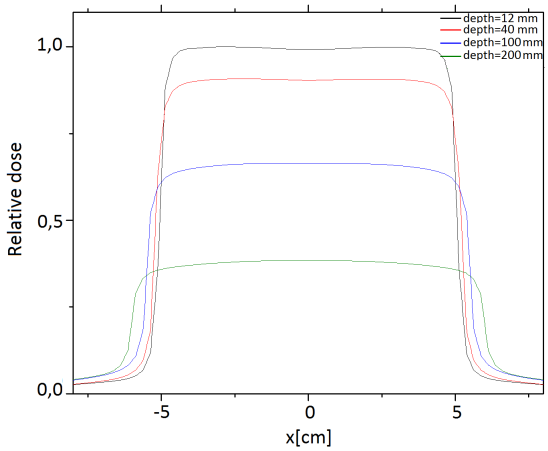

(a)

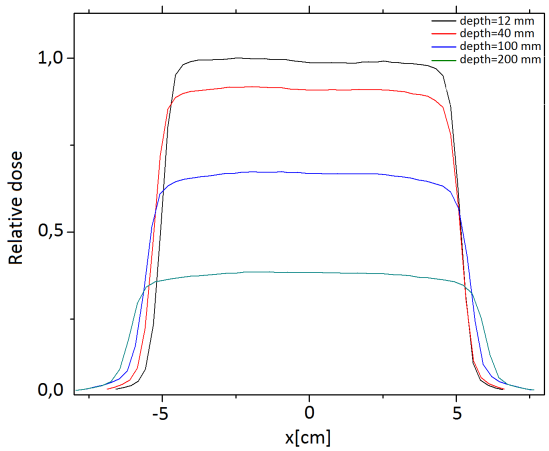

(b)

Figure 4-23.: Radiation profiles for the model case in the cross-plane direction for a) Calculated by the AAA algorithm and b) measured one.

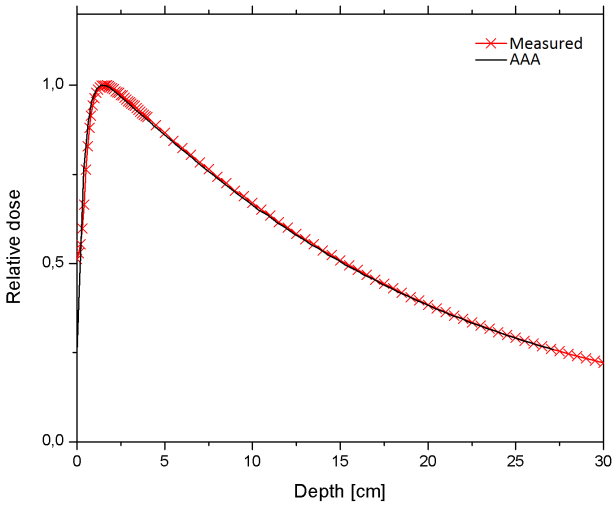

Figure 4-24.: Normalized PDD for test 1 with size field of 10×10 cm^2 and energy spectrum of 6 MeV.

In addition, a measured PDD was obtained and one calculated for each different adjustment of each test. The comparison was made only for the points inside the build-up zone and the tolerance values in the comparison shown above in Table **4-12** was taken into account, which for this test is 40 %. Because of the low tolerance constraint in this region, all points in the build-up zone pass the test. To be more specific, all the PDDs were normalized at the maximum value of dose so the higher value that the graphic can reach has to be 1 as can be seen in Figure **4-24**.

For the overall result for each region of the profile was calculated following the procedure done by Breitman et al [18] by the next relation:

$$Overall\ results = \frac{\sum_{all\ test\ cases} Point\ passing\ test\ case_i}{\sum_{all\ test\ cases} Points\ in\ test\ case_i} \tag{4-4}$$

It should be noted that to have statistically significant results it is necessary to perform more than 30 measurements for each test, this would give a total of 6240 dosimetric profiles for both available photon energies. However, in the hospital environment that is impossible because the time machine is limited and the expensive cost that those measurements would imply.
For this reason a dose profile was measured 30 times, evaluating the 3 zones: inner (point n° 3), penumbra (point n° 2) and outer (point n° 1), as it can be seen in Figure **4-25**. The field size was 10×10 cm^2 and the dose profile was obtained in the cross-plane direction at a depth of 10 cm, in Table **4-14** the results are shown for the 3 points analyzed.

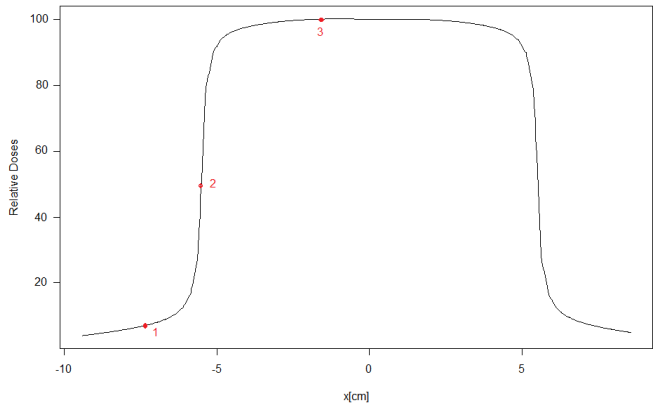

Figure 4-25.: Position of the points for characterization of the dosimetric profile of size of 10×10 cm^2.

Point number	1	2	3
Profile zone	Outer	Penumbra	Inner
Position [cm]	-7.2	-5.0	-1.6
Mean absolute dose	4.8	54.9	100.6
Standard deviation	0.017	0.18	0.22

Table 4-14.: Result of the measurement of the dosimetric profiles in points of the three evaluated zones.

Table **4-14** shows very small standard deviations for the inner, penumbra and outer zones, which means a low dispersion of the measurements made and therefore guarantees the repeatability of the measurements and a high stability of the ionization chamber used.

4.2.2. Absolute dosimetry

In order to compare the absolute dose values that the AAA algorithm calculates, the dose values for each of the tests listed in Table **4-11** were measured experimentally using a water tank with the previously mentioned specifications and their percentage difference was obtained. The procedure for obtaining the dose values and knowing whether or not the test passed the TG-53 criteria, the model case that was followed to perform with the rest of tests is shown below. It is useful to state the next steps.

4.2.2.1. Model case

Performing an experimental set-up in which the water phantom, the calibrated ionization chamber, the electrometer, a thermometer and a barometer were used; then the water tank was centered and

aligned with respect to the cross-hair and the lasers of the linear accelerator, and the ionization chamber were place at a depth of 10 cm and a distance SSD=90 cm was fixed, and then, it proceeded to irradiate with 100 MU.

In pursuance of having a reference point and to be able to calculate the Total Scattering Factor (TSF), absolute dosimetry was obtained with the aforementioned parameters for a field size of 10×10 cm^2 for the photon energy spectrum of 6 MeV. With the purpose of making the respective corrections to the dosimetry, three measurements were obtained for each of the voltages fixed to the electrometer (-300 V, 150V and 300 V) and electric charge values were obtained. Additionally, for the other corrections, the values of pressure and temperature were recorded as can be seen in Table **4-15**.

The calculation of the absolute dose absorbed in water was made taking into consideration the TRS 398 [35] and TG-51 [15] documents. Knowing the absolute dose calibration factor to water of the ionization chamber N_{D,w,Q_0}, 3 measurements were performed tree times for each potential difference, recording the absolute pressure and the water temperature to make the respective corrections to measure the dosimeter reading. The calculation of the absorbed dose is performed by the following equation:

$$D_{w,Q_0} = M_{Q_0} N_{D,w,Q_0} \tag{4-5}$$

Where M_{Q_0} is the reading of the ionization chamber with its respective corrections, the first correction that is necessary to do is due to the ionization process of the water molecules because it depends on the pressure and the temperature, and also because of the calibration of the ionization chamber was made in a different location with different pressure and temperature, it is necessary to make the corrections to obtain a correct measurement, the following equation gives us the correction factor:

$$k_{T,P} = \frac{(273{,}2 + T) \times P_0}{(273{,}2 + T_0) \times P} \tag{4-6}$$

The polarity correction is also necessary to have an appropiate measurement, because the charge collection is not always the same in an ionizing chamber for the negative polarity as for the positive polarity [34], the true reading is taken to be the average of the absolute values of readings taken at the two polarities, as it is shown in the next equation;

$$k_{pol} = \frac{\mid M_+ \mid + \mid M_- \mid}{2M}. \tag{4-7}$$

The recombination correction of the ions is made taking into account the average of the three measurements made when the electrometer potential difference is smaller (150 V), and this is because the response of the ionization chamber also depends on the voltage applied between the measuring and collecting electrodes of the detector. Such correction is done as follows;

$$k_s = a_0 + a_1 \left(\frac{M_1}{M_2}\right) + a_2 \left(\frac{M_1}{M_2}\right)^2 \tag{4-8}$$

where M_1 is the reading made by setting the voltage to +300 V and M_2 to +150 V, the constants a_0, a_1 and a_2 are given for pulsed radiation and for pulsed and swept radiation [35].
The corrected measurement of the dosimeter is given by the multiplication of the measurement obtained when the electrometer is configured to +300 V with all correction factors:

$$M_Q = M_1 \, k_{T,P} \, k_{pol} \, k_s \tag{4-9}$$

The final absorbed dose $D_{w,Q}$, for a reference depth z_{ref} is

$$D_{w,Q} = M_Q \, N_{D,w,Q_0} \, k_{Q,Q_0}, \tag{4-10}$$

where k_{Q,Q_0} is the correction factor for the quality of the radiation beam. This kind of factor k_{Q,Q_0} is different from the unit when the dosimeter used for the measurements is irradiated with a beam quality different from the quality of the beam that was calibrated.
Taking into account all previous corrections, for the model case the measurements reported in Table **4-15** were obtained and the respective absolute dose was reported in the penultimate column.

Parameters	**Electric charge** [nC]			**Dose**	**TSF**
	+300 V	-300 V	+150 V	[cGy]	
10×10 cm^2	1.950	1.976	1.947	76.48	0.999
P=76.21 kPa	1.951	1.973	1.944	75.59	1.00
T=17.1 ^{o}C	1.949	1.973	1.943	76.52	0.999

Table 4-15.: Absolute dose for a field size of 10×10 cm^2 and photon energy spectrum of 6 MeV.

An average dose of 76.53 cGy was obtained with a standard deviation of 0.058 cGy. In addition, the value calculated by the AAA algorithm for this case is 77.2 cGy, giving a percentage difference of 0.86 %; this small value gives a preliminary indicative that under reference conditions the algorithm works very well. The average of the Total Scatter Factor TSF calculated according to the Equation 3-4 and reported in Table **4-15** gives a value of 1 with a standard deviation of 7.6×10^{-4}. On the other hand, with the AAA algorithm, the respective TSF was calculated, having a value of 1, with a percentage difference respect to the experimental value of 0.0 % and taking into account the Table **4-12** it can be observed that this test has passed the TG-53 criteria.

Subsequently, absolute dosimetric tests were performed on an anthropomorphic and heterogeneous phantom designed taking into account the recommendations of the Task Group report 44 of the AAPM [45], in which they give a list of materials that are equivalent to some human tissues, with similar mass and electron densities, and, that were adopted in the current work for the equivalences in the tests to a phantom of thorax.

4.2.3. Absolute dosimetry test for anthropomorphic phantom

This test evaluates the ability of the AAA algorithm to calculate the absolute dose in the presence of heterogeneities such as the tissues substitutes of an average adult thorax: soft tissue (paraffin wax), lungs (cork) and spine (PVC). Eight points were evaluated: 3 in the soft tissue region, 4 in the lung and 1 in the spine, as can be seen in Figure **4-26**.

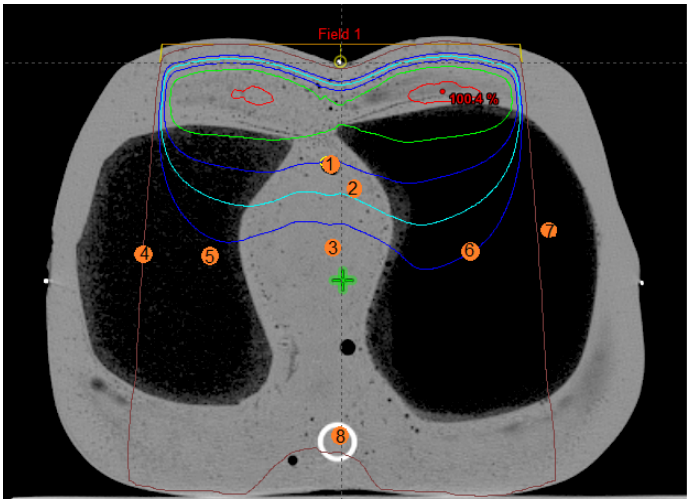

Figure 4-26.: Distribution of measurement points within the thorax phantom.

The measurements of the doses of the 8 points were made using a Pin Point ionization chamber, which due to its small volume is suitable for this type of measurements. In Figure **4-27** we can see the experimental setup used to obtain the absolute dose values.

(a) (b)

Figure 4-27.: Experimental setup for the measurement of the absolute dose in the thorax phantom.a) View of the phantom place on the table of the linear accelerator and b) the phantom with its holes and the ionization chamber.

Measurements were obtained for the two available photon energies of the linear accelerator, fixed SSD= 100 cm, with a field size of $20 \times 12\ cm^2$, MU=100, and the absolute dosimetry was performed in the same way as was done for the water phantom.
After obtaining the absolute dose value with their respective corrections, each value obtained is compared with that calculated by the algorithm, which requires a treatment planning on the CT images of the thorax phantom with the aforementioned configurations. This comparison was made by the following equation:

$$\%\ Dose_{difference} = 100 \times \frac{Dose_{meas} - Dose_{AAA}}{Dose_{meas}} \tag{4-11}$$

For example, radiating with photon energy spectrum of 6 MeV for point 1 an absolute dose of 82.73 cGy was measured and using the TPS Eclipse the absolute dose calculation of the AAA algorithm of 83.3 cGy was obtained, and applying the above equation gives a percentage difference of -0.68 %.

5. Results and Discussion

In order to evaluate the dosimetric accuracy of the AAA algorithm version 11.0.31 of Eclipse, a set of specific tests were developed for a particular clinical center (Instituto de Oncología Carlos Ardila Lulle of Fundación Santa Fe de Bogotá), which can be performed in any radiotherapy center that has a linear accelerator provided with MLC collimation system. Relative and absolute dosimetric tests were developed for the photon energy spectrums of 6 MeV and 15 MeV[1] taking into account different parameters that were later compared with the results obtained by the AAA algorithm. The algorithm was evaluated for parameters such as photon energy spectrum, field sizes, SSD surface-source distance, main collimator rotation, isocenter measurements, oblique incidences, beam asymmetries, MLC collimation system and its behavior in a heterogeneous and anthropomorphic tissue.

5.1. Relative dosimetry tests for photon energy spectrum of 6 MeV

The following results are related to the 8 tests reported in Table **4-11** for a complete relative dosimetry, taking into account the real scope of each one in the evaluation of the dose distribution in both directions: in-plane and cross-plane, as well as its distribution in depth. For each test is stated the purpose to realize it, and in what way this one evaluates to the AAA photon dose calculation algorithm.

5.1.1. Test 1: Open square fields

The purpose of this test is to assess the ability of the AAA algorithm to reproduce dose distributions in configurations similar to those used to measure initial input data. In this test 3 sizes of square fields were selected: 5×5, 10×10 and 25×25 cm^2, without any tilt of the gantry and at a distance SSD = 100 cm, no beam modifiers were used and measurements of radiation profiles were obtained centered in both direction in-plane an cross-plane in the aforementioned phantom of water. The measurements were performed at the depths mentioned in the model test.

Additionally the PDDs were measured and normalized to one for each of the fields and compared with those obtained by the planning system, they were compared point-to-point in the build-up

[1] In all the results when it is written photon energy spectrum 6 or 15 MeV refers to a large amount of photons of different energies been generated by interactions of electrons with kinetic energy of 6 or 15 MeV respectively.

region and the percentage of points that were within the tolerance range described by The Task Group Report 53.

5.1.1.1. Field size: 5 × 5 cm^2

From the model test, the same analysis was performed for the profiles of the radiation beam of the field size and photon energy specified, at all depths required, the calculated fields and the measured ones can be observed in Figure **5-1**, where the graphs of the left column are those calculated by the AAA algorithm and those of the right the measured ones.

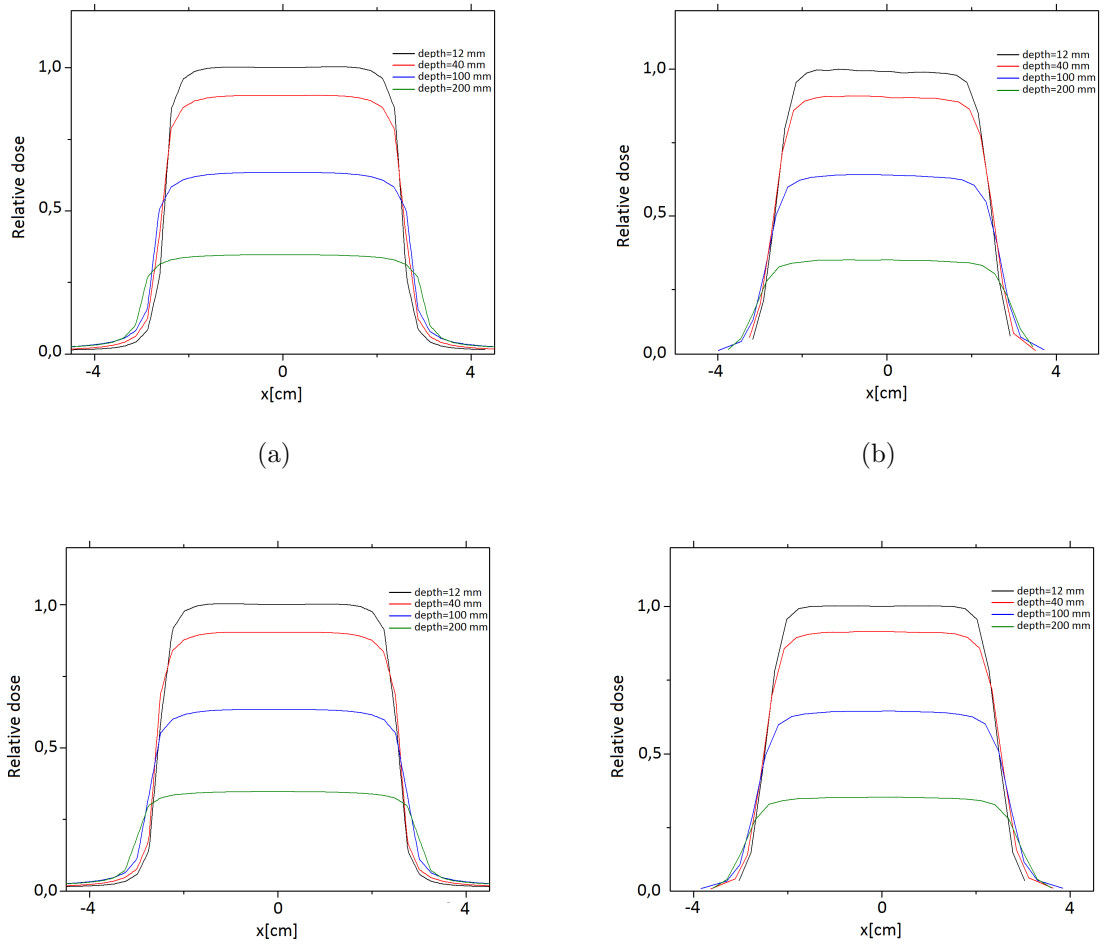

Figure 5-1.: Radiation profiles of test 1: 5×5 cm^2 a) AAA cross-plane profile, b) measured cross-plane profile, c) AAA in-plane profile and d) measured in-plane profile.

With a total of 16 profiles the comparative calculations were made between the profiles calculated by the AAA algorithm and the measured ones. The results obtained from this comparison, analyzed

the points of all the regions of the profiles could be extracted in the inner zone 96.9 % of the points that passed the test, for the zone of penumbra 94.8 % and for the outer zone only 7.4 % of the point have passed the TG-53 criteria.

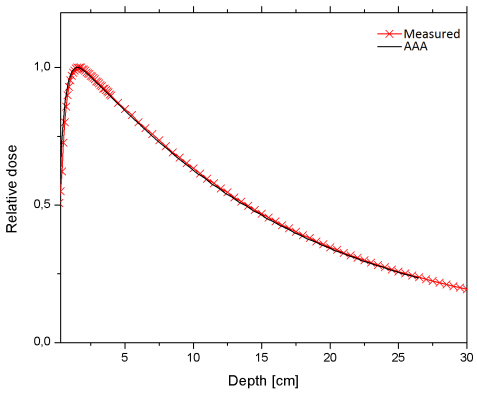

Figure 5-2.: Normalized PDD for test 1 with size field of 5×5 cm^2 and photon energy spectrum of 6 MeV.

For analysis of the PDD curves as can be seen in Figure **5-2** we compared 13 points of which all 13 passed the test, representing a 100 % concordance with TG-53 criteria. The maximum dose position was calculated at 16 mm from the surface by the AAA algorithm and experimentally found at 15 mm, with a difference of 6.25 %.

The results for the inner zone and penumbra are in agreement with the tolerance of TG-53, however in the outer zone, which was compared from the 5 % of the relative dose profile to 20 % and its results were much lower than expected, and this kind of results are recurrent for all the profiles compared of all the tests. Due to this result, it was analyzed in detail.

In Figure **5-3** a distribution of the percentage differences between measure values and values calculated by AAA algorithm for each position of the outer zone can be observed, and for the cross-plane direction in the 4 depths: 12, 40, 100 and 200 mm, having a respective average percentage difference[2] of -77.6 %, -33.6 %, -25.9 % and -13.49 %; showing that as the depth increases the lower the percentage of points that match the TG-53 criteria, but those points that do not pass the test do so with a smaller percentage difference. In order to be clear, some bar graphs in all this work only have the extreme values of the positions in each side of the umbra zone.

[2]The percentage differences are calculated taking the measured values as the theoretical values

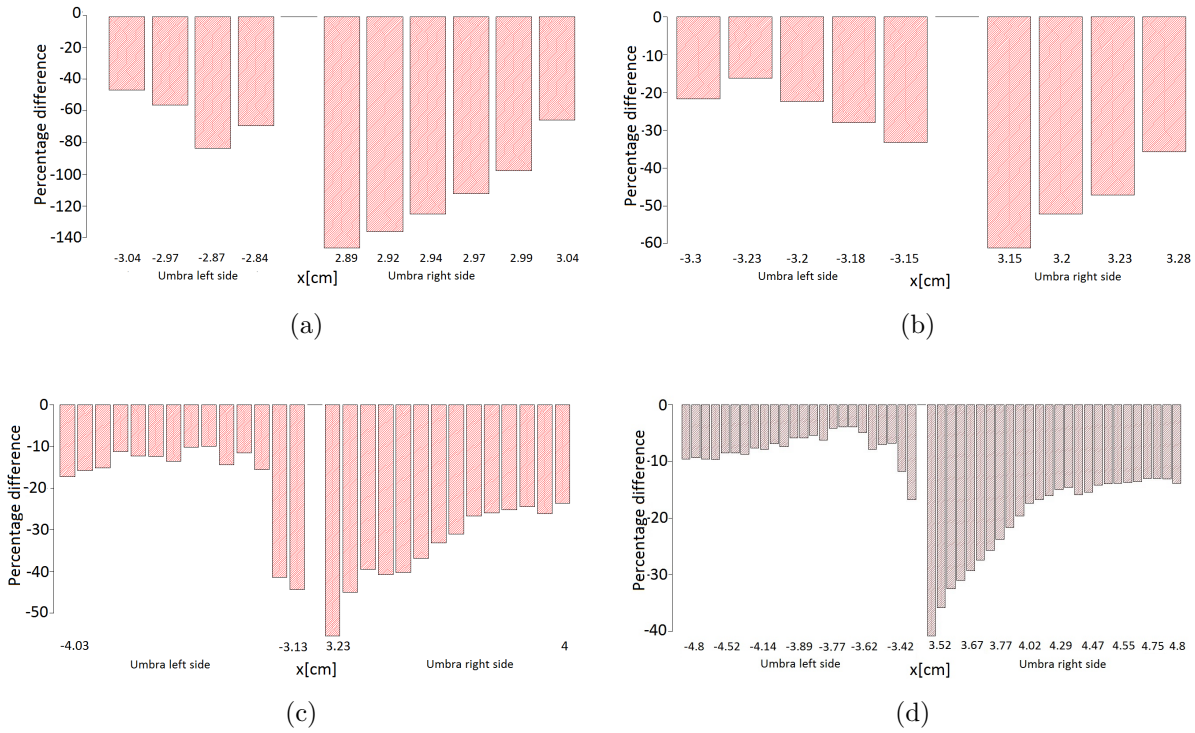

Figure 5-3.: Distribution of percentage differences from the outer zone for field size of 5×5 cm^2 in the cross-plane direction to the depths of: a) 12 mm, b) 40 mm, c) 100 mm and d) 200 mm.

In addition, the eight bar graphs (Figures **5-3** and **5-4**) show a negative percentage distributions for both the right and the negative side, which may mean that the AAA algorithm underestimates the calculation of the dose profile in this zone.

Cross-plane Depths [mm]	Mean percentage difference	**In-plane** Depths [mm]	Mean percentage difference
12	-77.6	12	-29.9
40	-33.7	40	-26.2
100	-25.9	100	-15.7
200	-13.5	200	-12.8

Table 5-1.: Mean percentage difference in the outer zone for each depth for 5×5 cm^2 field size.

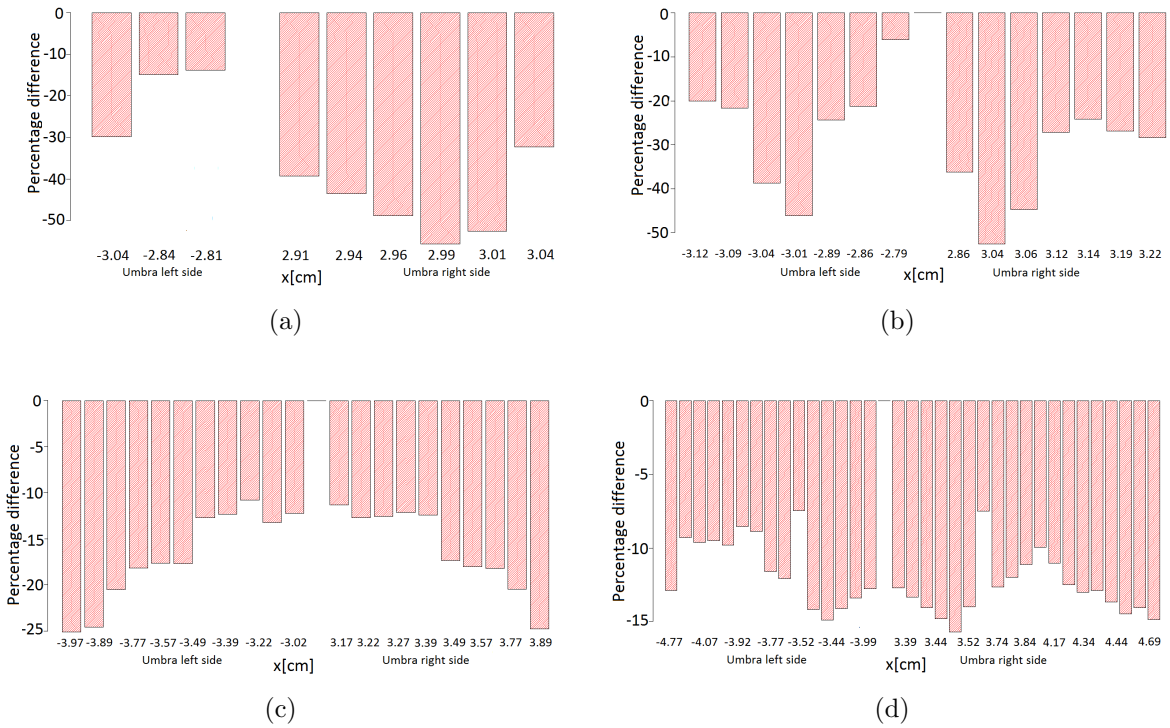

Figure 5-4.: Distribution of percentage differences of the outer zone for field size of 5×5 cm^2 in the in-plane direction to the depths of: a) 12 mm, b) 40 mm, c) 100 mm and d) 200 mm.

On the other hand, the percentage differences distribution shown in Figure **5-4** for the outer zone of the profiles compared in the in-plane direction shows a behavior similar to that seen in the cross-plane direction although with a little less percentage differences. Additionally, it can be observed that as the depth increases the number of points that do not pass the TG-53 criteria is greate. This is possible to see depending on the amount of bars in each picture because each bar represent a point in the outer zone of the profile that did not pass the test and has its respective percentage differences. Although those points do it with a smaller percentage difference.

5.1.1.2. Field size: 10 $\times$ 10 cm^2

For this part of the first test, a field size that use to be as a reference size for absolute and relative dosimetry in many protocols is evaluated. It is recommended to take into account its importance, monitoring the results of the dosimetric comparison profiles calculated by the AAA algorithm and the measured ones.

All the points of each profile were compared, the percentage of points that passed this test is divided in: the inner zone 96.5 % of the points passed the test, 92.8 % of the points in the zone of penumbra and 6.2 % of the outer zone passed the test. Due to the low amount of points in the outer zone passing the criterion TG-53, the distribution of errors in this area can be observed in Figures **5-7**

and **5-8**, in cross-plane and in-plane directions.

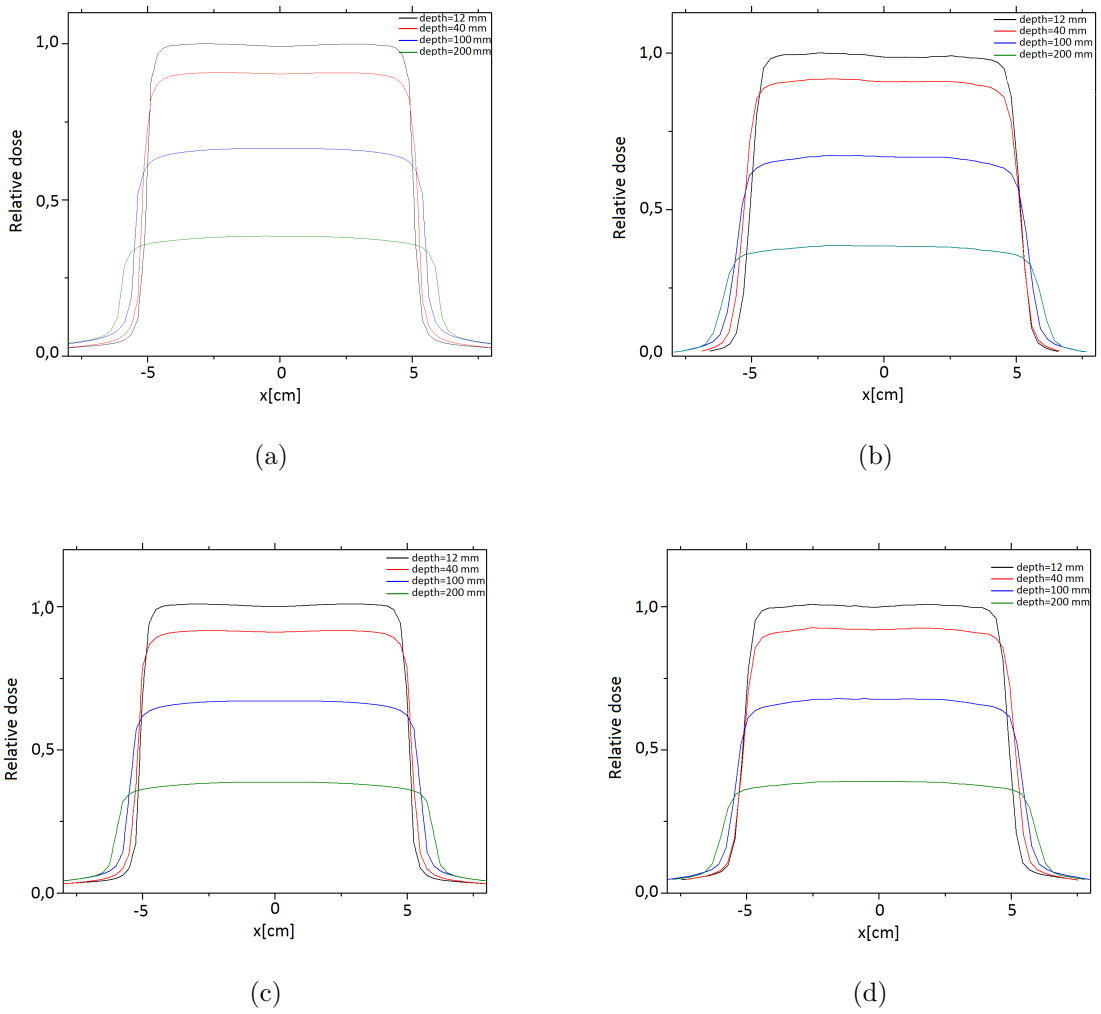

Figure 5-5.: Radiation profiles of test 1: 10×10 cm^2 a) AAA cross-plane profile, b) measured cross-plane profile, c) AAA in-plane profile and d) measured in-plane profile.

From this distribution of percentage differences can be observed that up to the depth of 100 mm the AAA algorithm overestimates the calculated dose in this zone, and in the depth of 200 mm it also does, but there are some points where it underestimates the calculation of the dose related to the measured values. As occurred for the 5×5 cm^2 field size part, as the depth increases, the number of points that do not pass the TG-53 criteria increase too, however they do with less percentage difference, in Table **5-2** it can observe this relation for both directions: cross-plane and in-plane. Although it is not a constant, can be seen a trend in almost all cases that as the depth increases the average percentage difference is smaller.

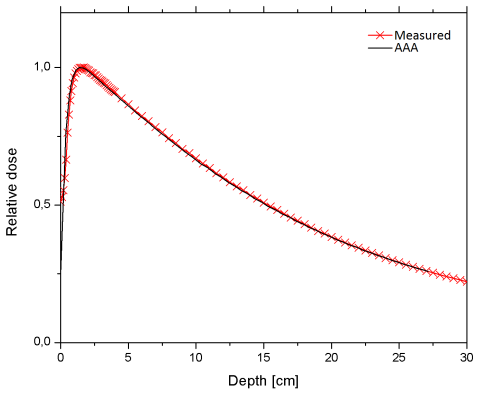

Figure 5-6.: Normalized PDD for test 1 with size field of 10×10 cm^2 and photon energy spectrum of 6 MeV.

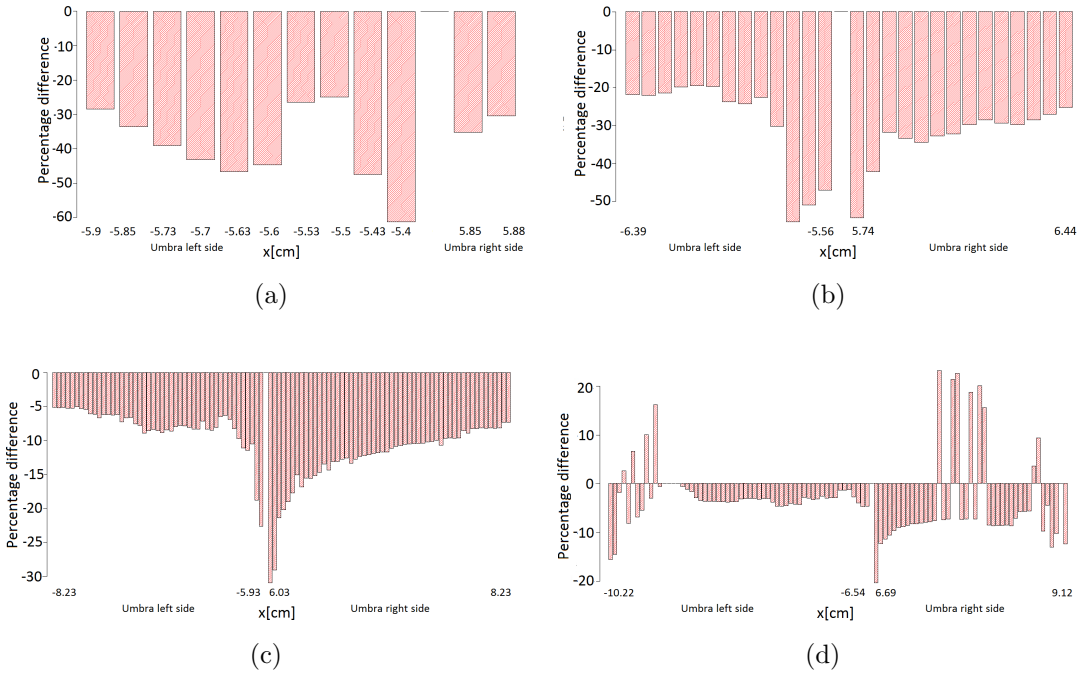

Figure 5-7.: Distribution of percentage differences from the outer zone for field size of 10×10 cm^2 in the cross-plane direction to the depths of: a) 12 mm, b) 40 mm, c) 100 mm and d) 200 mm.

Cross-plane Depths [mm]	Mean percentage difference	**In-plane** Depths [mm]	Mean percentage difference
12	-35.7	12	-23.4
40	-27.7	40	-18.2
100	-11.2	100	-11.5
200	-3.2	200	-5.8

Table 5-2.: Mean percentage difference in the outer zone for each depth for 10×10 cm^2 field size.

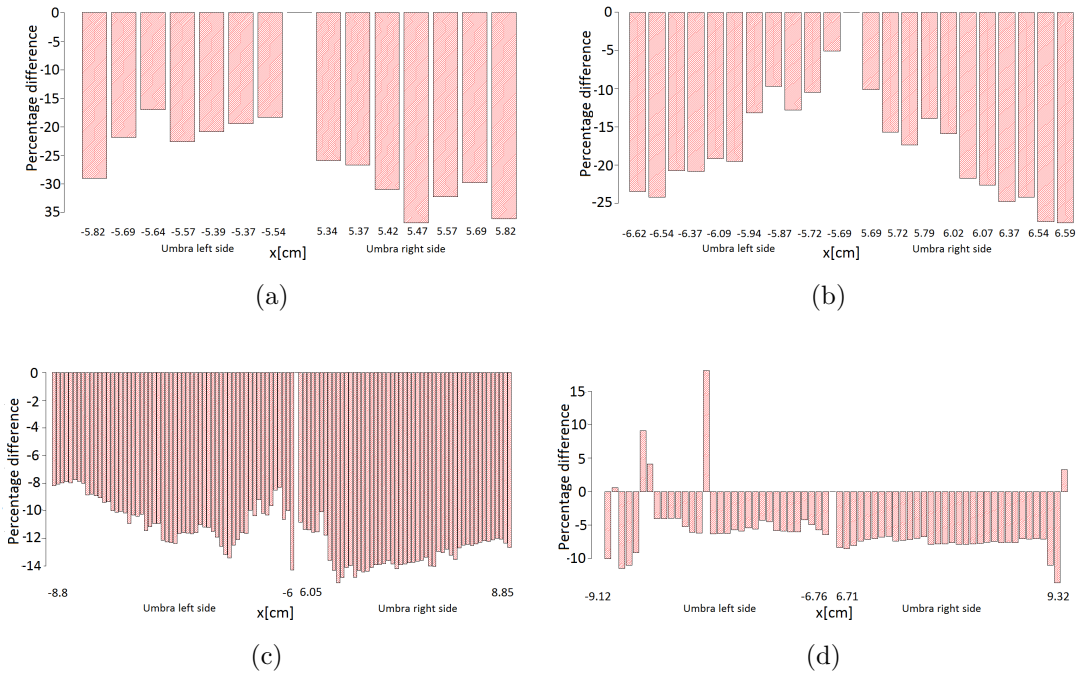

Figure 5-8.: Distribution of percentage differences from the outer zone for field size of 10×10 cm^2 in the in-plane direction to the depths of: a) 12 mm, b) 40 mm, c) 100 mm and d) 200 mm.

In the comparison of the two PDDs: measured and calculated, a complete agreement can be observed taking into account the criterion of comparison provided in the Task Group 53. All of the 11 points in the build-up zone compared are within the tolerance range and pass the test. The percentage difference between the depths of maximum dose is 1.44 %.

For this test, the evaluation criterion of PDDs, as reported by TG 53, has a tolerance of 20 % between the measured and the calculated by the algorithm. It means a very large tolerance and for

that reason all the points pass the test. In addition, it can be observed in Figure **5-6** that after the zone of build-up the same tendency of concordance is conserved than the zone evaluated.

5.1.1.3. Field size: 25 × 25 cm^2

In Figure **5-9** can be seen the dose profiles for the cross-plane and in-plane directions, for all suggested depths of the evaluation of the algorithm. The algorithm presents better performance in the calculation of the dose distributions for this field size in the inner and penumbra region than for the outer regions of the profile again.

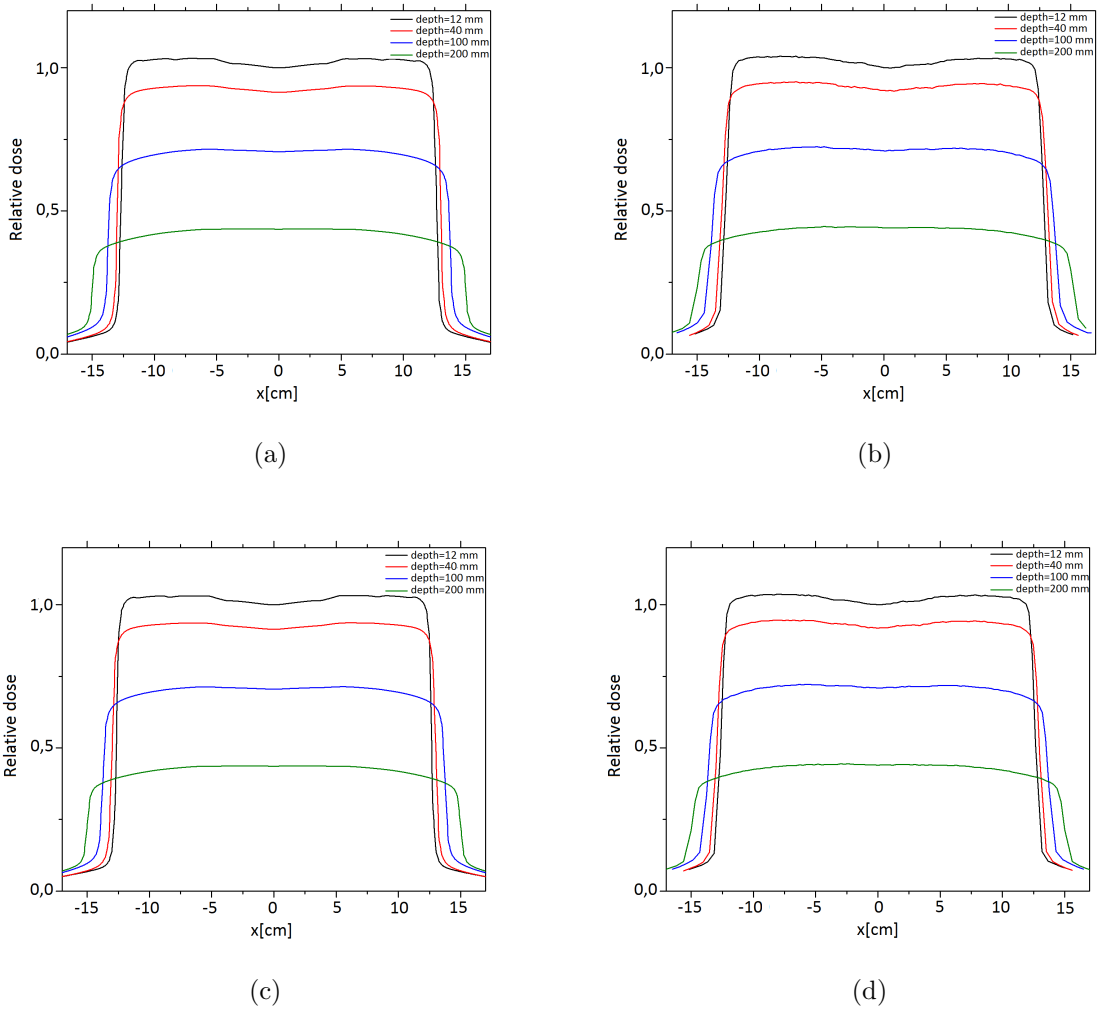

Figure 5-9.: Radiation profiles of test 1: 25×25 cm^2 a) AAA cross-plane profile, b) measured cross-plane profile, c) AAA in-plane profile and d) measured in-plane profile.

For this field size, the behavior of both cross-plane and in-planes profiles in the experimental part fits well in the inner zone, since 88.4 % of their points passed the test, whereas only 85.7 % of the

points in the penumbra zone passed the test and for the zone of umbra only 3.8 % of the points passed the test. Due to these results in the outer zone and for being an important test during the commissioning process, the analysis of percentage differences is performed.

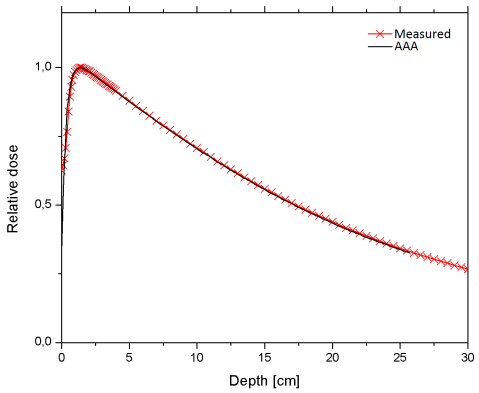

Figure 5-10.: Normalized PDD for test 1 with size field of 25×25 cm^2 and photn energy spectrum of 6 MeV.

The agreement decreases with increasing field size for this first test in the photon energy spectrum of 6 MeV, which can be abstracted by reducing the percentage of points passing the test in each zone for this field size. Another behavior was observed, as with the field size 10×10 cm^2 occurred, it was that as the depth increases, the mean of the percentage difference decreases, although the number of points that do not pass the test are higher as it can see in Table **5-3**. For this test it was also observed that the agreement between the measured and the planned is slightly higher in the in-plane direction.

Cross-plane Depths [mm]	Mean percentage difference	**In-plane** Depths [mm]	Mean percentage difference
12	-21.6	12	-18.3
40	-16.8	40	-11.5
100	-11.9	100	-7.3
200	-10.9	200	-6.2

Table 5-3.: Mean percentage differences in the outer zone for each depth for 25×25 cm^2 field size.

In Figures **5-11** and **5-12** that represents the distribution of percentage differences for the outer zone in which it is seen that there is an underestimation in calculation of the dose in this region

again. On the other hand, the maximum dose depth calculated by the AAA algorithm is 1.37 cm and the experimental depth is 1.4 cm, with a difference of 2.14 %. 100 % of the 11 points pass the test, which is easily achieved since the tolerance value for this region is 20 %.

Test 1, represented by the three square field sizes for the photon energy spectrum of 6 MeV, can be summarized as following: in the inner region 91.5 % of the points pass the test, in the penumbra region 90.1 % of the points, in the outer region only 5.4 % of the points pass and finally, in the build-up region 100 % of the compared points pass the test according to Task Group 53. The results for the whole test 1 can be observed in Table **5-4**.

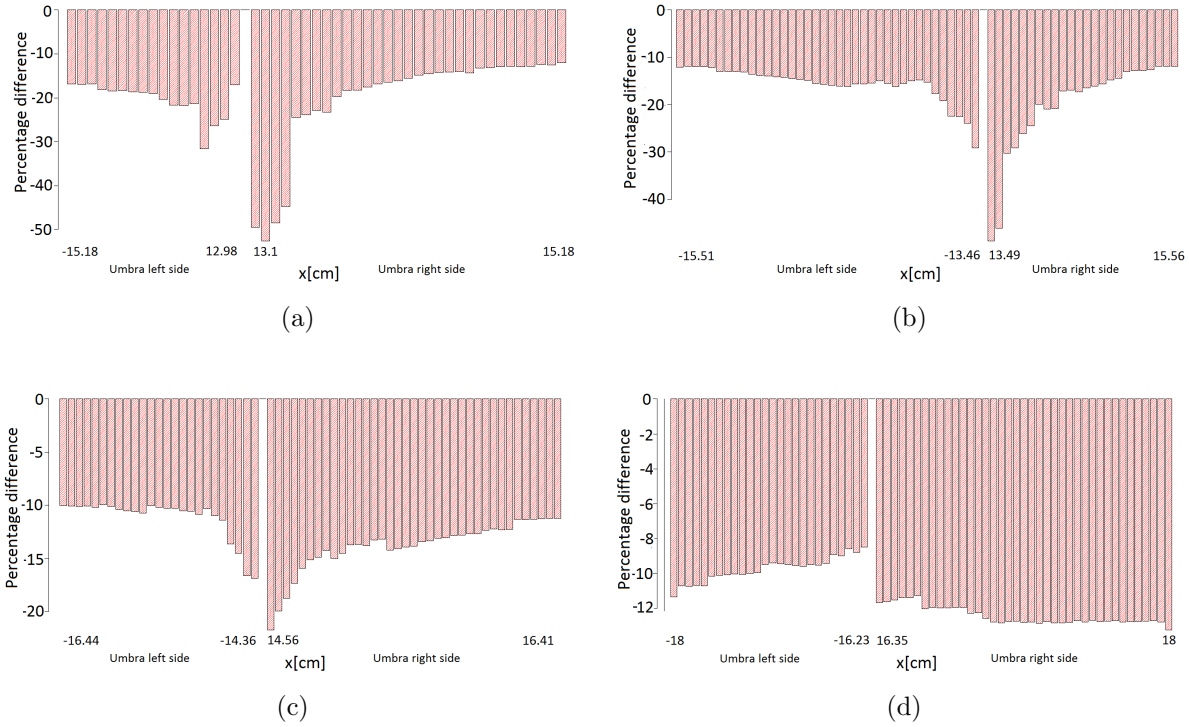

Figure 5-11.: Distribution of percentage errors from the outer zone in the cross-plane direction to the depths of: a) 12 mm, b) 40 mm, c) 100 mm and d) 200 mm.

The results reported in Table **5-4** can be attributed to possible changes over time in the TPS input data used during the commissioning stage and that will be explained at the end of the analysis of all tests. However, the data compared to be part of the commissioning data and that the AAA algorithm is calculating the dose values larger than what is measured in the outer zone, it could indicate that in the 3D-CRT treatments the doses being received by the organs at risk are being overestimated by the algorithm. Solving this problem is possible to have higher dose coverage in the PTV and at the same time complying with the constrains for the organs at risk (OAR).

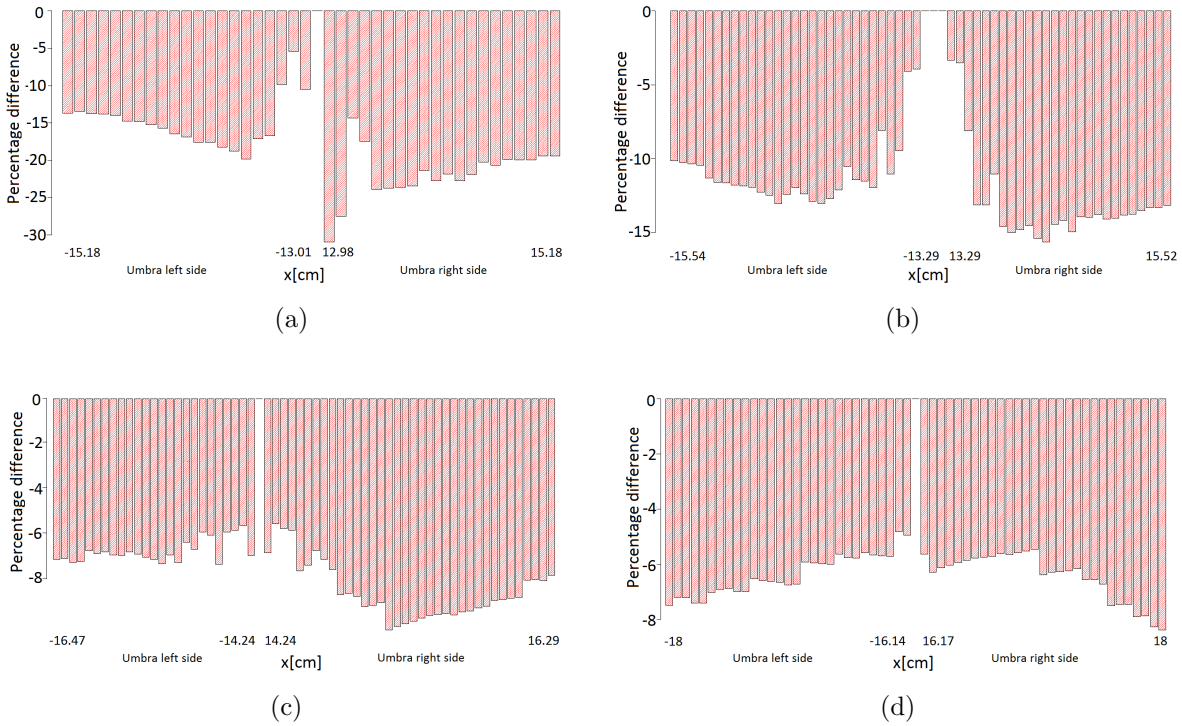

Figure 5-12.: Distribution of percentage differences from the outer zone in the in-plane direction to the depths of: a) 12 mm, b) 40 mm, c) 100 mm and d) 200 mm.

Results reported for this test by Gifford et al. [27] found that for the field size of 25 × 25 cm^2 beyond the positions of ±13.6 cm no point passed the TG-53 criteria. This position is located in a part of the outer zone, depending on how large this area is taken the results vary significantly. In the present work the outer zone was taken from 5 % to 20 % of the relative dose.

Region of the beam	% Points pass the TG-53
Inner	91.5
Penumbra	90.1
Outer	5.42
Build-up	100

Table 5-4.: Results of the comparison between measured and AAA calculated points for the test 1 for each beam profile region.

5.1.2. Test 2: Extended SSD square fields

The purpose of this test is to verify the ability of the AAA algorithm to predict the increase of the width of the penumbra with the change of the depth. The characteristics of this test that differ from the previous one mainly is to set a distance SSD = 125 cm for two sizes of fields: 8×8 and 20×20 cm^2. The profiles were obtained at the respective depths for photon energy spectrum of 6 MeV.

5.1.2.1. Field size 8×8 cm^2

For this test, profiles were measured in both direction: in-plane and cross-plane, and comparing the measured values with the AAA calculated we can verify that they are in agreement for the profiles in the depths of 12 mm and 40 mm, for the last two depths the calculation made by the AAA algorithm differs from the measured ones in the inner region. For the outer region the results are more unfavorable and will be analyzed later.

The comparative points produced the following result: in the inner zone 91.1 % of them passed the test, in the penumbra 98.0 % and 5.8 % for the outer zone. These results show that this algorithm presents great agreement with the measured values in the penumbra zone which is the region being evaluated in this test.

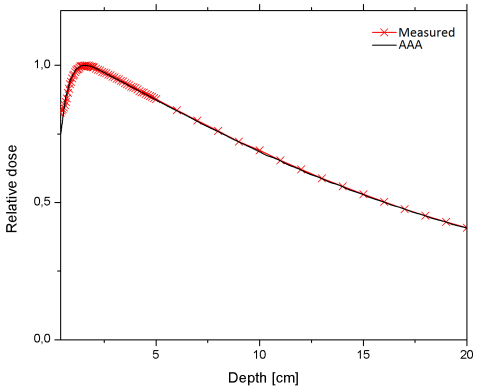

Figure 5-13.: Normalized PDD for test 2 with size field of 8×8 cm^2 and photon energy spectrum of 6 MeV.

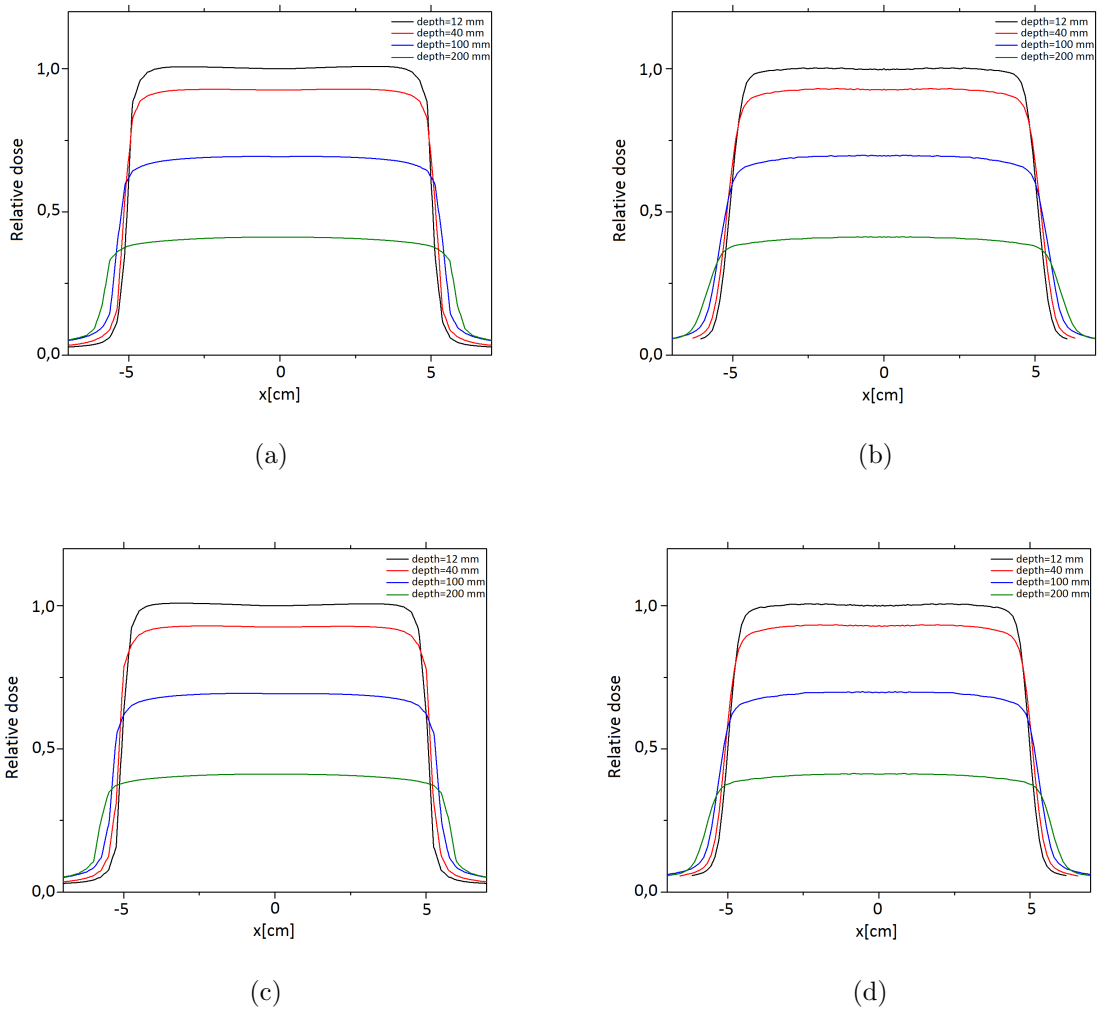

Figure 5-14.: Radiation profiles of test 2: 8×8 cm^2 a) AAA cross-plane profile, b) measured cross-plane profile, c) AAA in-plane profile and d) measured in-plane profile.

The percentage differences distributions for the outer zone for the direction of cross-plane (Fig. **5-15**) show that these differences are greater in the vicinity of the penumbra zone for the 4 depths, whereas for the in-plane direction (Fig. **5-16**)the opposite behavior occurs and the percentage differences are higher as it moves away from the penumbra zone.

Regarding the analysis in the comparison of the PDDs, it is observed that the 100 % of the points compared in the build-up area pass the test, 27 points compared 27 passed the test. The maximum dose depth calculated was 1.63 cm and the experimental depth was 1.65 cm, giving a percentage difference of 1.22 %. It can be observed in Figure **5-13** the values calculated by AAA algorithm agree with the measured values even after the zone of build-up that is only recommended to analyze in Task Group 53.

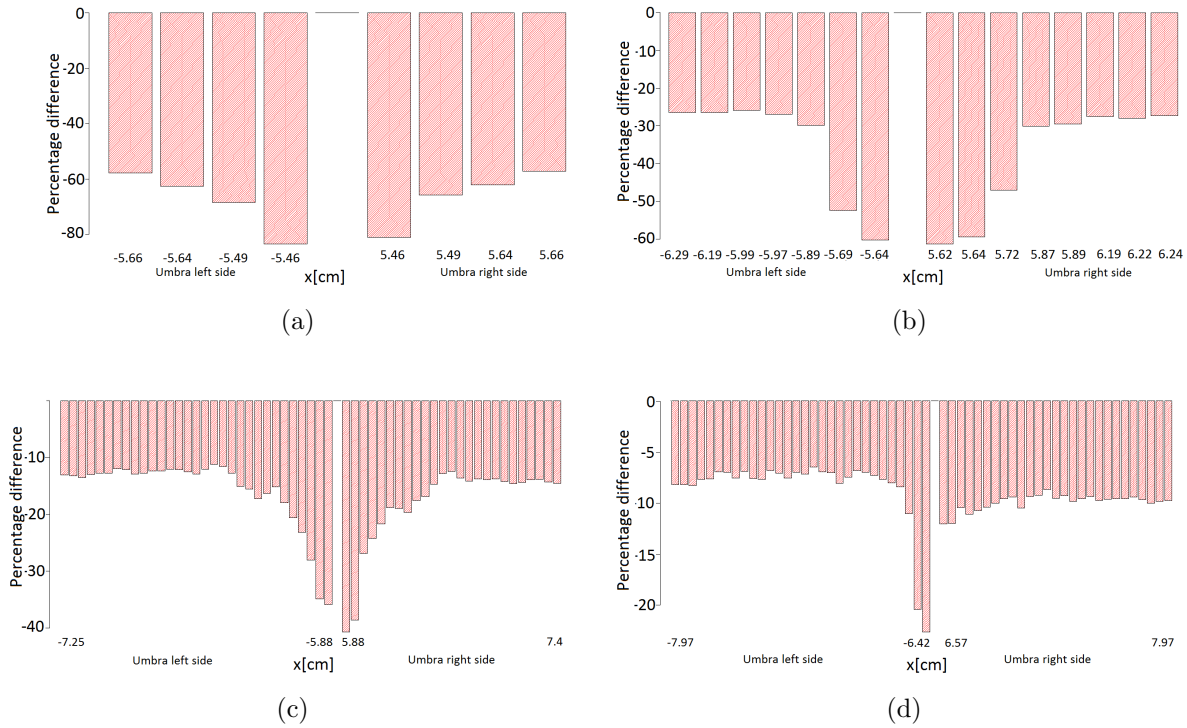

Figure 5-15.: Distribution of percentage differences from the outer zone in the cross-plane direction to the depths of: a) 12 mm, b) 40 mm, c) 100 mm and d) 200 mm.

Cross-plane Depths [mm]	Mean percentage difference	**In-plane** Depths [mm]	Mean percentage difference
12	-52.9	12	-24.6
40	-37.6	40	-17.2
100	-18.4	100	-14
200	-8.2	200	-7.4

Table 5-5.: Mean percentage differences in the outer zone for each depth for 8×8 cm^2 field size.

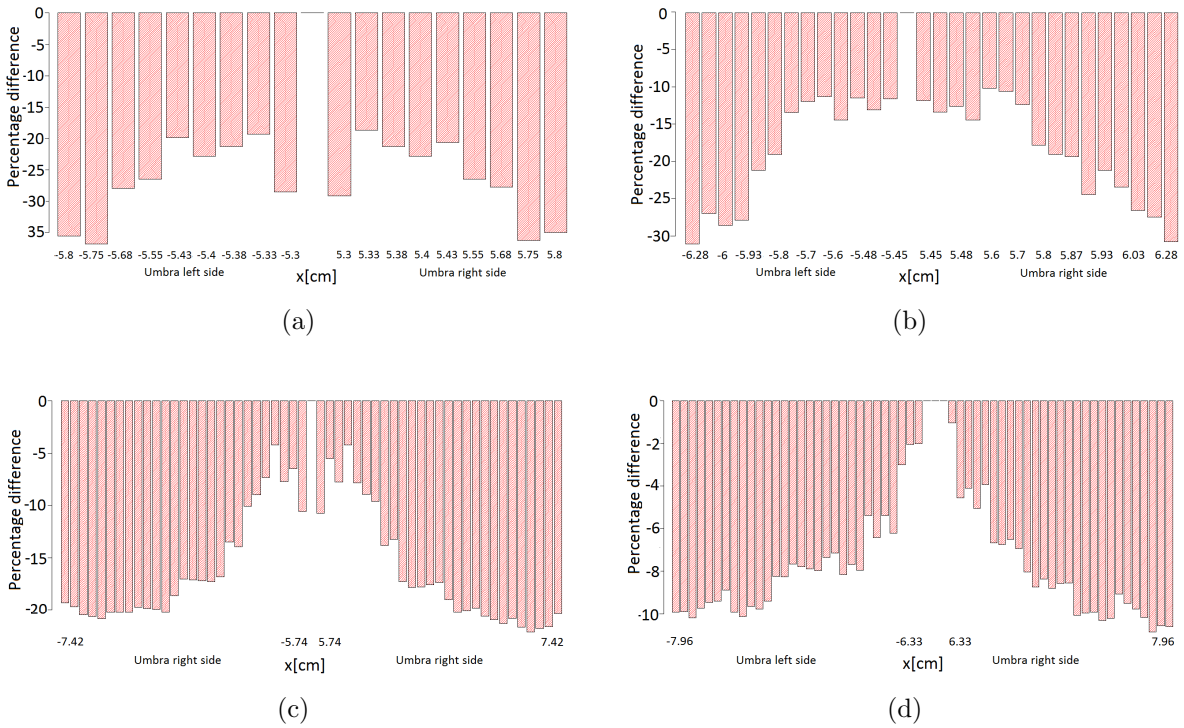

Figure 5-16.: Distribution of percentage differences from the outer zone in the in-plane direction to the depths of: a) 12 mm, b) 40 mm, c) 100 mm and d) 200 mm.

5.1.2.2. Field size 20 $\times$ 20 cm^2

In addition, it is performed for a larger field size, maintaining the same distance SSD = 125 cm, to evaluate the change of the penumbra with respect to the depth but with a greater field of radiation.

The results of the comparison show that 83.5 % of the points pass the test in the inner zone, while for the most important area to evaluate that it is the penumbra, 77.3 % of the points pass and for the outer region 1.1 % of the points pass. These results show that for a greater SSD distance and a large field size the algorithm is less accurate comparing to the measured values in the penumbra zone, and in the outer zone is also affected since it is much less accurate than for the previous field size. It was observed that in the penumbra zone, as the depth increased, the concordance between the measured and calculated points decreased.

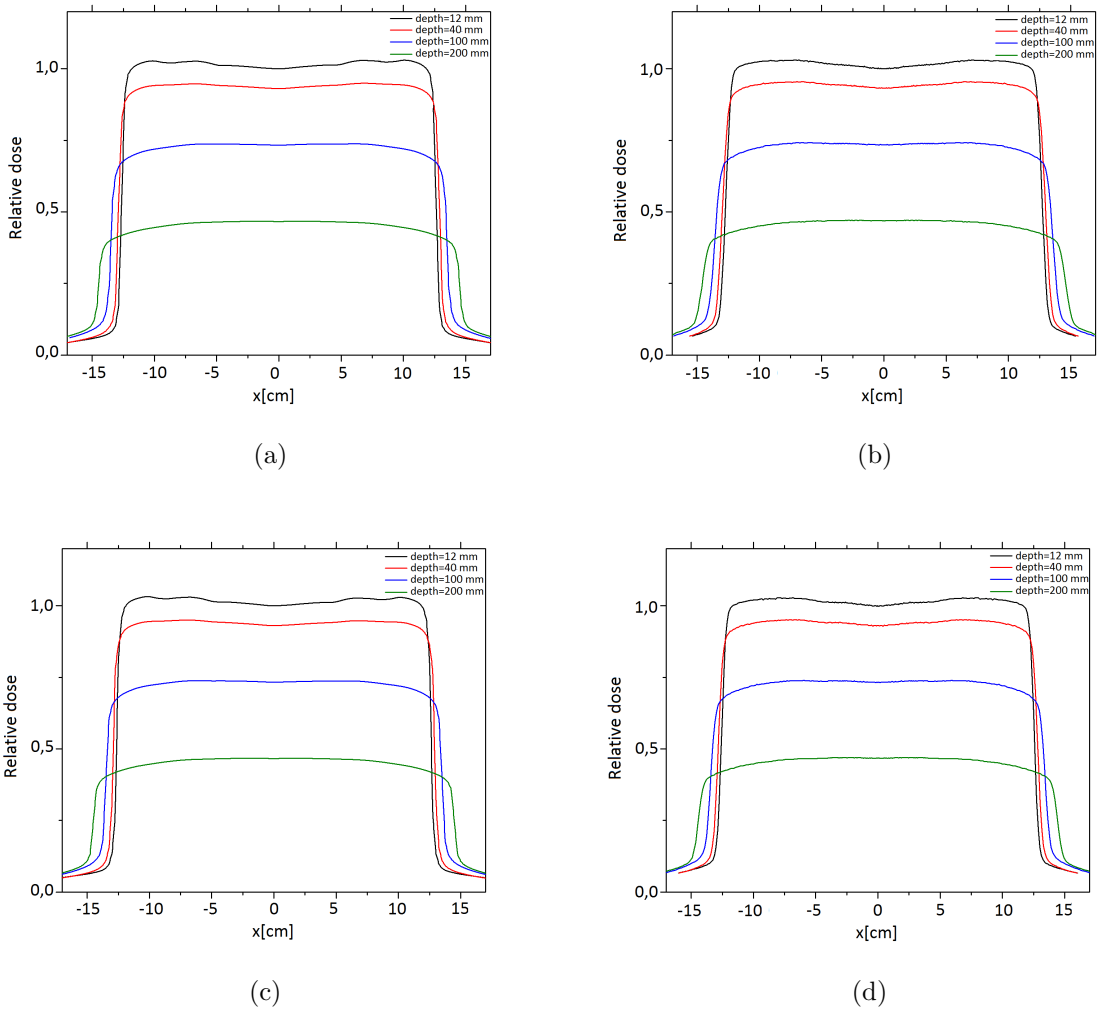

Figure 5-17.: Radiation profiles of test 2: 20×20 cm^2 a) AAA cross-plane profile, b) measured cross-plane profile, c) AAA in-plane profile and d) measured in-plane profile.

The results reported in Tables **5-6** and **5-5** show that increasing the SSD distance and depth, the mean values of percentage differences decrease, although the number of compared points that fail the TG-53 criteria are larger. Additionally, in both tables it can be seen that the results in in-plane direction are better than those in cross-plane direction for this zone.

The comparison of both PDDs, the measured points with the calculated ones gave a result of 22 points that pass the test, this amount represents 100 % of the points. The calculated maximum dose depth is 1.37 mm and measured at 1.4 mm, with a difference of 2.2 %. As in the previous configuration the good match of the two curves after the build-up region can be observed.

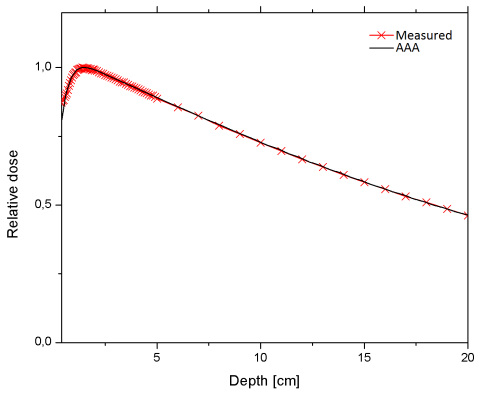

Figure 5-18.: Normalized PDD for test 2 with size field of 20×20 cm^2 and photon energy spectrum of 6 MeV.

The total results for both sizes of radiation fields, for the photon energy spectrum of 6 MeV it was possible to obtain that 85.7 % of the points of the inner zone passed the test, 85.8 % of the points of the zone of penumbra, 2.2 % of the points of the outer zone passed the test and in the zone of build-up 100 % of the points.

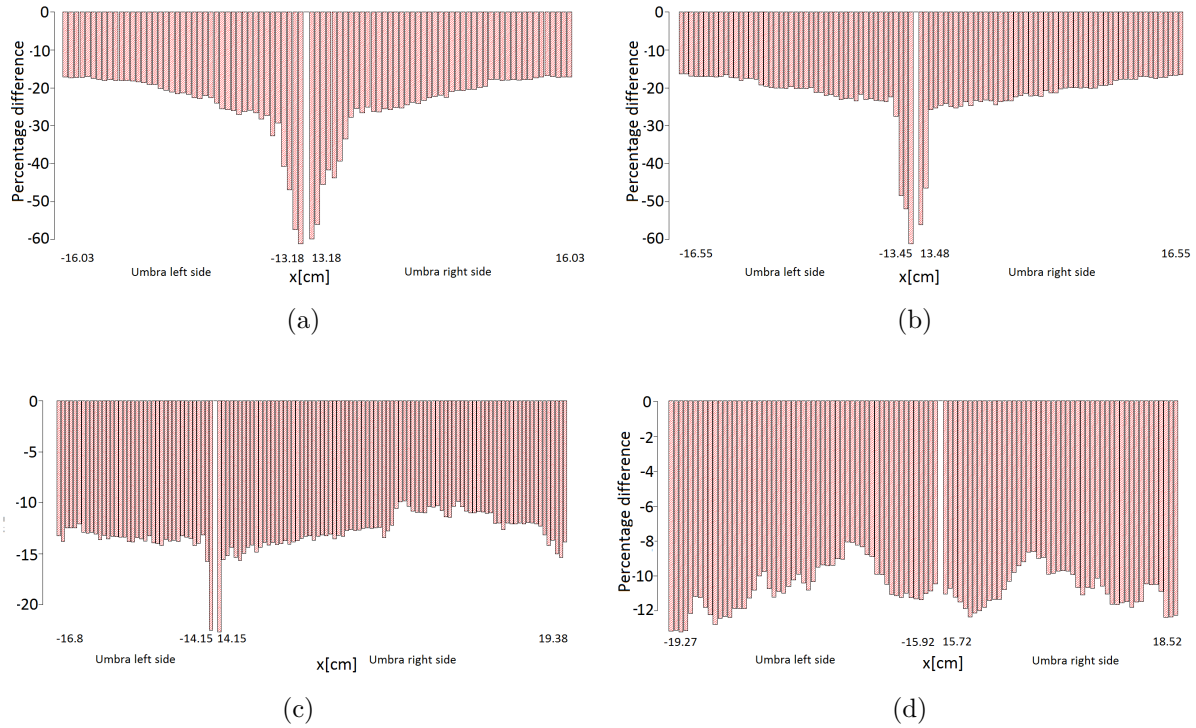

Figure 5-19.: Distribution of percentage differences from the outer zone in the cross-plane direction to the depths of: a) 12 mm, b) 40 mm, c) 100 mm and d) 200 mm.

Cross-plane Depths [mm]	Mean percentage difference	**In-plane** Depths [mm]	Mean percentage difference
12	-27	12	-18.0
40	-21.7	40	-15.0
100	-12.9	100	-10.0
200	-10.8	200	-10.2

Table 5-6.: Mean percentage difference in the outer zone for each depth.

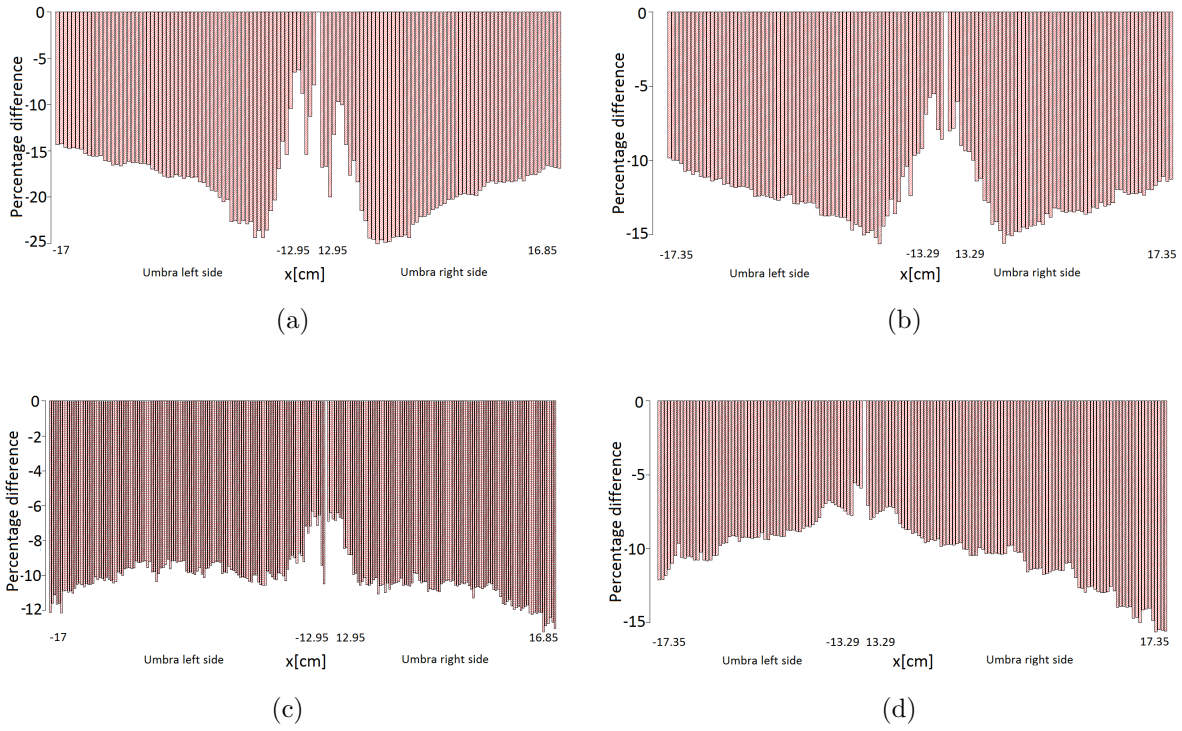

Figure 5-20.: Distribution of percentage differences from the outer zone in the in-plane direction to the depths of: a) 12 mm, b) 40 mm, c) 100 mm and d) 200 mm.

The results of the comparisons in the outer zone for the two field sizes show that by increasing the SSD distance the concordance between the algorithm and the measured points in the three zones of the profile: inner, penumbra and outer, although for the field size of 8x8 the results show greater accuracy in the area to be evaluated. In addition, analyzing the graphs of the figures **5-20** and **5-16** we can observe that for the two field sizes the algorithm is more accurate in calculations in the in-plane direction. The results for the whole test 2 are summarized in Table**5-7**.

Region of the beam	% Points pass the TG-53
Inner	85.7
Penumbra	85.8
Outer	2.2
Build-up	100

Table 5-7.: Results of the comparison between measures and AAA algorithm calculated points for the test 2 for each beam profile region.

5.1.3. Test 3: Rectangular fields

This test evaluates the algorithm's ability to calculate dose distributions on elongated rectangular surfaces. This test is performed for two different field sizes, 5×25 and 25×5 cm^2, with a distance SSD = 100 cm and at gantry angle and collimator of 0°, comparisons of the profiles of the radiation beam are made for each four depths.

5.1.3.1. Field size 5×25 cm^2

The profiles to be evaluated in the two directions: cross-plane and in-plane for the 4 depths are shown in Figure **5-22**. The field sizes were fixed as follows: X= 5 cm and Y= 25 cm in the linear accelerator console, this arrangement as it will see later influences the matching of the points calculated by the AAA algorithm and the measured ones.

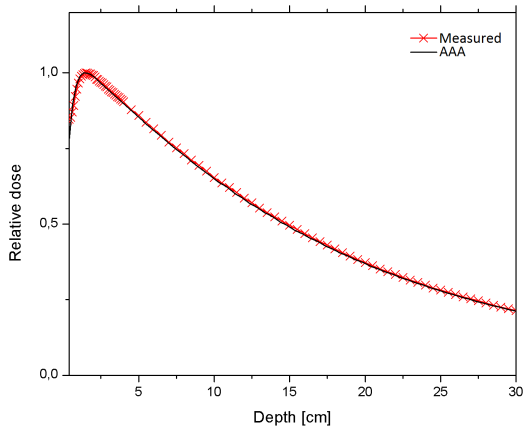

Figure 5-21.: Normalized PDD for test 3 with size field of 5×25 cm^2 and photon energy spectrum of 6 MeV.

The results of this test show a great performance of the algorithm for the calculations of rectangular distributions. 96 % of all points passed the test in the inner zone, highlighting the results in

penumbra zone since in both cross-plane and in-plane directions: 100 % of the points have passed the test.

For the outer zone, the results are better than in the previous test, however only 17.3 % of the compared points passed the criterion TG-53. In Test 1 it was mentioned that the greater agreement occurs for in-plane direction and this is due to the a larger profiles are obtained in this direction and therefore contribute more points in the comparisons.

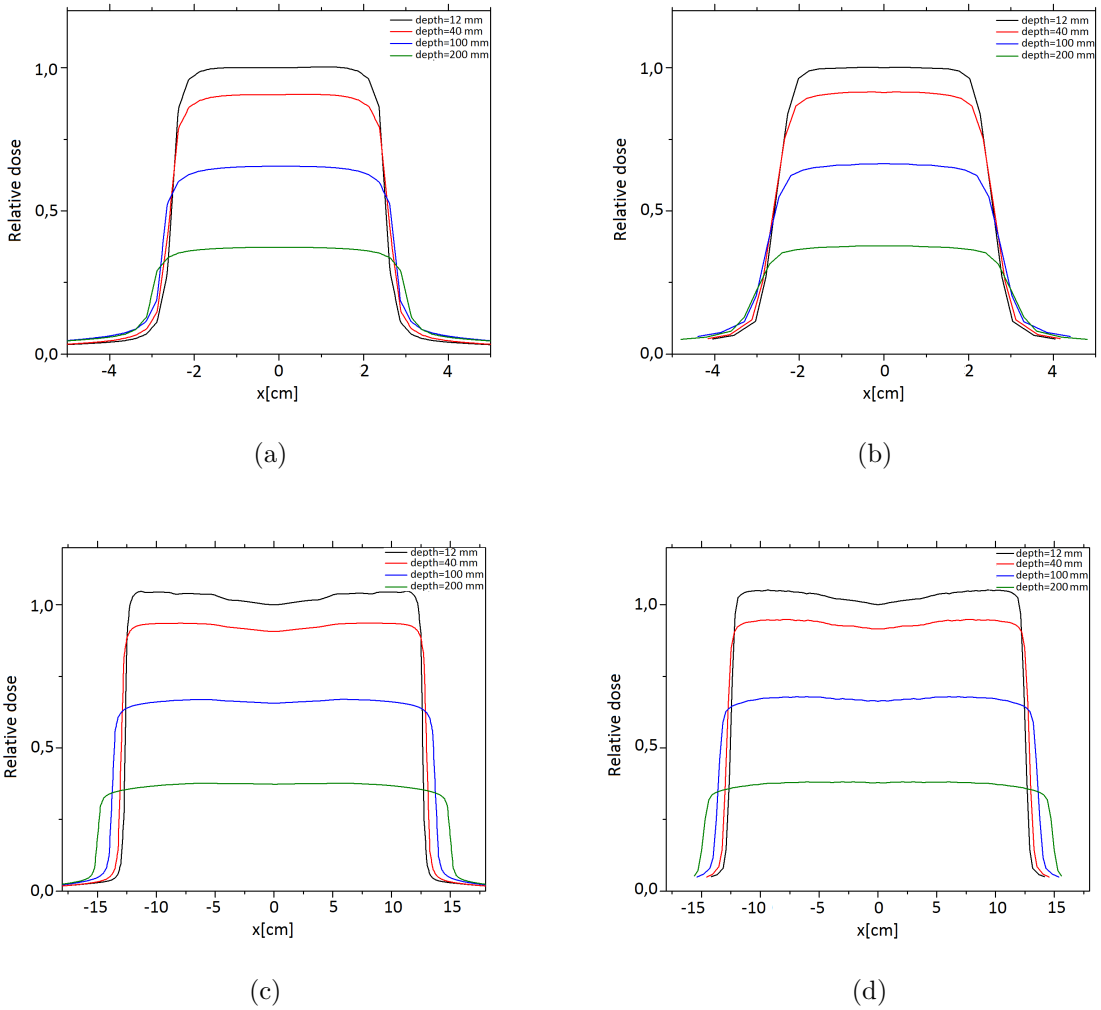

Figure 5-22.: Radiation profiles of test 3: 5×25 cm^2 a) AAA cross-plane profile, b) measured cross-plane profile, c) AAA in-plane profile and d) measured in-plane profile.

The evaluation for the profiles for the outer zone in the cross-plane direction show a greater number of points that do not pass the criteria of the TG-53, with a greater percentages differences near the penumbra zone, all the points that do not pass this criterion in the umbra region present an

overestimation in the calculation of the dose distribution.

The percentage differences distributions for the outer area for in-plane direction (see Figure **5-24**) can be seen for the deeper profiles, the amount of points that do not pass the TG-53 criteria is higher; and for the depths of 40, 100 and 200 mm are underestimated in the calculation of the dose in the vicinity of the penumbra area and as it moves away from this area an overestimation of the dose calculation is presented. In this manner, this overestimation is related to comparison made between the AAA algorithm values and the measured ones.

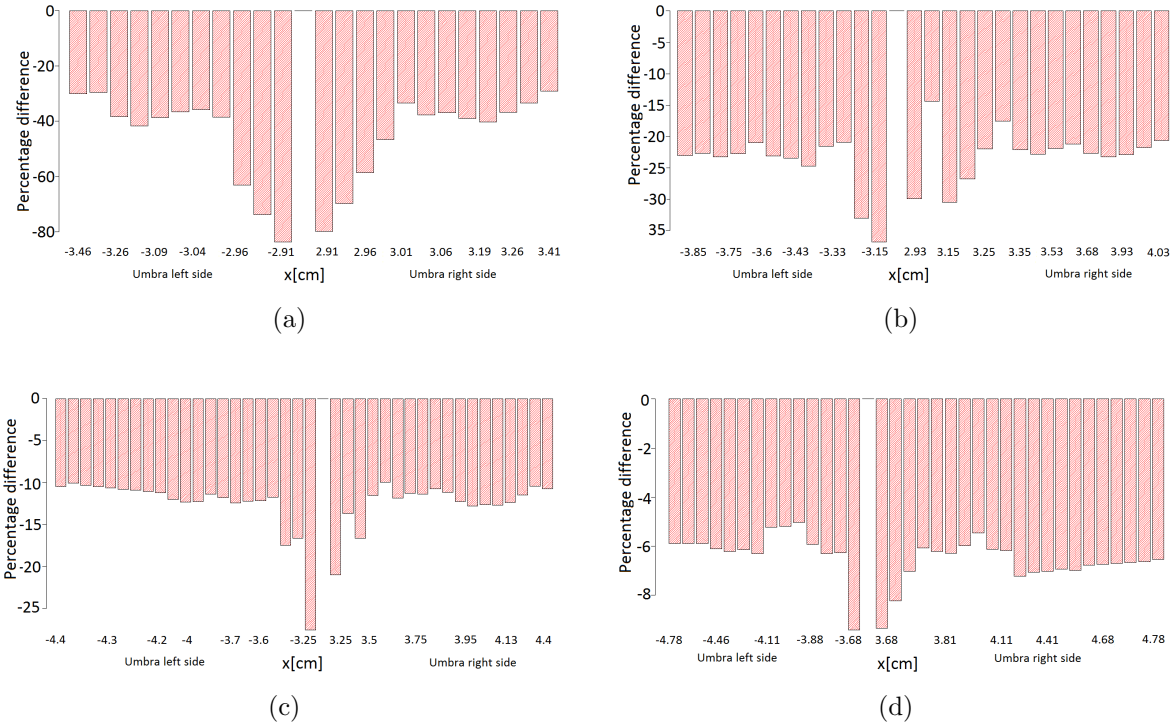

Figure 5-23.: Distribution of percentage differences from the outer zone in the cross-plane direction to the depths of: a) 12 mm, b) 40 mm, c) 100 mm and d) 200 mm.

Cross-plane Depths [mm]	Mean percentage difference	**In-plane** Depths [mm]	Mean percentage difference
12	-41.9	12	-7.3
40	-21.9	40	-6.9
100	-11.9	100	-9.4
200	-6.2	200	-2.6

Table 5-8.: Mean percentage differences in the outer zone for each depth.

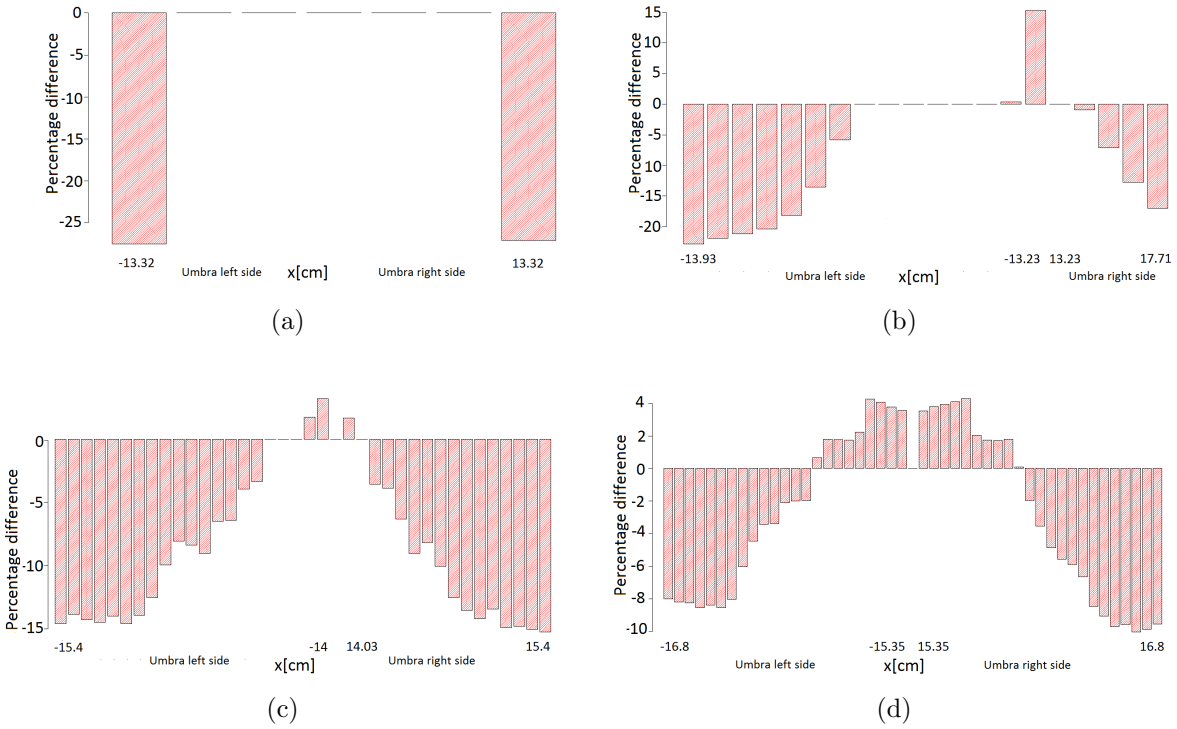

Figure 5-24.: Distribution of percentage differences from the outer zone in the in-plane direction to the depths of: a) 12 mm, b) 40 mm, c) 100 mm and d) 200 mm.

In the comparison of the PDDs it could find that 100 % of the 11 points evaluates in the build-up area pass the test. The comparison of the depths of maximum dose between the measured and the calculated by the algorithm is of 9.48 %. The reason why the excellent result in the comparison is because of the high tolerance value in the TG-53.

5.1.3.2. Field size 25 × 5 cm^2

In the second part of test 3, the field size is set as: X = 25 cm and Y = 5 cm, as in the first part, the profiles are compared in both directions and at four depths as can be observed Figure **5-25**. The results differ from the previous one because of the amount of compared points in longer side of the profile in each case.

The results of the second part of this test show less agreement between the measured and calculated profiles. In the inner zone 93.8 % of the compared points passed the TG-53 criteria, in the penumbra zone 93.3 % and finally in the outer zone only the 6.6 % of the points passed the test.

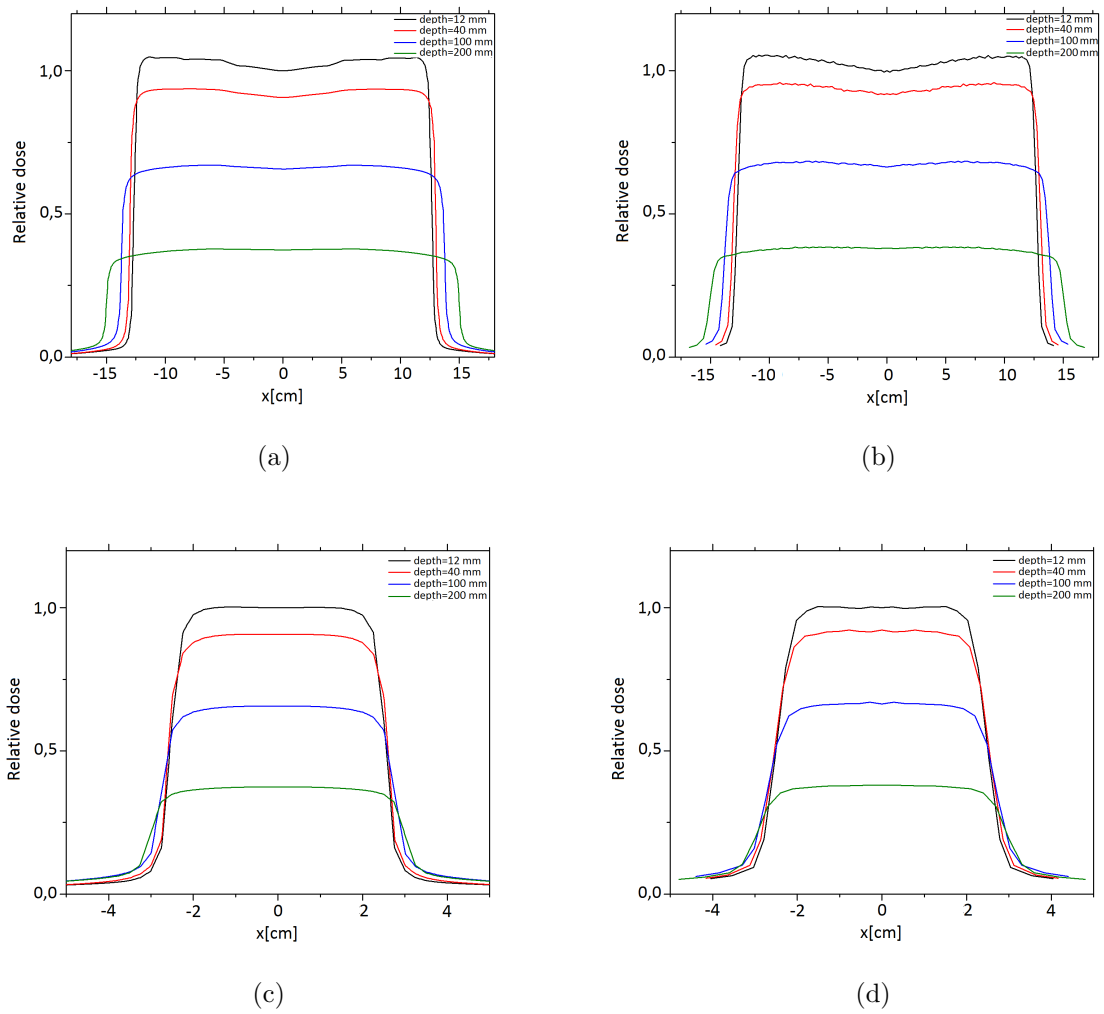

Figure 5-25.: Radiation profiles of test 3: 25×5 cm^2 a) AAA cross-plane profile, b) measured cross-plane profile, c) AAA in-plane profile and d) measured in-plane profile.

The percentage of points that pass the test are lower for the second part of the test, and this is due to a possible assumption that the algorithm calculates better in in-plane direction than cross-plane, and in this direction there are fewer points than in the cross-plane direction as was mention before, thus contributing less to the total number of points passing the test.

Due to the low percentage of points found within the tolerance values, the distribution of percentage differences in the outer zone, both in the cross-plane and in-plane directions, it is analyzed in detail below (see figures **5-27** and **5-28**).

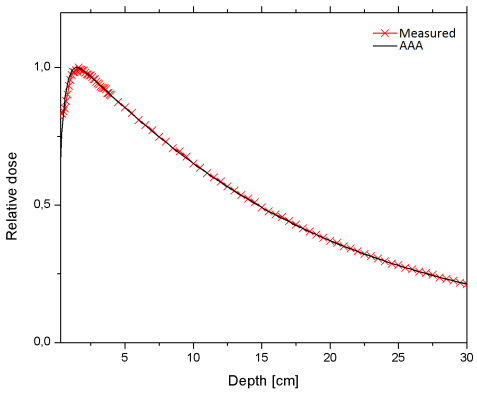

Figure 5-26.: Normalized PDD for test 3 with size field of 25×5 cm^2 and photon energy spectrum of 6 MeV.

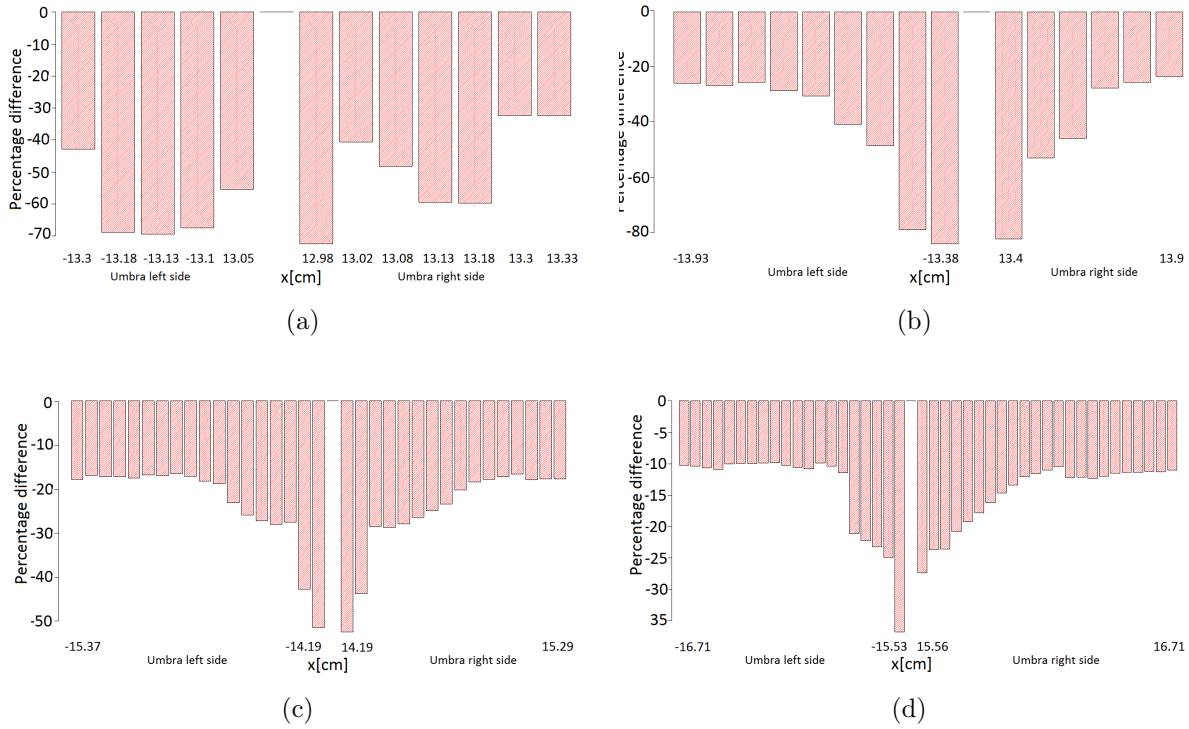

Figure 5-27.: Distribution of percentage differences from the outer zone in the cross-plane direction to the depths of: a) 12 mm, b) 40 mm, c) 100 mm and d) 200 mm.

The percentage differences distribution shows that the more depth, the greater amount of points that do not match the criteria TG-53, but as the previous results, their percentage differences are less large than in the comparisons of less deep profiles.

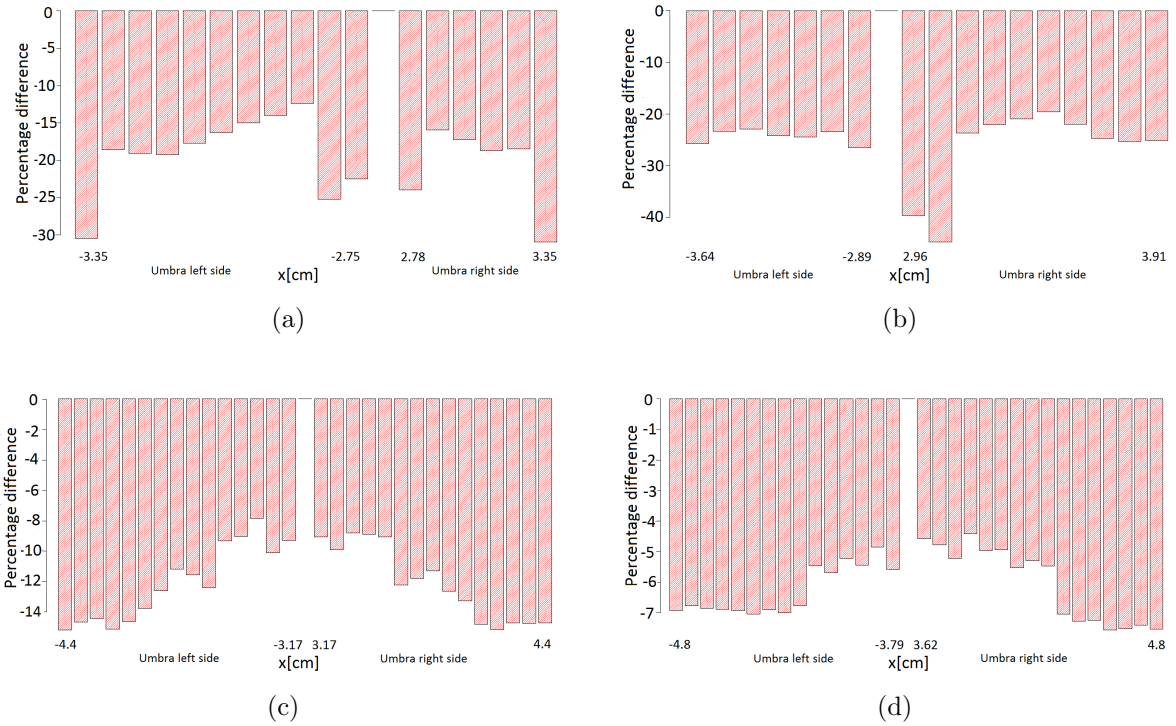

Figure 5-28.: Distribution of percentage differences from the outer zone in the in-plane direction to the depths of: a) 12 mm, b) 40 mm, c) 100 mm and d) 200 mm.

Cross-plane Depths [mm]	Mean percentage difference	**In-plane** Depths [mm]	Mean percentage difference
12	-48.6	12	-17.3
40	-45.1	40	-23.4
100	-23.7	100	-10.6
200	-13.6	200	-5.8

Table 5-9.: Mean percentage differences in the outer zone for each depth.

In the comparison of the two PDDs it was possible to verify the great concordance between those calculated by the algorithm AAA and measured ones because the 11 points compared passed the test by 100 %.
The results for the whole test 3 are summarized in Table **5-10**.

In Table **5-10** high agreement is seen in the inner and penumbra zones, however, in the outer zone the low agreement persists and, in general, an overestimation can be observed in the calculation

of the relative dose by the AAA algorithm[3] in the umbra zone. With the results obtained in this test it can be verified that in the in-plane direction the algorithm has more agreement with the measured data.

Region of the beam	% Points pass the TG-53
Inner	94.9
Penumbra	96.7
Outer	6.6
Build-up	100

Table 5-10.: Results of the comparison between measures and AAA calculated points for the test 3 for each beam profile region.

5.1.4. Test 4: Open with 45° collimator

The objective of this test is to evaluate how the AAA algorithm performs the dose distributions when the collimator is at an angle different from 0°. In addition, to evaluate the behavior of the algorithm in the calculation of the dose distribution in a diagonal direction with respect to the shape of the field. To perform this test, a field of 20×20 cm^2 is fixed and then the collimator is rotated 45°, as can be seen in Figure **5-29**, so that the dosimetric measurements are realized by the diagonals of the square, such diagonals measure 28.28 cm.

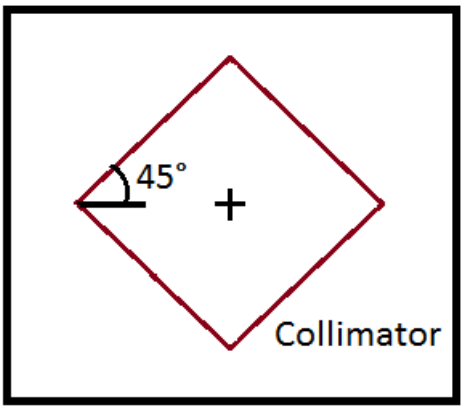

Figure 5-29.: Scheme of the set-up of the collimator at 45°.

[3]This overestimation is analyzed as a result comparison between the values calculated for the algorithm and the measured values, one of them could have failed due to possible reasons that in conclusions section are mentioned

For this test, Task Group 53 is a little less demanding in its tolerance values, having a 5 % difference in the comparisons for the inner and outer zones, and 3 % for the zone of penumbra. In the respective comparison of the behavior of the radiation beam in the build-up zone, Task Group 53 is even more lax allowing a maximum of 50 % in the tolerance differences for its validation.

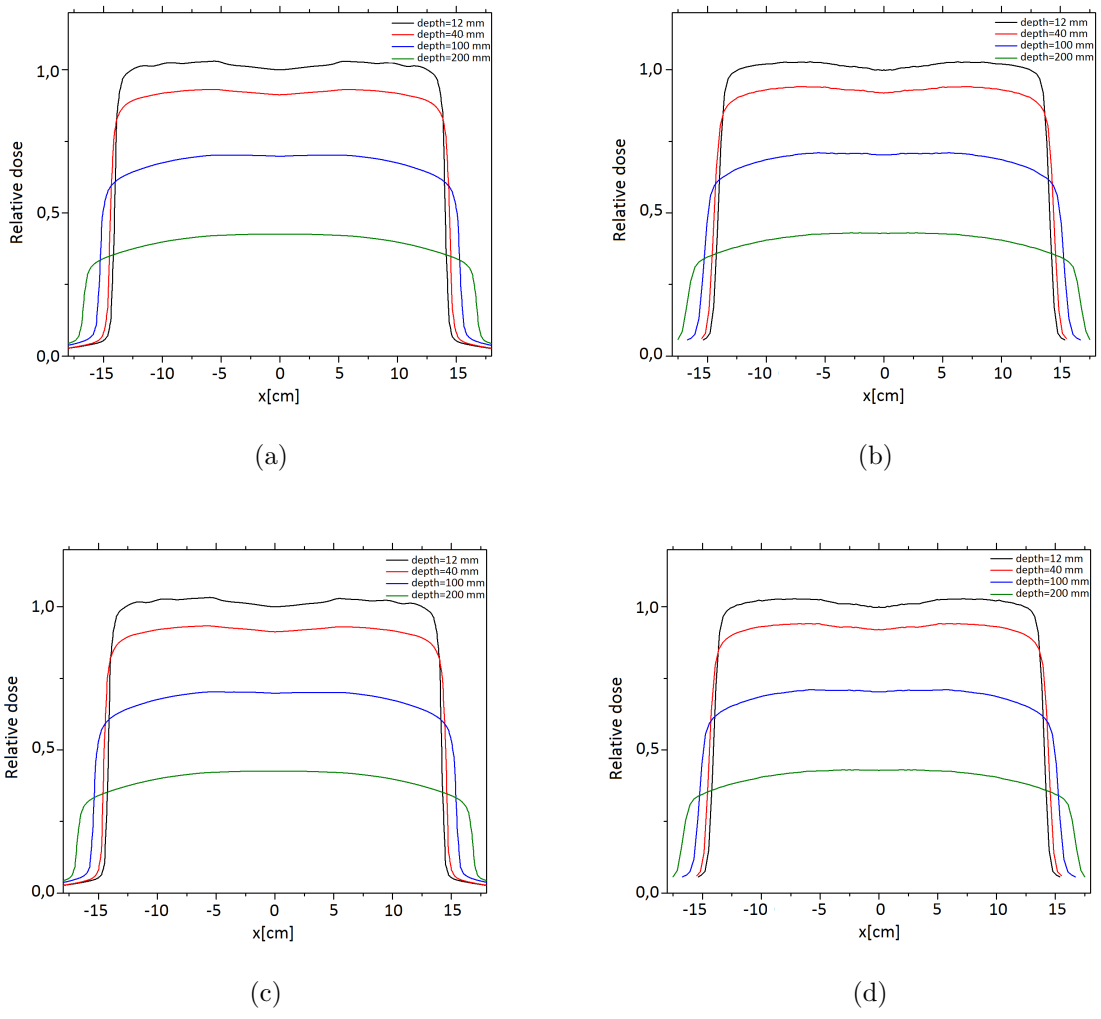

Figure 5-30.: Radiation profiles of test 4: collimator at 45° 20 × 20 cm^2 a) AAA cross-plane profile, b) measured cross-plane profile, c) AAA in-plane profile and d) measured in-plane profile.

The results of the comparison of the dosimetric profiles show very high agreement in the inner and penumbra areas, with 99.7 % and 100 % of points passing the TG-53 criteria, while for the outer zone only 4.2 % the points pass the test.
Although the size of the profiles are the largest analyzed, the results about agreement in inner and penumbra zones are excellent, because it can be affirmed that the rotation of the collimator in the

calculations of dose do not affect the accuracy of the dose calculation by the AAA algorithm.

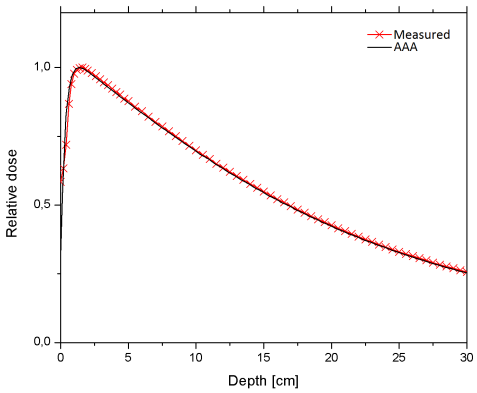

Figure 5-31.: Normalized PDD for test 4 with size field of 20×20 cm^2 and photon energy spectrum of 6 MeV.

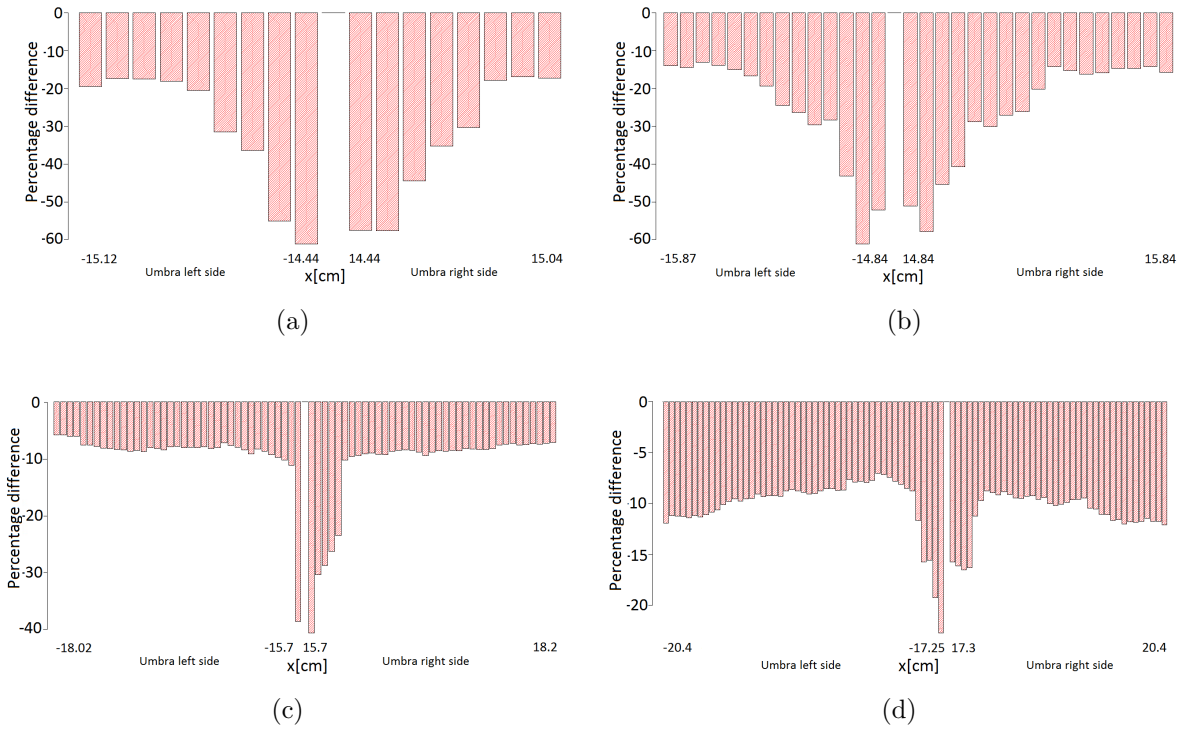

Figure 5-32.: Distribution of percentage differences from the outer zone in the cross-plane direction to the depths of: a) 12 mm, b) 40 mm, c) 100 mm and d) 200 mm.

The results obtained in the analysis of the percentage differences distributions for the outer zone of

all the profiles of this test show that the largest values were located near the penumbra zone limit, and the percentage of points that passed the test decrease as the depth increases.

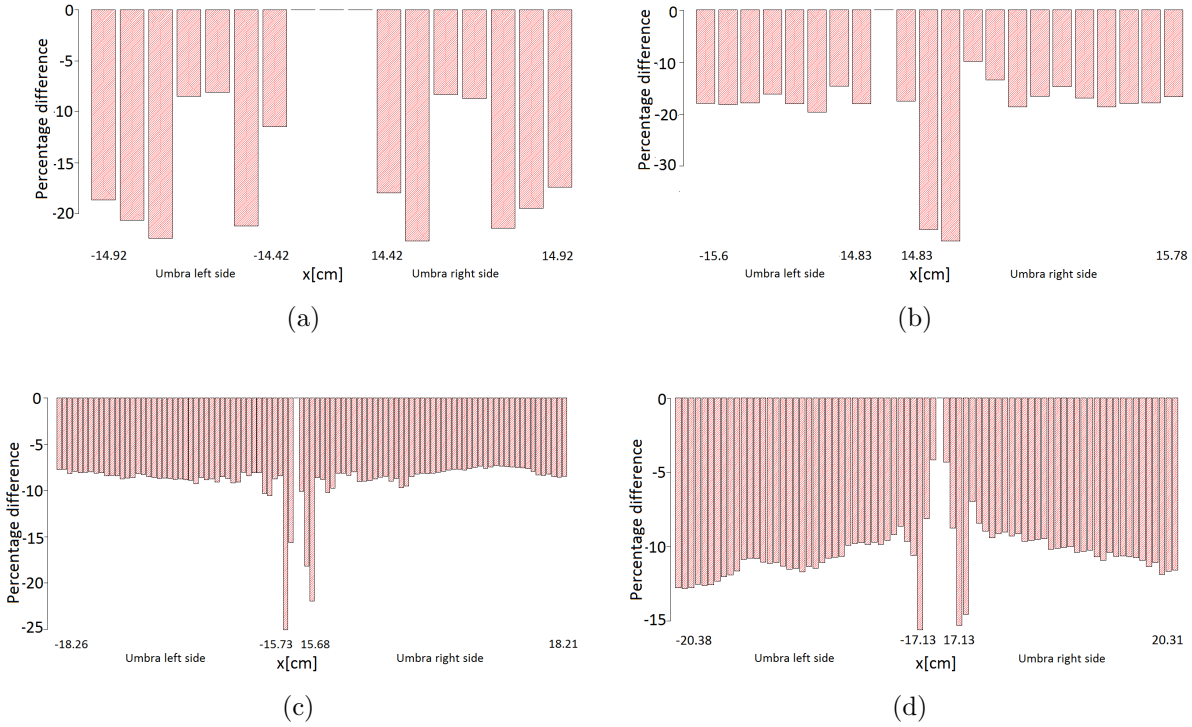

Figure 5-33.: Distribution of percentage differences from the outer zone in the in-plane direction to the depths of: a) 12 mm, b) 40 mm, c) 100 mm and d) 200 mm.

Cross-plane Depths [mm]	Mean percentage difference	**In-plane** Depths [mm]	Mean percentage difference
12	-33.0	12	-13.7
40	-25.9	40	-15.7
100	-9.8	100	-9.1
200	-10.7	200	-10.2

Table 5-11.: Mean percentage differences in the outer zone for each depth.

The results obtained in the point-to-point comparison for the two PDDs show great agreement: 6 of 6 analyzed points, 100 % of the points to pass the test. After the build-up zone the behavior of the two curves overlap giving an indicative of affinity between the two. The results for the test 4 are summarized in Table**5-12**.

Region of the beam	% Points pass the TG-53
Inner	99.7
Penumbra	100
Outer	4.2
Build-up	100

Table 5-12.: Results of the comparison between measures points and AAA calculated points for the test 4 for each beam profile region.

5.1.5. Test 5: 10 × 10 cm^2 at surface

Because of many patients are treated isocentrically, it is necessary to test the algorithm at SSD distances shorter than source-axis distance (SAD). This configuration corresponds to isocenter depth of 10 cm. Moreover, this test also helps us to understand the possibles differences between a treatment normalized at isocenter and other normalizations from the point of view of dosimetric by comparing this test with the second part of the first test.

The measurements of the profiles were made using a 10 × 10 cm^2 size field at the surface, this was done by fixing the jaws at 11,1 × 11,1 cm^2 at a distance SSD = 90 cm for the selected photon energy spectrum of 6 MV, for the four depths 1.2, 4 , 10 and 20 cm.

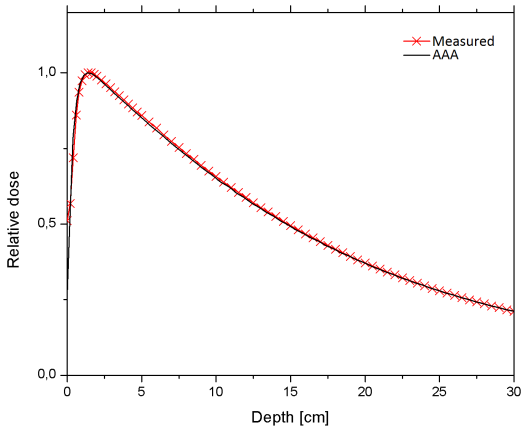

Figure 5-34.: Normalized PDD for test 5 with size field of 10 × 10 cm^2 at surface and energy of 6 MeV.

It has already seen the results of evaluating the algorithm for a SSD distance greater than 100 cm, now, the AAA algorithm was evaluated for a shorter SSD distance. The corresponding graphs in cross-plane and in-plane directions can be seen in Figure **5-35**.

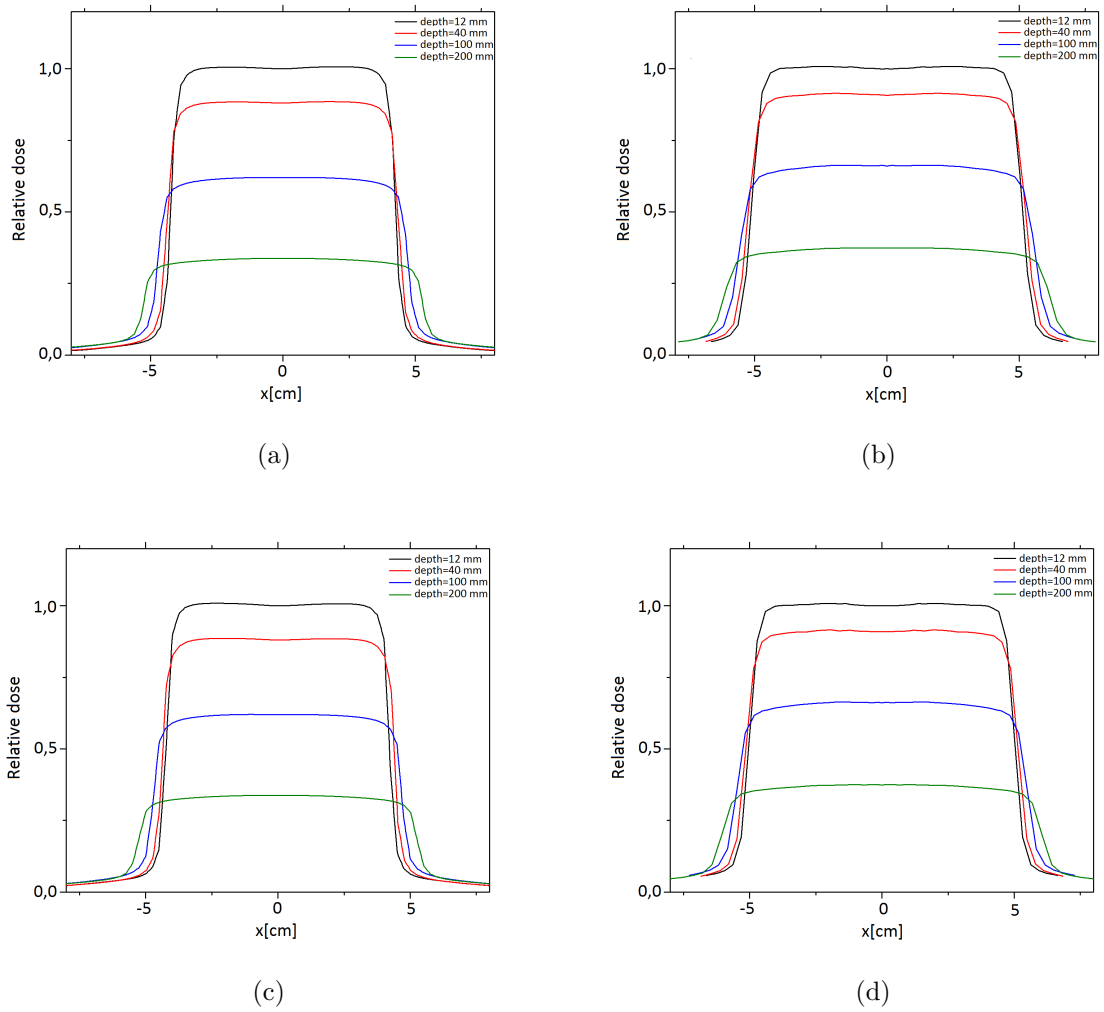

Figure 5-35.: Radiation profiles of test 5: 10×10 cm^2 field size at surface a) AAA cross-plane profile, b) measured cross-plane profile, c) AAA in-plane profile and d) measured in-plane profile.

Cross-plane Depths [mm]	Mean percentage difference	**In-plane** Depths [mm]	Mean percentage difference
12	-37.2	12	-20.5
40	-29.0	40	-17.1
100	-14.3	100	-8.1
200	-6.9	200	-5.4

Table 5-13.: Mean percentage differences in the outer zone for each depth.

The results for this test are very favorable in the inner zone because 95.5 % of the points passed the test, and the behaviour is excellent in the penumbra zone with 100 % of the points passing criterion TG-53. In the outer zone the results were not good since only 6.5 % of the points pass the test. Due to this result, it was analyzed in detail all the distribution of percentage differences (see Fig. **5-36** and **5-37**) for the outer zone.

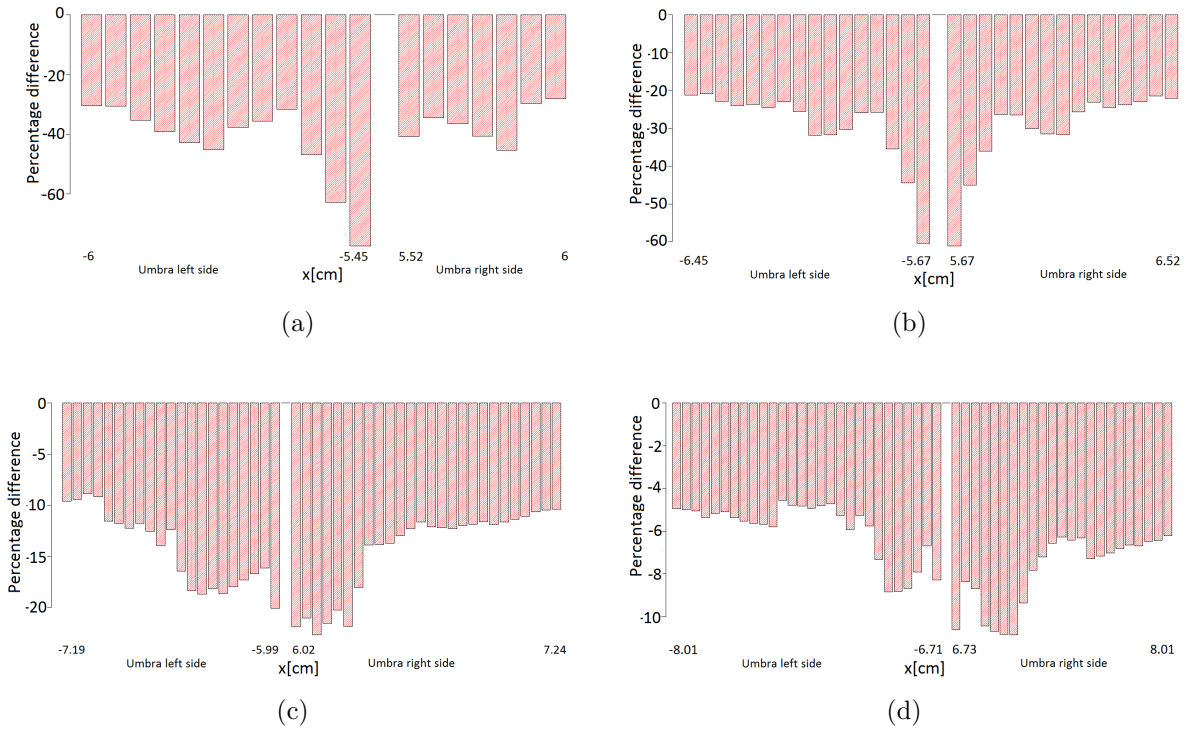

Figure 5-36.: Distribution of percentage differences from the outer zone in the cross-plane direction to the depths of: a) 12 mm, b) 40 mm, c) 100 mm and d) 200 mm.

The percentage differences distributions of the outer zone show that as the depth increases, the percentage of points passing the TG-53 criterion decreases, although the higher percentage differences are found in the less deeper profiles for both directions. The mean percentage difference for each depth can be observed in Table **5-13**, from which it can see that the percentage differences are larger in the profiles less deeper for this zone. Additionally, the negative sign could indicate that the AAA algorithm is calculating an overestimation of the dose value in the region of umbra.

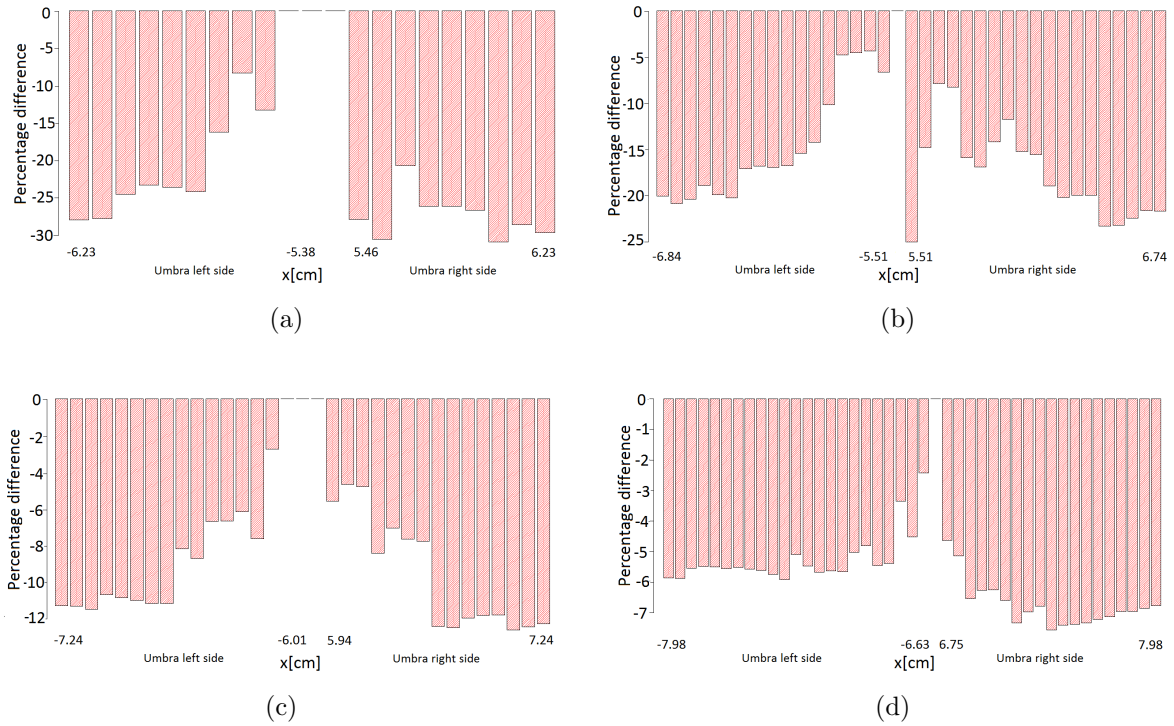

Figure 5-37.: Distribution of percentage differences from the outer zone in the in-plane direction to the depths of: a) 12 mm, b)40 mm, c) 100 mm and d)200 mm.

In the comparison of the two PDDs a great concordance between the calculated and the planned case was obtained, as a result of 100 % of the points passed such comparison in the zone of build-up, after this zone, a good behavior remains. It has already seen that in the inner zone the agreement between the compared values is high, and therefore the result is expected since the two PDDs compared were realized in central axis (CAX).
The results for the test 5 are summarized in Table **5-17**.

Region of the beam	% Points pass the TG-53
Inner	93.5
Penumbra	100
Outer	6.5
Build-up	100

Table 5-14.: Results of the comparison between measures and AAA calculated points for the test 5 for each beam profile region.

5.1.6. Test 6: Oblique incidence

In this case, the ability of the algorithm to calculate the dose for an oblique incidence of the radiation beam is evaluated. The dose distribution at an oblique incidence is expected to vary from a normal occurrence due to the amount of scatter that occurs from different parts of the phantom. The distance that the photons travel through the air are longer in some parts of the radiation beam than in others.

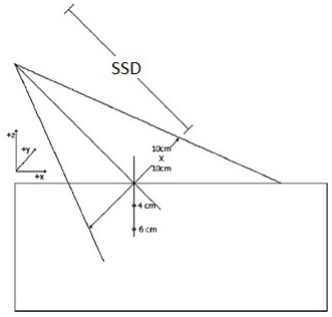

Figure 5-38.: Gantry and water phantom configuration for an oblique incidence beam.

5.1.6.1. Oblique incidence at 305°

For this test the field size is fixed 10×10 cm^2 and the gantry is rotated at 305°. Due to technical conditions for the measurement, only the dosimetric profiles could be obtained in the cross-plane direction at the depth of 1.2 and 4 mm. In the in-plane direction for depths of 100 and 200 mm, although it could be measured, the dose distribution did not have the profile shape, therefore for the comparisons they were discarded since it was not possible to differentiate each zone (see Figures **5-39c**) to apply the respective TG-53 tolerance criteria.

The results for this test show high accuracy of the algorithm and the measured values in calculating the dose distribution for the inner zone by passing the TG-53 criterion at 99.5 % of the points. For the penumbra zone the concordance drops significantly because 86.4 % of the points passed the test, while in the outer zone the results were even worst due to only 4.4 % of the points pass the test.

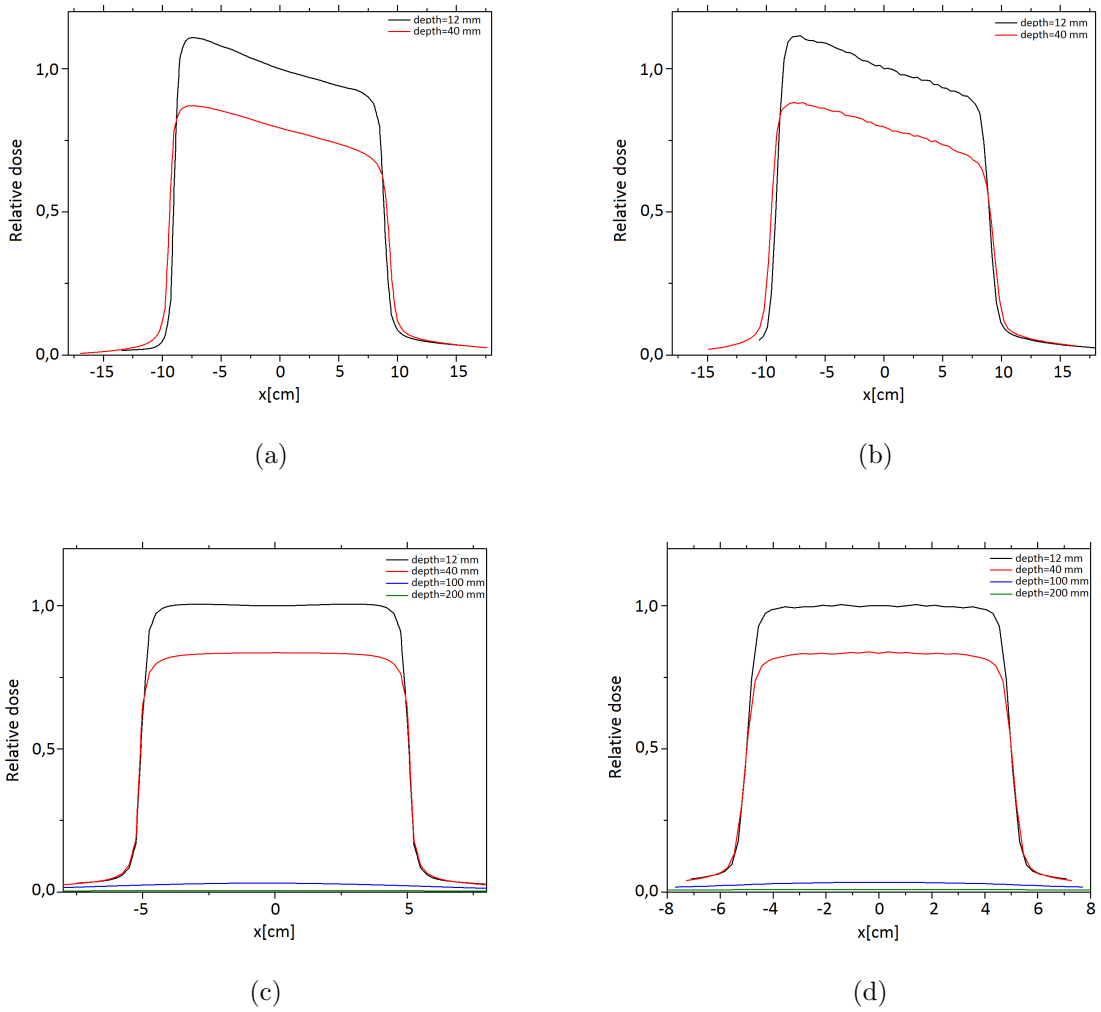

Figure 5-39.: Radiation profiles of test 6: gantry angle at 305° a) AAA cross-plane profile, b) measured cross-plane profile, c) AAA in-plane profile and d) measured in-plane profile.

Cross-plane Depths [mm]	Mean percentage difference	**In-plane** Depths [mm]	Mean percentage difference
12	-27.7	12	-25.5
40	-16.8	40	-21.2

Table 5-15.: Mean percentage differences in the outer zone for each depth.

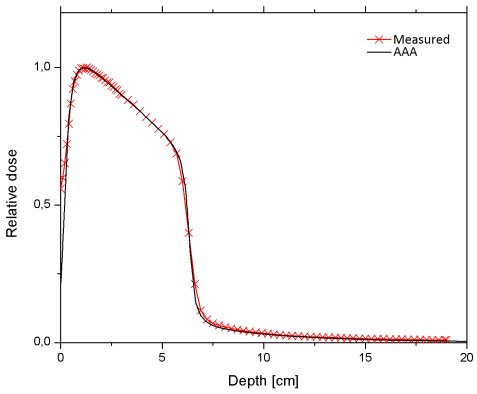

Figure 5-40.: Normalized PDD for test 6 with gantry angle at 305° and photon energy spectrum of 6 MeV.

The distribution of percentages differences for the outer zone in the cross-plane direction can be seen in Figure **5-39 a)** and **b)**, from which can find that for this zone the highest number of points that do not pass the test are to the right of the profile, but the points that are to the left of the profile that are closest to the source of radiation are those that have higher percentages of differences.

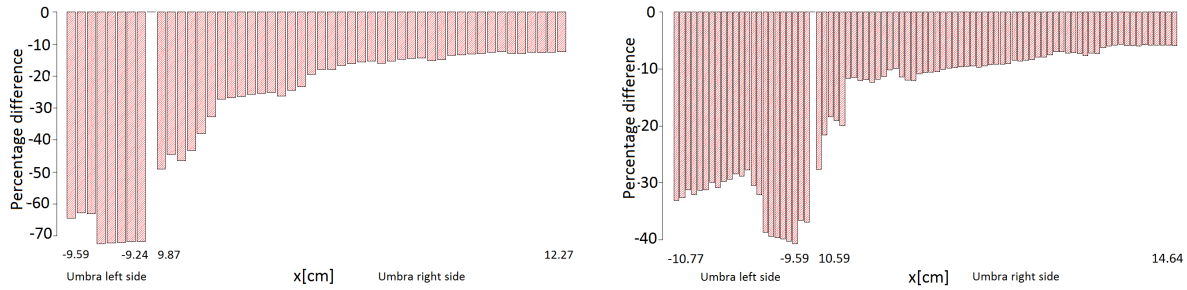

(a) (b)

Figure 5-41.: Distribution of percentage differences from the outer zone in the cross-plane direction to the depths of: a) 12 mm and b) 40 mm

Comparing the PDD measured from the calculated by the algorithm for a oblique incidence, it can be seen that 100 % of the 9 points passed the test despite abrupt dose changes, such comparison are performed in the build-up region.

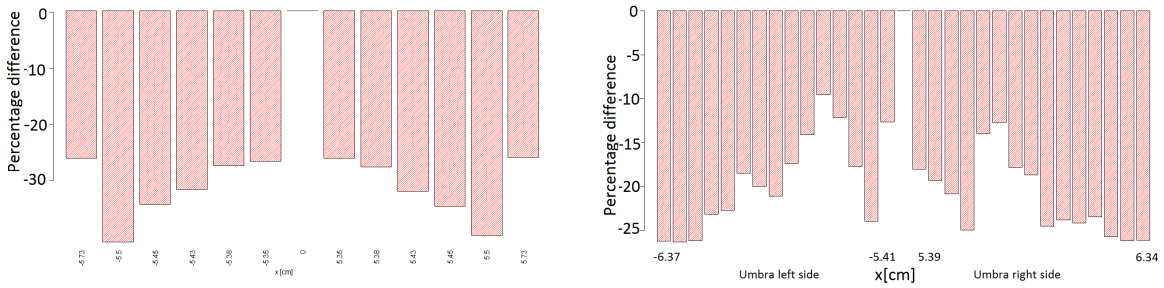

(a) (b)

Figure 5-42.: Distribution of percentage differencess from the outer zone in the in-plane direction to the depths of: a) 12 mm and b) 40 mm

Another information that can be abstracted from the distribution of percentage differences is that the algorithm continues overestimating the calculation[4] of the dose distribution in this area and for oblique incidences is significant because radiotherapy treatments of breast cancers are performed with a oblique radiation beams, and therefore, the doses that the organs at risk as lungs and heart are receiving are being overestimated.

5.1.6.2. Oblique incidence at 330°

The second part of the present test is to perform the same previous comparisons but at different gantry angle, in order to compare if with another oblique angle of the gantry changes the accuracy in the calculation of the dose distribution performed by the AAA algorithm.

The results of this test are excellent for the inner zone because it was found that AAA calculation values agree with measured ones in 99.9 % of the points taking into account the criterion of the TG-53, and for the penumbra zone the results are also favorable since 96.2 % of the points pass the test, while for the outer zone a low percentage of points passed the test again, being only 7.3 %.

[4]This overestimation is related with the comparison with values measured under clinical conditions.

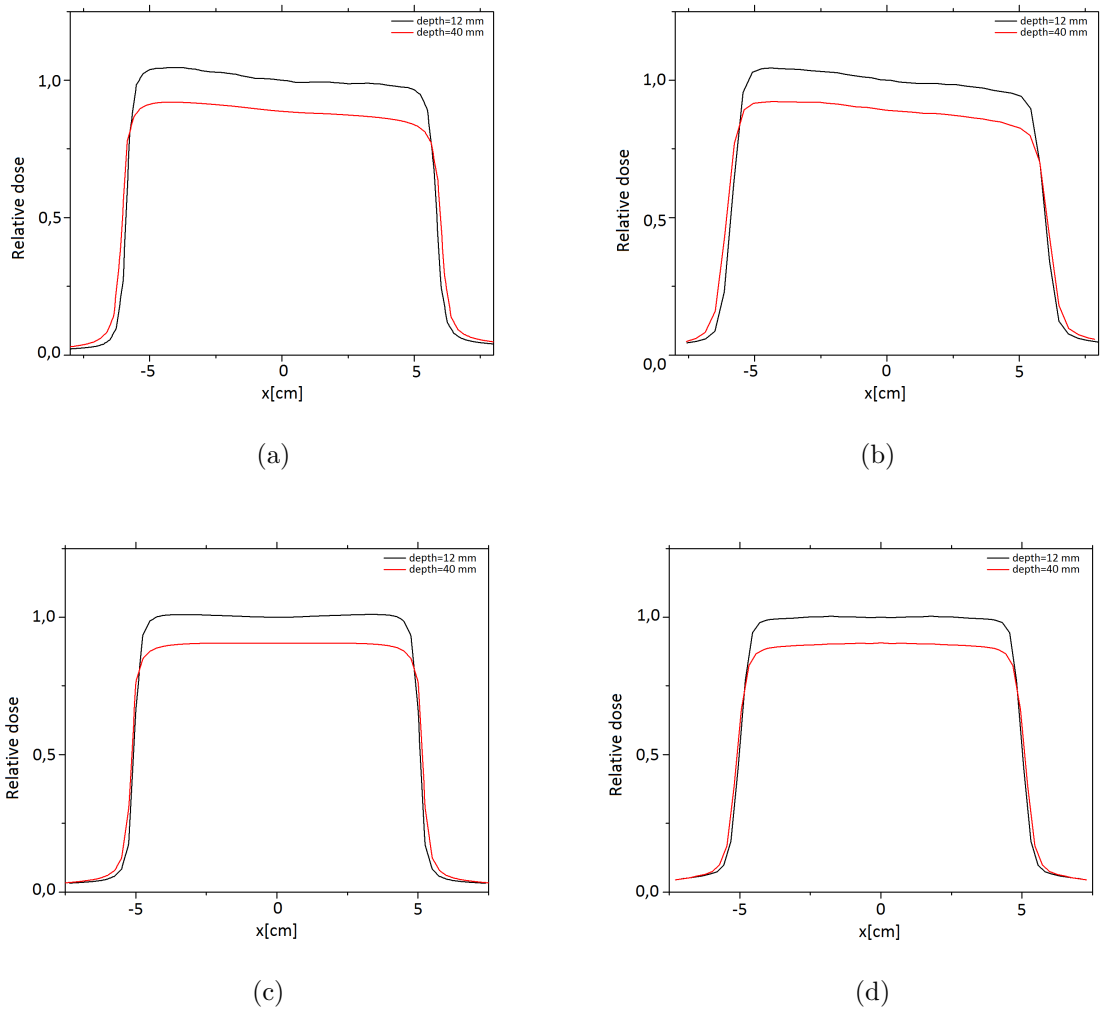

Figure 5-43.: Radiation profiles of test 6: gantry angle at 330° a) AAA cross-plane profile, b) measured cross-plane profile, c) AAA in-plane profile and d) measured in-plane profile.

In the distribution of percentage differences that can be observed in Figures **5-44** and **5-45** it is possible to see values of very high percentage differences.

Furthermore, the distribution of percentage differences of cross-plane profiles can be seen that there are more such differences on the outer right zone than on the left due to the longer length of this side of the umbra. Finally, it can also observe that in the bar graph all the bars have a negative sign, which means an overestimation in the calculation of the distribution of doses in the outer zone by the AAA algorithm[5].

[5]This overestimation is related with the comparison with values measured under clinical conditions.

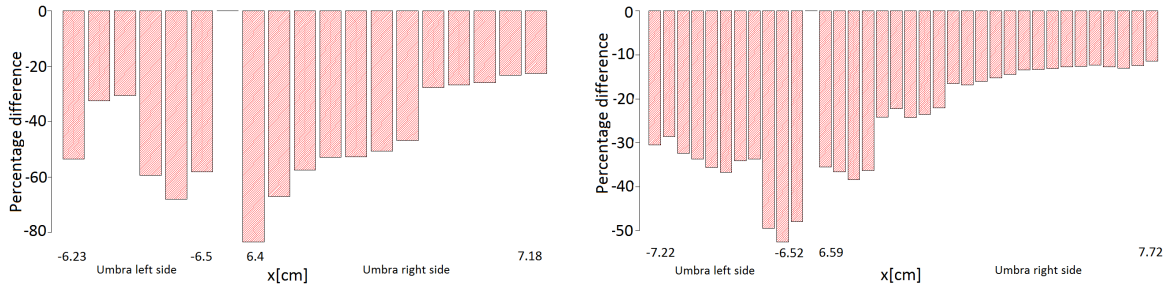

(a) (b)

Figure 5-44.: Distribution of percentage differences from the outer zone in the cross-plane direction to the depths of: a) 12 mm and b) 40 mm.

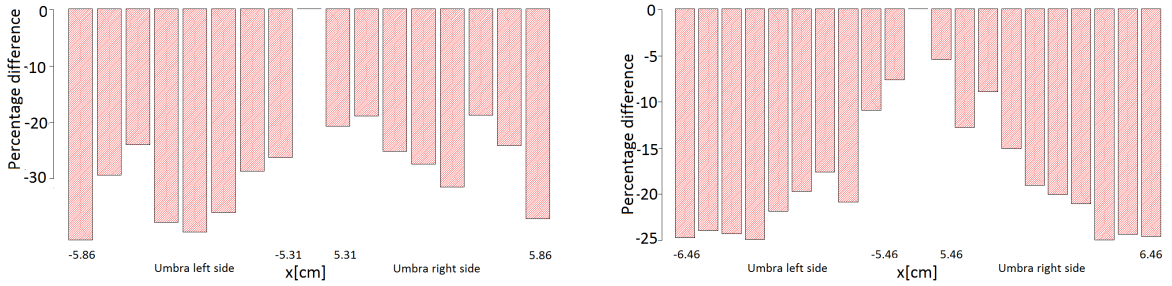

(a) (b)

Figure 5-45.: Distribution of percentage differences from the outer zone in the in-plane direction to the depths of: a) 12 mm and b) 40 mm

Cross-plane Depths [mm]	Mean percentage difference	**In-plane** Depths [mm]	Mean percentage difference
12	-41.9	12	-25.3
40	-24.8	40	-17.9

Table 5-16.: Mean percentage differences in the outer zone for each depth.

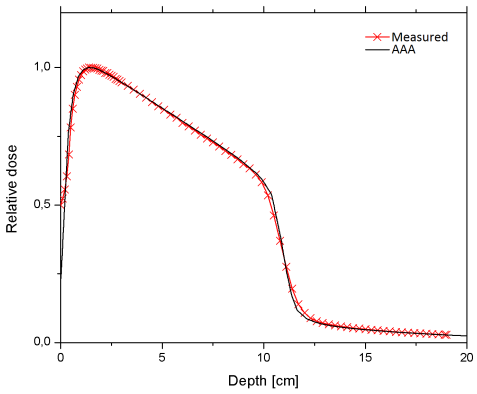

Figure 5-46.: Normalized PDD for test 6 with gantry angle at 330° and photon energy spectrum of 6 MeV.

The reproducibility of the PDD calculated by the AAA algorithm could represent a challenge in its calculation for its variation in the SSD distance and because of the gantry angulation, however, 100 % of the 11 points compared passed the test. The maximum dose values were obtained and the good fit was evident, the calculated value is 1.37 cm and the measured 1.4 cm, with a percentage difference of 2.2 %.

Comparing the results of the two oblique incidences, it can observe that the algorithm is much more accurate in the calculation of the dose distributions for the gantry angle at 330°; for this case the profile has a smaller slope in the cross-plane direction and for this reason the penumbra zone is less extensive and has a more homogeneous fall. The results for the whole test 6 are summarized in Table **5-17**.

Region of the beam	% Points pass the TG-53
Inner	99.3
Penumbra	90.5
Outer	4.4
Build-up	100

Table 5-17.: Results of the comparison between measures and AAA calculated points for the test 6 for each beam profile region.

5.1.7. Test 7: Asymmetric half-beam

The purpose of this test is to evaluate the algorithm in the reproducibility accuracy of the dose distributions in hemiblocked fields. Its configuration is at SSD = 100 cm, and with a field size

initially set as 10×10 cm^2 and the collimator Y (jaw closest to the gantry console[6]) is absolute closed, as shown in figure **5-48**.

The results of the comparisons of the dose profiles shown in Figure **5-47** give as a result in the inner region a 96 % of agreement of the compared points, while for the penumbra zone 80.8 % of the points pass the test, and finally in the outer zone only 13.5 % of the points pass the TG-53 criterion.

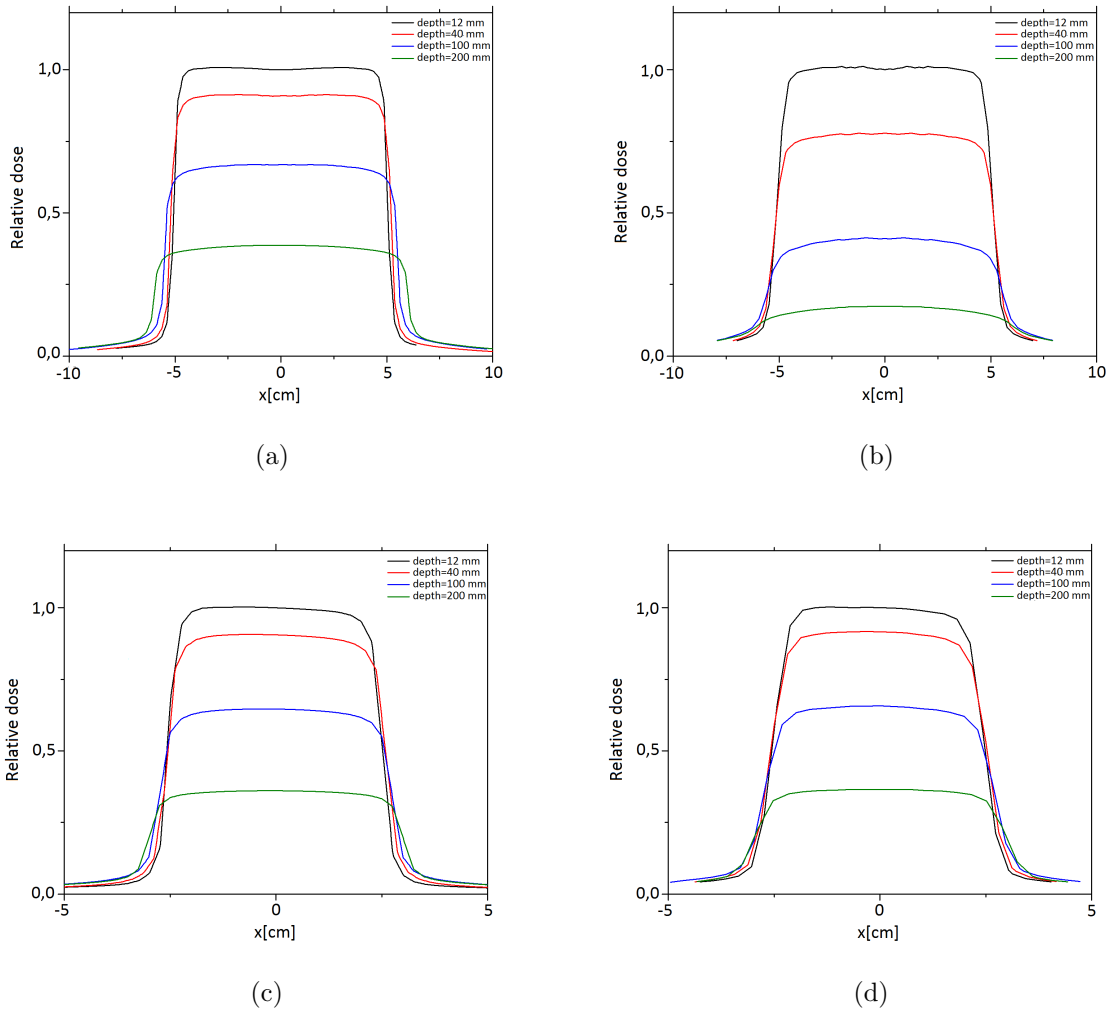

Figure 5-47.: Radiation profiles of test 7: Asymmetric half-beam a) AAA cross-plane profile, b) measured cross-plane profile, c) AAA in-plane profile and d) measured in-plane profile.

[6]This test is also possible to perform in whatever configuration of the jaws Y1 and Y2, setting up one of them wide open and the other half open while X1=X2= 5 cm.

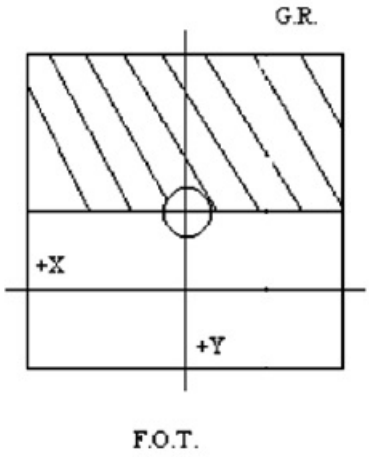

Figure 5-48.: Configuration of the jaws to fix the radiation field for the development of the test 7

The analysis of distribution of percentage differences in outer zone can be divided into two, the first one for the comparison of profiles obtained in cross-plane direction which have a very high percentage differences (see Figure **5-50**) and this agrees with the results obtained in the outer zone of the previous tests, and also it reaffirms that there is a problem when the dose profiles are obtained at the edge of the radiation field where the penumbra and umbra zone are affected. For this same reason, the results of the evaluation of the test in the penumbra zone are the worst for a field size 10×10 cm^2 and SSD= 100 cm.

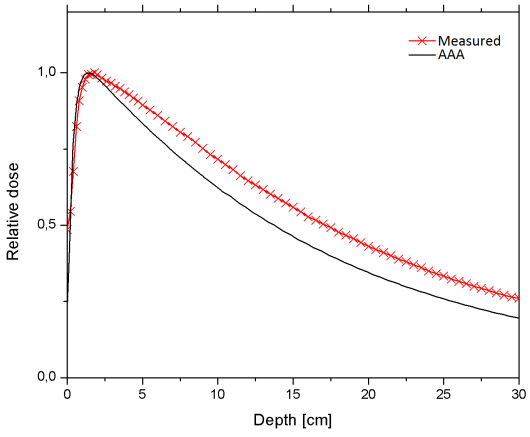

Figure 5-49.: Normalized PDD for test 7: Asymmetric half-beam and photon energy spectrum of 6 MeV.

On the other hand, the distribution of the percentage differences in the comparison of the profiles obtained in the in-plane direction shows for the depths of 12 and 40 mm a positive and negative

percentage differences, which indicates that the algorithm would fail to overestimate and underestimate the calculation of the dose distribution, also this behavior shows a failure in the dose calculation for this zone of the profile. For depths of 100 and 200 mm it can be observed that near the penumbra zone the percentage differences are lower than in the far side of the umbra.

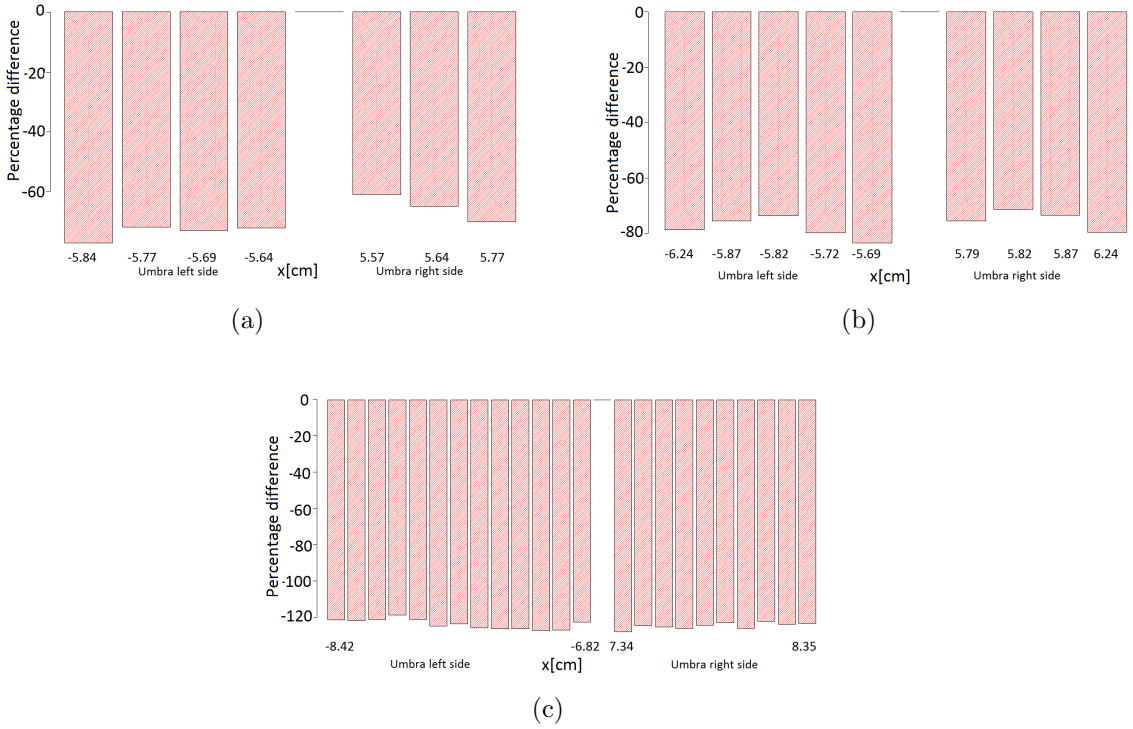

Figure 5-50.: Distribution of percentage differences from the outer zone in the cross-plane direction to the depths of: a) 12 mm, b) 40 mm and c) 100 mm.

Cross-plane Depths [mm]	Mean percentage difference	**In-plane** Depths [mm]	Mean percentage difference
12	-54.6	12	-0.1
40	-61.9	40	-1.9
100	-114.0	100	-18.5
200	N.A.	200	-46.9

Table 5-18.: Mean percentage differences in the outer zone for each depth

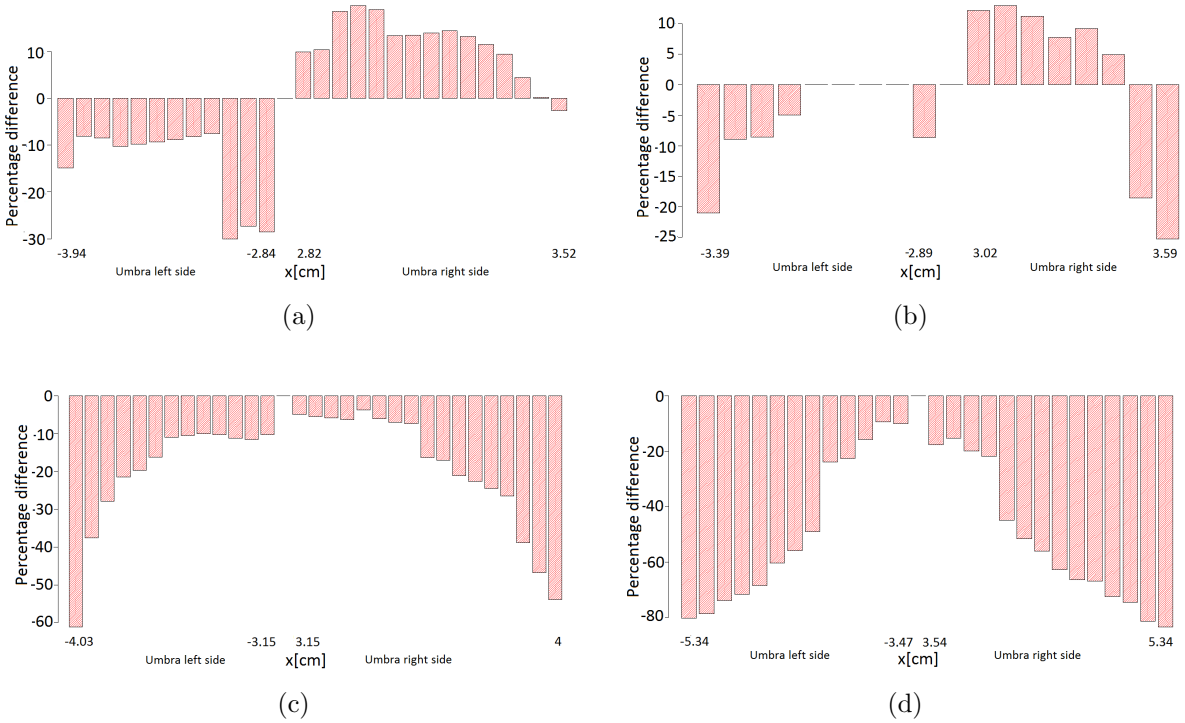

Figure 5-51.: Distribution of percentage errors from the outer zone in the in-plane direction to the depths of: a) 12 mm, b) 40 mm, c) 100 mm and d) 200 mm.

The comparison of the PDDs for this test shows a good agreement in the area to be evaluated, since 100 % of the points pass the test, which has a tolerance of 20 %. If it analyzes the graph after the depth of maximum dose it can observe a pronounced separation between the two curves, that although it complies with the tolerance value, differs more from the behavior obtained by the PDDs in the previous tests, and this is due to the position where the ionization chamber is located during the irradiation, it means that the PDDs are obtained at the edge of the radiation field. The results for the test 7 are summarized in Table **5-19**.

Region of the beam	% Points pass the TG-53
Inner	96.0
Penumbra	80.8
Outer	13.5
Build-up	100

Table 5-19.: Results of the comparison between measures and AAA calculated points for the test 7 for each beam profile region.

5.1.8. Test 8: Multileaf collimator (MLC)

This test evaluates how accurately the algorithm is by modeling the MLC multi-leaf collimator system (MLC), since most of the algorithms make their approximations taking into account the transmission of radiation between leaf and leaf, and the effects of the edges of each leaf.

For this test it is necessary to make the Figure **5-52** in a triangle shape using the multi-leaf, and having the configuration of the jaws of the collimator in X1=3 cm, X2=12 cm, Y1=4 cm and Y2=19 cm. The dose profiles were obtained at x = 5 cm (in-plane) and at y = 4 cm (cross-plane), for the 4 depths; and also at the point where these two lines intersect the PDDs were obtained.

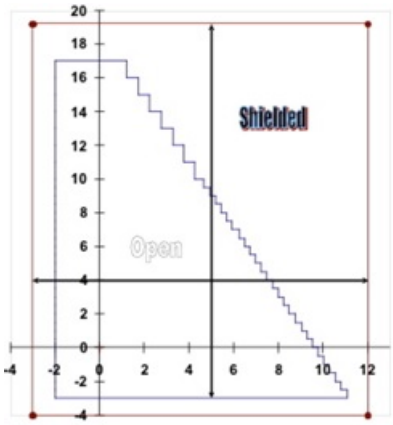

Figure 5-52.: Gantry-water phantom configuration for oblique incidence test development.

The results obtained from the comparisons of the dosimetric profiles show high agreement between the AAA values and the measured ones in the inner zone with 98.3 % of the points passed the test, while for the penumbra area 84.4 % of the points passed the test, and in the outer zone 73.4 %, which represents the best concordance between the umbra zone of the measured profiles and the calculated ones in all the evaluated tests.

The collimation of the field is mainly given by the multi-leaf system (MLC), so it could infer that the data of the dose profiles for this area have been modified, either by modifications in the hardware of the linear accelerator or because the data entered during the commissioning phase were not accurate enough.

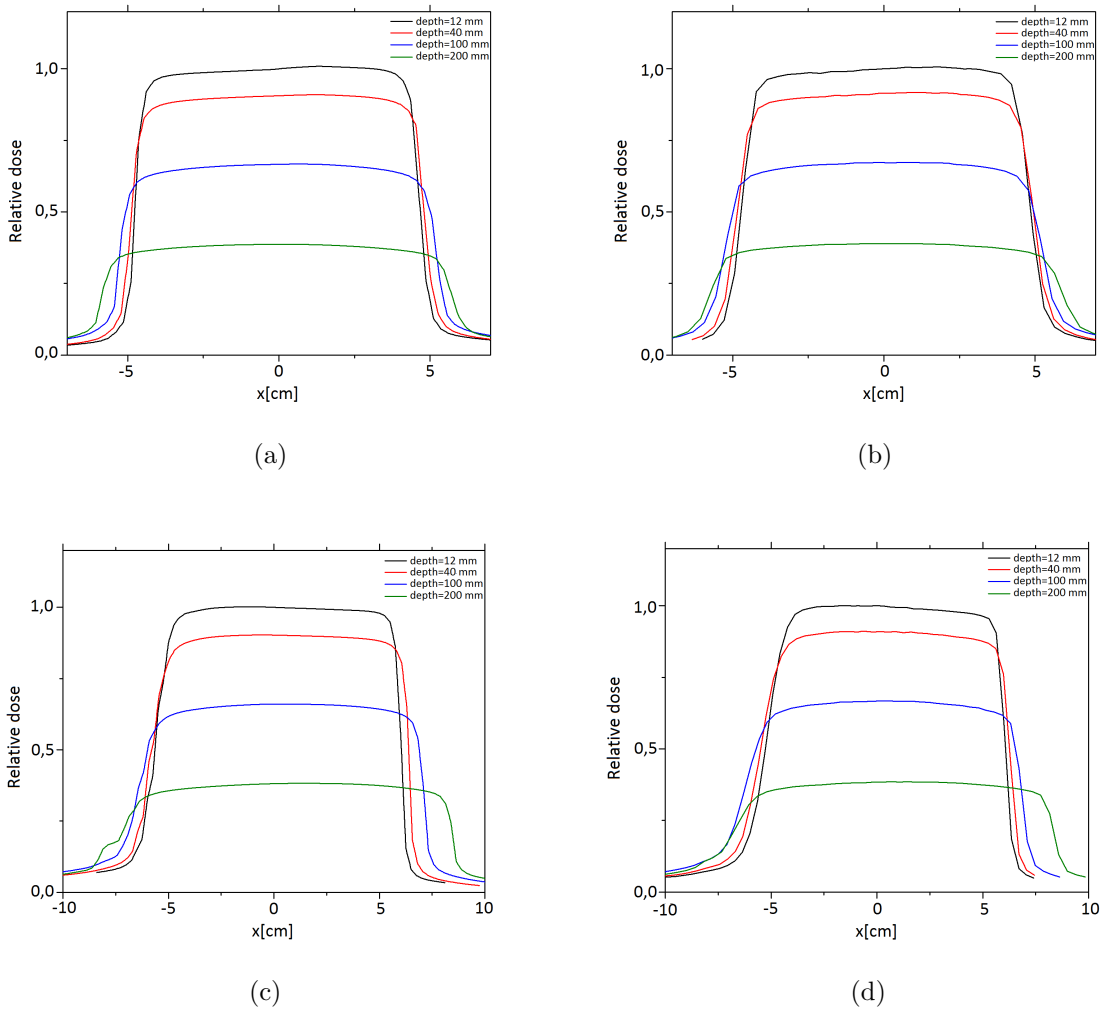

Figure 5-53.: Radiation profiles of test 8: Multileaf collimator (MLC) a) AAA cross-plane profile, b) measured cross-plane profile, c) AAA in-plane profile and d) measured in-plane profile.

The percentage differences distribution for the umbra zone shows that bars larger than 5 %, which is the tolerance value in this zone, and are less than those within the tolerance range for the in-plane while for the dose profiles assessed in cross-plane direction, they show that the distribution of percentage differences has larger values but they decrease as the depth increases. Depending on the direction of the dose profiles compared and the depth, there may be an overestimation and underestimation of the calculation of the dose distribution in this zone of the profile.

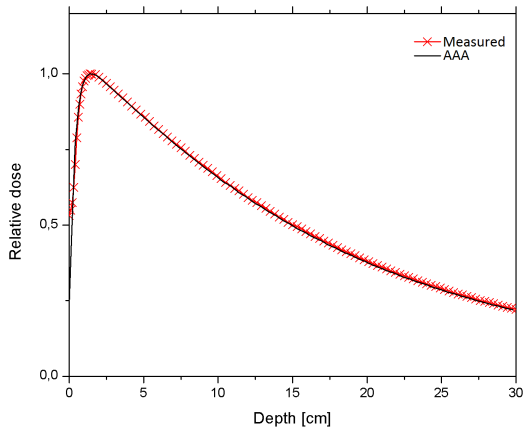

Figure 5-54.: Normalized PDD for test 8: Multileaf collimator (MLC) and photon energy spectrum of 6 MeV.

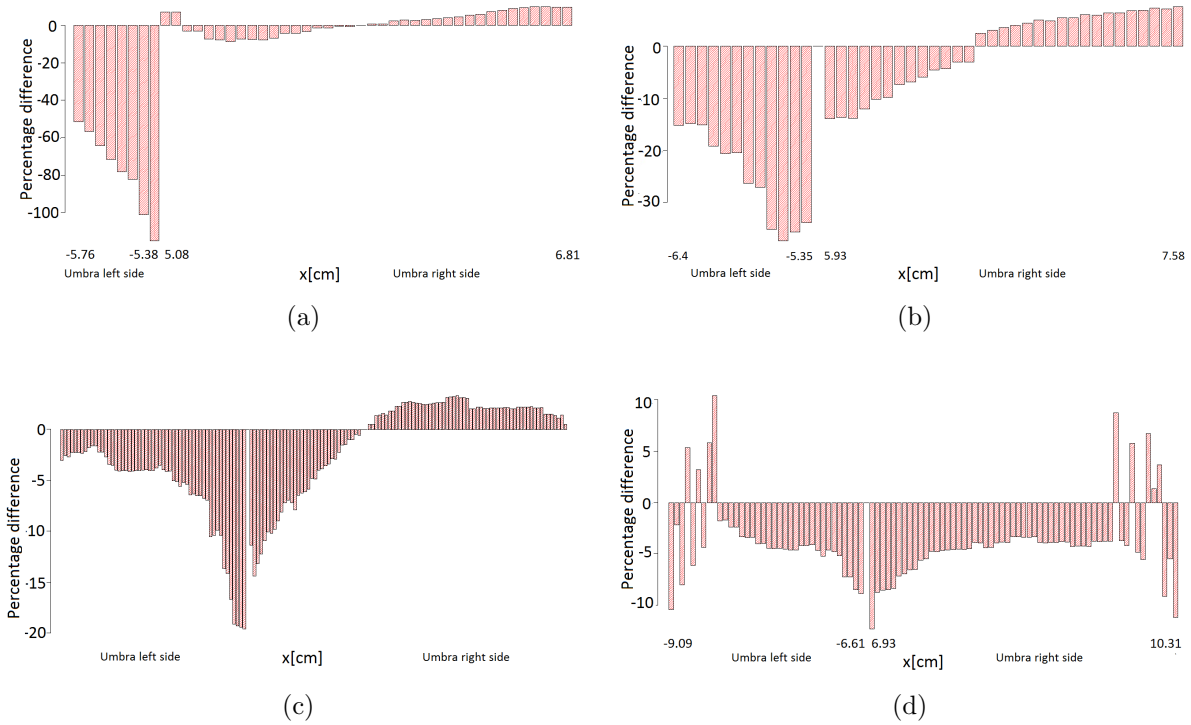

Figure 5-55.: Distribution of percentage differences from the outer zone in the cross-plane direction to the depths of: a) 12 mm, b) 40 mm, c) 100 mm and d) 200 mm.

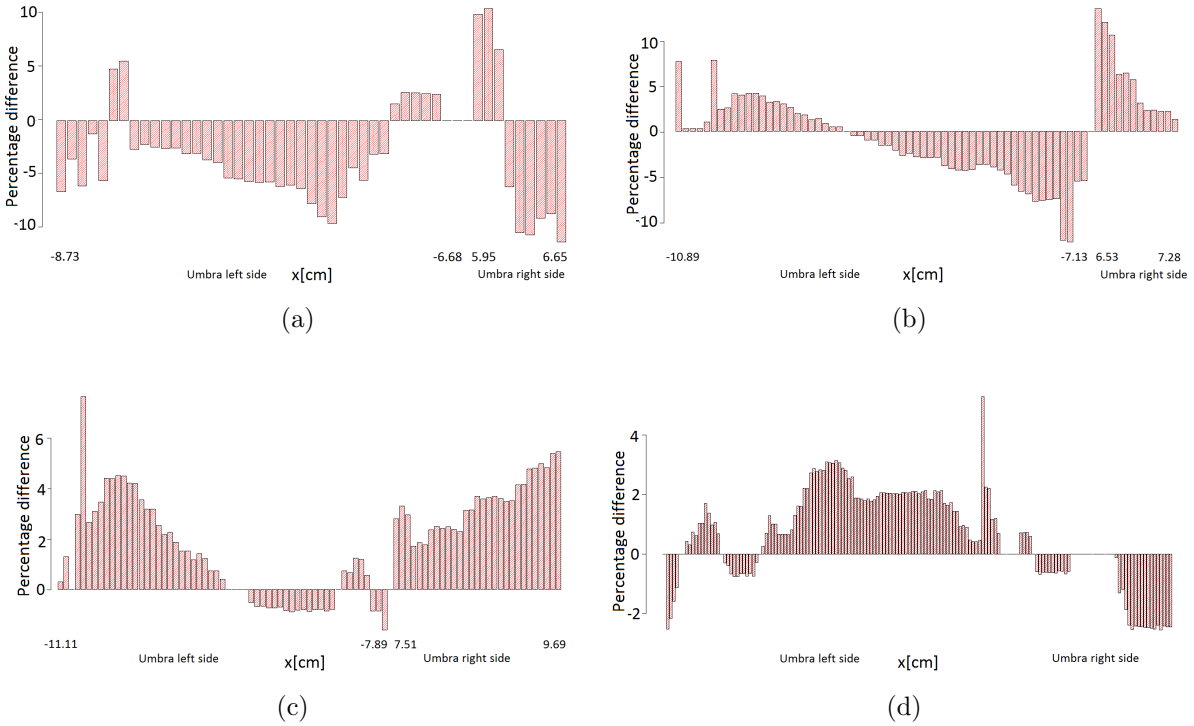

Figure 5-56.: Distribution of percentage differences from the outer zone in the in-plane direction to the depths of: a) 12 mm, b) 40 mm, c) 100 mm and d) 200 mm.

In the comparison of the PDDs it was found that 100 % of the points passed the test in the build-up region, and additionally the behavior of the two curves is maintained throughout the range of the comparison. The difference between the depths of the maximum dose, one calculated and one measured is 0.5 %. The results for the test 8 are summarized in Table **5-21**.

Cross-plane Depths [mm]	Mean percentage difference	**In-plane** Depths [mm]	Mean percentage difference
12	-12.2	12	-3.1
40	-6.8	40	-0.3
100	-3.3	100	1.9
200	-4.1	200	0.6

Table 5-20.: Mean percentage differences in the outer zone for each depth.

Region of the beam	% Points pass the TG-53
Inner	98.3
Penumbra	84.4
Outer	73.4
Build-up	100

Table 5-21.: Results of the comparison between measures and AAA calculated points for the test 8 for each beam profile region.

The evaluation of the relative dosimetry for the 8 tests for the photon energy spectrum of 6 MeV is performed following the Equation 4-3, and the calculation of its overall result is based on the equation 4-4, that are summarized in Table **5-22**.

Test	Field size [cm^2]	% Inner	% Penumbra	% outer	% Buid-up
1. Open square fields	5×5	96.9	94.8	7.4	100
	10×10	96.5	92.8	6.2	100
	25×25	88.4	85.7	3.8	100
2. Extended SSD square fields	8×8	91.1	98.0	5.8	100
	20×20	83.5	77.3	1.1	100
3. Rectangular fields	5×25	96.0	100	17.3	100
	25×5	93.8	93.3	6.6	100
4.Open with 45-degree collimator	20×20	99.7	100	4.2	100
5.Isocentric 10^2 cm^2 at surface	11.1×11.1	93.5	100	6.5	100
6a. Oblique incidence 305°	10×10	98.7	86.4	4.4	100
6b. Oblique incidence 330°	10×10	99.9	96.2	7.3	100
7.Asymmetric half-beam	$10 : 0$	96.0	80.8	13.5	100
8.Multileaf collimator (MLC)	Triangle	98.3	84.3	73.4	100

Table 5-22.: Summary of the results of the comparison (percentage differences) of the relative dosimetry measured values with those calculated by the AAA algorithm for the photon energy spectrum of 6 MeV.

One of the possible causes for the results of the outer zone that have been mentioned throughout the development of the different tests may be due to variations in the input data of the linear accelerator which were introduced during the commissioning stage. For the photon energy spectrum of 15 MeV the behavior and percentage points meeting the TG-53 criteria are very similar and that will be analyzed in a later section, by which it could indicate that is necessary to perform a recommissioning of the algorithm. In addition, this set of tests is recommended for equipment that has been working for many years or when some parts of the linear accelerator, involved in the emission of the primary ionizing radiation or in scatter generation, have been replaced.

Region of the beam	% Points pass the TG-53
Inner	93.6
Penumbra	91.0
Outer	15.3
Build-up	100

Table 5-23.: Overall results of the comparison between measurement and AAA calculations for all the tests for photon energy spectrum of 6 MeV.

5.2. Absolute dosimetry tests for photon energy spectrum of 6 MeV

For each tests mentioned in Table **4-11**, absolute dosimetry was performed, setting SSD = 100 cm and the depth of measurement to 10 cm within the water phantom, and following all the methodology explained in the previous chapter. The values of absolute dose and the Total Scatter Factors (TSF) that can be observed in Table **5-24**.

Test	Field size[a]	AAA TSF	Measure TSF	% Diff.[b] TSF	Met TG-53 criteria
1. Open square fields	5×5	0.891	0.894	0.35	YES
	10×10	1	1	0	YES
	25×25	1.143	1.133	0.86	NO
2. Extended SSD square fields	8×8	0.545	0.546	0.17	YES
	20×20	0.621	0.617	0.59	YES
3. Rectangular fields	5×25	0.975	0.972	0.25	YES
	25×5	0.954	0.847	0.71	NO
4.Open with 45-degree collimator	20×20	1.110	1.095	1.27	YES
5.Isocentric 10^2 cm^2 at surface	11.1×11.1	1.016	1.025	0.85	NO
6a. Oblique incidence 305°	10×10	0.717	0.707	1.46	NO
6b. Oblique incidence 330°	10×10	0.945	0.945	0.06	YES
7.Asymmetric half-beam	10 : 0	0.498	0.518	3.96	NO
8.Multileaf collimator (MLC)	Triangle	0.989	0.997	0.82	YES

[a] In cm^2

[b] Percentage difference

Table 5-24.: Comparison between the calculated TSFs by the AAA algorithm calculations and the measured values for the photon energy spectrum of 6 MeV.

The results reported in Table **5-24** demonstrate the high agreement of the AAA algorithm calculations of the absolute dose with the measured values, and for most all the cases its percentage

differences are within the tolerance values given by TG report 53. All the cases that do not pass, or those that pass by a slight margin, except for the test 7, its difference possibly is due to the volume of the ionization chamber; it is recommended to do the measurements of this test with the pin point ionizing chamber. However, it is noteworthy to mentioned that the values of the tolerance table are very strict and the results obtained are within the clinical range.

In test 5, which evaluates the absolute dose calculation to a lower SSD distance, it fails slightly. For these absolute dose values it was observed that the algorithm works better for large SSD distances than smaller. It could be observed in table **5-24** that for test 6b, for a large gantry tilt the algorithm does not pass the TG 53, this may due in part to the decrease of the distance SSD when the gantry. is rotated.

5.3. Absolute dosimetry measured in antrophomorfic phantom for photon energy spectrum of 6 MeV

This test evaluates the behavior of the AAA algorithm in the absolute dose calculation when there are presence of heterogeneities. It evaluated 8 points that can be observed in figure **4-26**, and taking into account the steps described in the previous chapter it shows in Table **5-25** the results obtained in the measurements and their percentage difference with that calculated by the AAA algorithm:

Point / Substituted tissue	AAA calculated [cGy]	Measured [cGy]	% Difference
1 / Paraffin wax	83.30	82.73	-0.68
2 / Paraffin wax	80.30	78.37	-2.46
3 / Paraffin wax	71.80	69.65	-3.08
4 / Cork	35.40	44.0	24.4
5 / Cork	72.40	74.7	3.17
6 / Cork	76.50	74.22	-2.98
7 / Cork	14.20	16.97	19.50
8 / PVC	44.30	44.75	1.01

Table 5-25.: Result of a comparison between calculated absolute doses and measured values for a heterogeneities test with photon energy spectrum of 6 MeV.

The results show that six of the eight points pass the TG-53 criteria, only points 4 and 7 do not, and this is in agreement with the previously reported percentage differences in relative dosimetries for the outer zone.

The AAA algorithm for the photon energy spectrum of 6 MeV meets the TG-53 criteria when the compared points are within the inner zone of the radiation field, and calculations on heterogeneities

are not a problem for the algorithm. At point 4 the ionization chamber is located at the edge of the radiation field and at point 7 in the outer zone as it can be seen in Figure **5-57**. The poor result in point 4 has the same causes as that obtained in the absolute dosimetry in the water phantom for test 7 (see in Table **5-24**) where it may be as a consequence of the location of the sensitive volume of the ionization chamber regard to the radiation field. And the result of point 7 is attributable to the location of the ionization chamber in the outer zone, where it has seen the results are not as expected.

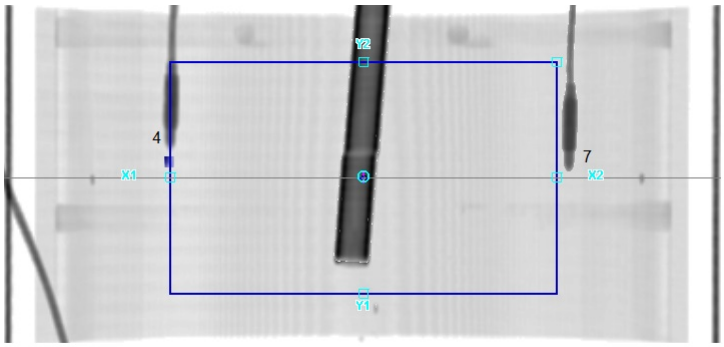

Figure 5-57.: Location of the PinPoint ionization chamber at points 4 and 7

5.4. Relative dosimetry tests for photon energy spectrum of 15 MeV

In order to make a comparison of the results of two photon energy spectrums, measurements of relative dosimetry for the photon energy spectrum of 15 MeV were carried out with the same experimental arrangement with which the profiles and PDDs of the photon energy spectrum of 6 MeV were obtained. Although the agreement with the compared points for the penumbra zone was slightly improved in this energy spectrum, the behavior in the results of the comparisons of the profiles and PDDs with the energy spectrum of 15 MeV for each of the tests was very similar to the energy spectrum of 6 MeV and the percentage differences in the outer zone can be verified this statement. In Table **5-26**, the summary of the results obtained for each zone of the radiation profile can be observed for each one of the performed tests.

For test 1, it has results similar to those obtained with the photon energy spectrum of 6 MeV, in which for the larger field size, the accuracy of the algorithm decreases. And because of the reason for performing the relative dosimetry to evaluate the algorithm's ability to reproduce the original input data and its results, we can infer that the outer zone are affected and these input data are necessary to review and possibly introduce new ones.

In test 2, we can observe that it evaluates the ability of the algorithm to predict the increase in the penumbra width with the increase in the depth. Additionally, it can observe that with the photon

energy spectrum of 15 MeV the agreement of the algorithm in the calculations for that zone of the profile increases considerably. In the outer zone, the results improve slightly with respect to the photon energy spectrum of 6 MeV, but they are still very low and worse than the results obtained in test 1, so it may infer that increasing in the SSD distance, depth and field size are involved in decreasing of the agreement in the calculation of dose distributions by the AAA algorithm, and this may be is because of all these factors that increase the amount of photons and interactions simulated for the algorithm.

Test	Field size[a]	% Inner	% Penumbra	% outer	%Buid-up
1. Open square fields	5×5	96.3	99.7	10.0	100
	10×10	91.1	100	10.9	100
	25×25	78.9	91.9	6.0	100
2. Extended SSD square fields	8×8	89.4	99.5	6.4	100
	20×20	89.7	96.2	2.6	100
3. Rectangular fields	5×25	92.7	100	4.0	100
	25×5	91.6	95.8	5.2	100
4.Open with 45-degree collimator	20×20	99.4	100	5.4	100
5.Isocentric 10^2 cm^2 at surface	$12.5\times$ 12.5	91.9	99.4	5.97	100
6a. Oblique incidence 305°	10×10	95.3	75.7	5.3	100
6b. Oblique incidence 330°	10×10	93.4	66.1	18.3	100
7.Asymmetric half-beam	$10 : 0$	96.7	82.8	15.4	100
8.Multileaf collimator (MLC)	Triangle	98.6	93.9	57.8	100

[a]In cm^2

Table 5-26.: Summary of the results of the comparison of the relative dosimetry measured with those calculated by the AAA algorithm for the photon energy spectrum of 15 MeV.

For the test 3, the ability of the algorithm to calculate the dose distributions in elongated rectangular fields that are based on the input data of square fields is evaluated. The meeting grade with the TG-53 criterion of the algorithm in inner and penumbra zones increases, maintaining the previous reported values that the results improve for the field size configuration of 5×25 cm^2 greater than 25×5 cm^2, for this reason it can state that the calculation of the dose distributions is slightly more accurate in the in-plane direction than in cross-plane.

For test 4, we can observe that the great concordance between the measured dose profiles and those calculated by the AAA algorithm for the inner and penumbra zones is maintained, however, for the outer zone the results are not favorable, being affected mainly by the field size and by the same problems that affect all the tests in this zone of the profile in those results with photon energy

spectrum of 6 MeV. Consequently, the overestimation in the calculation of the dose distribution by the AAA algorithm persists.

The configuration for test 5, which evaluates the calculation of dose distributions for a SSD distance of less than 100 cm, for the photon energy spectrum of 15 MeV, the SSD distance was reduced to 80 cm and the field size was fixed to $12{,}5 \times 12{,}5$ cm^2 to have a field size of 10×10 cm^2 in isocenter. The results show an excellent concordance in the penumbra zone, while in the inner zone the results are less better. For the outer zone it can be seen that the results are not better than those obtained in test 1 for the size of 10×10 cm^2, indicating that the smaller SSD distance and the slightly larger field size affect the calculations due to the increase of photons and interactions that are necessary to simulate for obtaining such volumetric dose distributions.

In the results of the test 6 that evaluates the ability of the algorithm to perform calculations of dose distributions for incidences of the oblique beam, it can observe that in the penumbra zone the results are not good, in fact they are the worst of all the tests evaluated for this energy. For the energy spectrum of 6 MeV the results were better, which could indicate that due to the neutron production by photon energy spectrum of 15 MeV in the interaction first with the acrylic of the tank and subsequently with the water could modify the results

As with the photon energy spectrum of 6 MeV, in this test we evaluate the ability of the algorithm to reproduce the dose distributions made by a hemiblocked field, which although is not a standard practice, is common for developing various conformal treatments. It can be seen that the results in the penumbra and outer zone are not good and it could have been as a result of the mentioned problem that the algorithm would have changed its input data due to modifications in the linear accelerator hardware. In summary, this results of this test help us to give an overall conclusion of the problems in the possible de-calibration of the AAA algorithm over the years and the physical changes that the linear accelerator has had.

Region of the beam	% Points pass the TG-53
Inner	91.1
Penumbra	93.5
Outer	14.2
Build-up	100

Table 5-27.: Overall results of the comparison between measures and AAA calculated points for all the tests for photon energy spectrum of 15 MeV.

In the last test, in which of the ability of the AAA algorithm is evaluated by modelling dose distributions that occurs when having an MLC collimator shaping the radiation field, and the ability of

the same algorithm to calculate the transmission of the dose between MLC leaves and its respective the effects of edge for the production of escatter radiation. It was observed a kind of similar behavior in the results with the photon energy spectrum of 6 MeV, but in the zone of umbra the results are better than those obtained in all previous tests of the same energy, which would confirm the suspicion of the need to recommissioning the AAA algorithm after substantial changes that have been made to the linear accelerator hardware involved in the generation of ionizing radiation.

In build-up zone, as mentioned before has more flexible tolerance values so all the points for both photon energy spectrums pass the criteria TG-53. The summary of the overall results for photon energy spectrum of 15 MeV can be seen in Table **5-27**. All the figures of the dose profiles can be seen in Appendix **A** for each test.

In brief, the overall results combined for the two energy spectrums: 6 MeV and 15 MeV can be seen in Table **5-28**.

Region of the beam	% Points pass the TG-53
Inner	92.3
Penumbra	92.4
Outer	14.8
Build-up	100

Table 5-28.: Overall results of the comparison between measures and AAA calculated points for all the tests for photon energy spectrums of 6 MeV and 15 MeV.

5.5. Absolute dosimetry tests for photon energy spectrum of 15 MeV

Absolute dosimetry for photon energy spectrum of 15 MeV was performed with the same procedure as for photon energy spectrum of 6 MeV, the results are listed in Table **5-29**, where it is mentioned if each test met or not the TG-53 criteria.

In this set of tests, in which there are photons with energies higher than 10 MeV, and therefore, the production of neutrons is presented, the algorithm correctly works, and in the results of all tests of absolute dosimetry and total scatter factor it can seen in Table **5-29** that 4 of the 8 tests passed their TG- 53 criteria, and one test passed it partially, despite the strictness of each tolerance value.

Test	Field size[a]	AAA TSF	Measure TSF	% Diff.[b] TSF	Met TG-53
1. Open square fields	5×5	0.921	0.925	0.5	YES
	10×10	1	1	0	YES
	25×25	1.083	1.075	0.73	NO
2. Extended SSD square fields	8×8	0.543	0.544	0.19	YES
	20×20	0.589	0.587	0.39	YES
3. Rectangular fields	5×25	0.983	0.995	1.15	NO
	25×5	0.965	0.975	0.98	NO
4.Open with 45-degree collimator	20×20	1.065	1.069	0.36	YES
5.Isocentric $10^2\,cm^2$ at surface	$12{,}5 \times 12{,}5$	0.787	0.795	1.06	NO
6a. Oblique incidence 305°	10×10	0.816	0.818	0.16	YES
6b. Oblique incidence 330°	10×10	0.961	0.957	0.39	YES
7.Asymmetric half-beam	$10 : 0$	0.979	0.952	2.78	NO
8.Multileaf collimator (MLC)	Triangle	1.046	1.055	0.84	YES

[a] In cm^2
[b] Percentage difference

Table 5-29.: Comparison between the calculated TSFs by the AAA algorithm and the measured values for the photon energy spectrum of 15 MeV.

In test 5, for the photon energy spectrum of 15 MeV as well as for 6 MeV can be seen that the algorithm did not meet the TG-53 criterion by a slight margin, this might have been due to the SSD distance that is reduced. For test 7, it was possible to observe that the calculated values of the algorithm also fails slightly, so it is recommended for this test with an ionization chamber of a smaller volume.

The TG-53 criteria do not include errors when determining the absolute dose under standard calibration conditions which would have had the consequence that the tolerance values were higher. Additionally, these criteria do not provide for errors in determining the TSF in their estimation for acceptable agreement [27].

5.6. Absolute dosimetry measured in antrophomorfic phantom for photon energy spectrum of 15 MeV

As for the photon energy spectrum of 6 MeV, the meeting grade of the AAA algorithm was evaluated in the calculation of absolute doses in heterogeneous and anthropomorphic media with photon energy spectrum of 15 MeV, obtaining results that are listed Table **5-30** and which have a similar behavior to those obtained with the energy spectrum of 6 MeV.

The points 1, 2 and 3 are less accurate for photon energy spectrum 15 MeV than for 6 MeV, but they all passed the tolerance value given by the TG-53 criterion of 7 % for the inner zone. The

points 4 and 7 have the same problem as with photon energy spectrum of 6 MeV.

The algorithm for this energy spectrum has high grade of agreement when calculates doses in heterogeneities, to be precise, the results of points 5, 6 and 8 are within the tolerance range. The point 5, in spite of being more distant from the radiation source, receives a higher dose than points 4 and 7 due to the electron density of PVC is much larger than electron density of cork, and also because this point is located in the inner zone of the radiation field.

Point / Substituted tissue	AAA calculated [cGy]	Measured [cGy]	% Difference
1 / Paraffin wax	90.0	86.25	-4.34
2 / Paraffin wax	87.1	82.81	-5.18
3 / Paraffin wax	78.6	75.02	-3.08
4 / Cork	35.2	47,24	25.48
5 / Cork	78.7	78.75	0.06
6 / Cork	80.9	78.68	-2.82
7 / Cork	18.4	19.97	7.86
8 / PVC	52.3	54.98	4.87

Table 5-30.: Result of a comparison between calculated and measured values for a heterogeneities test with photon energy spectrum of 15 MeV.

5.7. Comparison of relative dosimetries with other authors

These relative results show a good agreement of the AAA algorithm in the overall results (taking into account both photon energy spectrums) for the inner and penumbra zones, which are within the results reported by Breitmat et al. [18], where they show that in one clinical center for the inner zone they obtained an accuracy of 99 % and in another center 88 %, whereas for the zone of penumbra in the first center they obtained 97 % and the results for the second clinical center was 89 % by evaluating the accuracy of the AAA algorithm version 6.5 [18] or both photon energy spectrums. In contrast, for the outer zone or umbra, the percentage of points that pass all the tests in the present work is very low and very inferior to those reported in both centers: 97 % and 96 % respectively.
The group leadered by Gifford [27] performed a complete evaluation of the Pinacle algorithm taking into account all the recommendation of the TG-53. They found that 90 % of the points in the inner zone passed TG-53 criteria, 93 % in the penumbra zone, 88 % in the outer zone and 99 % in the build-up zone. The photon energy spectrum that they evaluated were 6 MeV and 18 MeV[7].

[7]Photon energy spectrum 6 or 18 MeV refers to a large amount of photons of different energies been generated by interactions of electrons with kinetic energy of 6 or 18 MeV respectively.

Region profile \ Algorithm evaluated	Present work	Institute TBCC [a]	Difference	Institute CCI[b]	Difference
	AAA 11.0.31	AAA 6.5		AAA 6.5	
Inner	92.3	97.0	-4.4	89.2	3.1
Penumbra	92.4	99.0	-6.6	88.0	4.4
Outer	14.8	97.0	-82.2	96.0	-81.2
Build-up	100	99.8	0.2	100	0.1

[a]Tom Baker Cancer Center
[b]Cross Cancer Institute

Table 5-31.: Comparison of the present work with two works [18] taking into account the TG-53 for both photon energy spectrum of 6 MeV and 15 MeV.

There were another evaluations of different algorithms but they no followed the recommendations of the Task Group Report 53, for this reason is not appropriate make a comparison with the present work. In Tables **5-31** and **5-32** are reported the comparison of the present work with those mentioned previously with its respective differences.

Region profile \ Algorithm evaluated	Present work	Institute ACC [27][a]	% Difference
	AAA 11.0.31	Pinnacle 4.2 [b]	
Inner	92.3	90	2.3
Penumbra	92.4	93	-0.6
Outer	14.8	88	73.2
Build-up	100	99	1

[a]Anderson Cancer Center
[b]Photon energy spectrum of 6 and 18 MeV

Table 5-32.: Percentage of points meeting the TG-53 criteria of the present work and the work performed in another dose calculation algorithm at ACC [27] for the photon energy espectrums of 6 MeV and 18 MeV.

The results obtained in Tables **5-31** and **5-32** in outer zone row show the high difference between the results of three medical institutes and these reported in this work that must have proved something different is happened in this area. The input data, in the commisionating stage, could have change over the years that the linear accelerator have been working; in addition, all the hardware, that had been replaced in it, may have altered those data.

6. Conclusions and Recommendations

The AAA algorithm shows great agreement with their respective measured values of absolute doses, and also calculating of dose distributions for the inner and penumbra zones of the radiation field taking into account the TG-53 criteria, for both relative and absolute dosimetries these results were confirmed in almost all the cases. In the penumbra zone, in the majority of the tests, a good results was obtained, having an overall result similar to the inner zone; however, for the tests in which the SSD distance was increased and in which there was an incidence oblique beam their agreement grade of the AAA algorithm decreased significantly, taking into account that the agreement obtained is indirectly related to the input data accessed during the commissioning stage.

The evaluation of each test shows that there is not a pattern in the behavior of the relative dosimetry results in function of the depth, for the inner zones and penumbra in most cases were almost steady. On the other hand, for the outer zone it was seen that as the depth increased the number of points that did not pass the TG-53 criteria was higher, but the percentage differences decreased with depth. This results were that indicates us that something wrong could have happened with the AAA algorithm or with the input data previously mentioned.

The results obtained do not differ much between the two photon energy spectrums analyzed, the behavior of the percentage differences is very similar for each of the tests except for some exceptions, such as those found for the photon energy spectrum of 15 MeV[1] in test 2, where two field sizes were analyzed and for the inner zone the agreement was similar.

Within the analysis of the percentage differences distributions, it was observed that in the outer zone, the AAA algorithm in general overestimates the calculation of the dose regarding to the measured values. It is necessary to clarify that the calculated values are totally depended of the data accessed during the commissioning stage. To ilustrate, in the 3D-CRT plans, the organs at risk are receiving less doses than it is calculated, which is not bad at all because a healthy organ is expected to receive as less doses as possible, but if the algorithm calculated dose distribution in the umbra zone properly, the dose plan could have coveraged the tumor volumen better where there is an overlaping with healthy tissue, without any uncertainty of overdosing them.

It was observed that with the increase of the field size, the percentage of points passing the TG-53 criteria are higher; however, the less deeper points have greater the percentage difference between the measured and calculated points by the AAA algorithm, taking into account that this algorithm

[1] As it was mentioned before, it refers a energy spectrum generated by the interaction of electrons with kinetic energy of 15 MeV

works, considering many data stored during the commissioning that could have changed.

The absolute dosimetry performed on the thorax phantom must have shown that the AAA algorithm does not present difficulties in the calculation of doses in the heterogeneities, for instance the measurements performed inside the substituted material of the lung showed great agreement with the dose calculated by the algorithm in the inner zone of the radiation field, as well as the results obtained for paraffin wax and PVC areas. However, for the points that were outside of the inner zone the results showed less agreement and did not pass the TG-53 criteria. These results are consistent with those obtained in the relative and absolute dosimetry performed in homogeneous phantom for this zone.

Due to all mentioned previously for the outer zone and the results reported by other authors differ markedly from those obtained in the present work, one could conclude that the high percentage differences reported in the outer zone is related to the physical modifications that have been made to the linear accelerator which all the tests were performed, and these hardware modifications are involve directly with the generation of the ionizing radiation. This modification might have affected the input parameters in the commissioning of the linear accelerator and now they are not adequated. For this reason it is recommended to perform a commissioning of the algorithm and the accomplishment of dosimetric tests with high accuracy to enter the new input data.

Other authors showed great agreement between measured values and those calculated by the dose calculation algorithm. However, it should be noted that most of them only performed measurements at one superficial depth. For this work, a complete relative dose comparisons were performed and that allows to observe that in some test the algorithm slightly decreases its agreement values as increases depth. Considering this aspect, we compared only with two works that also did a complete dosimetry tests for all four depths.

The tolerances values recommended by the Task Group Report 53 for the comparison of the dosimetric profiles and the Total Scatter Factor (TSF) are very strong in some cases. The comparisons performed could have been better if this evaluation would use the recommendations that are made for the evaluation of the dose distributions in the quality controls of the treatments. In contrast, for the evaluation of the PDDs the tolerance table shows very lax values, for that reason 100 % of all points pass, and this happens to all test results and those reported by other authors.

The results of the evaluation of the accuracy of the AAA algorithm in its version 11.0.31 couldn't have been reliable for the outer region, and indirectly they might have affected the results of the inner and penumbra zones due to the problems mentioned above. However, the development of the tests that were done in this work could help to identify problems such as: dosimetric decalibration of the linear accelerator and change in the input parameters, that were obtained during the commissioning stage, as a result of modifications in the hardware of the linear accelerator or because of the overuse of equipment over the years.

Bibliography

[1] *CIRS, Tissue Simulation and Phantom Tech.* urlhttp://www.cirsinc.com/products/iso-cube-daily-qa-phantom/. 2016

[2] *Clinac iX System.* urlhttps://www.varian.com/oncology/products/treatment-delivery/clinac-ix-system. 2016

[3] *Detectors including Codes of Practice.* urlhttp://www.ptw.de/.../blaetterkatalog. 2016

[4] *Iso-Aling Mechanical Alignment.* urlhttp://civcort.com/ro/physics-qa/isoalign/isoalign-MTIAD1.htm. 2016

[5] *Magnetic Front Pointer For Elekta SL20/25.* urlhttp://www.rpdinc.com/magnetic-front-pointer-for-elekta-sl25-3822.html. 2016

[6] *PTW 31010, 0.125cc Semiflex Chamber.* urlhttp://www.rpdinc.com/ptw-31010-0125cc-semiflex-chamber-972.html. 2016

[7] *PTW 31016, 0.016cc PinPoint 3D Chamber.* urlhttp://www.rpdinc.com/ptw-31016-0016cc-pinpoint-3d-chamber–977.html. 2016

[8] *PTW Water Phantoms, MP3, MP2, MP1 Water Scanning Systems.* urlhttp://www.ptw-usa.com/2032.html. 2016

[9] *QA Beam Checker Plus.* urlhttps://standardimaging.com/support/product/qa-beamchecker-plus. 2016

[10] *TANDEM Dual Channel Electrometer.* urlhttp://www.ptw.de/tandem-electrometer-ad0.html. 2016

[11] *UNIDOS E Universal Dosemeter.* urlhttp://www.ptw.de/unidos-e-dosemeter-ad0.html. 2016

[12] Akhlaghi, Parisa ; Hakimabad, Hashem M. ; Motavalli, Laleh R.: Determination of tissue equivalent materials of a physical 8-year-old phantom for use in computed tomography. En: *Radiation Physics and Chemistry* 112 (2015), p. 169–176

[13] Alam, Rejina ; Ibbott, Geoffrey S. ; Pourang, Rahman ; Nath, Ravinder: Application of AAPM Radiation Therapy Committee Task Group 23 test package for comparison of two treatment planning systems for photon external beam radiotherapy. En: *Medical physics* 24 (1997), Nr. 12, p. 2043–2054

[14] Allen, XL: Peak scatter factors for high energy photon beams. En: *Med. Phys.* 26 (1999)

[15] Almond, Peter R. ; Biggs, Peter J. ; Coursey, BM ; Hanson, WF ; Huq, M S. ; Nath, Ravinder ; Rogers, DWO: AAPM TG-51 protocol for clinical reference dosimetry of high-energy photon and electron beams. En: *Medical physics* 26 (1999), Nr. 9, p. 1847–1870

[16] B. Heymsfield, Steven ; Wang, ZiMian ; Baumgartner, Richard N. ; Ross, Robert: Human body composition: advances in models and methods. En: *Annual review of nutrition* 17 (1997), Nr. 1, p. 527–558

[17] Benedict, Stanley H. ; Schlesinger, David J. ; Goetsch, Steven J. ; Kavanagh, Brian D.: *Stereotactic radiosurgery and stereotactic body radiation therapy.* CRC Press, 2014

[18] Breitman, Karen ; Rathee, Satyapal ; Newcomb, Chris ; Murray, Brad ; Robinson, Donald ; Field, Colin ; Warkentin, Heather ; Connors, Sherry ; Mackenzie, Marc ; Dunscombe, Peter [u. a.]: Experimental validation of the Eclipse AAA algorithm. En: *Journal of Applied Clinical Medical Physics* 8 (2007), Nr. 2

[19] Cao, Daliang: Volumetric Modulated Arc Therapy (VMAT): The future of IMRT. En: *Swedish Cancer Institute* 20 (2015)

[20] Chang, Kwo-Ping ; Hung, Shang-Ho ; Chie, Yu-Huang ; Shiau, An-Cheng ; Huang, Ruey-Jing: A comparison of physical and dosimetric properties of lung substitute materials. En: *Medical physics* 39 (2012), Nr. 4, p. 2013–2020

[21] Cho, SH ; Ibbott, GS: Reference photon dosimetry data: a preliminary study of in-air off-axis factor, percentage depth dose, and output factor of the Siemens Primus linear accelerator. En: *Journal of Applied Clinical Medical Physics* 4 (2003), Nr. 4, p. 300–306

[22] Claude, Kezo P. ; Tagoe, Samuel Nii A. ; Schandorf, Cyril ; Amuasi, John: Fabrication of a tissue characterization phantom from indigenous materials for computed tomography electron density calibration. En: *The South African Radiographer* 51 (2013), Nr. 1, p. 9–17

[23] Datta, Niloy R. ; Kumar, Shaleen ; Das, Koilpillai Joseph M. ; Pandey, Chandra M. ; Halder, Shikha ; Ayyagari, Sunder: Variations of intracavitary applicator geometry during multiple HDR brachytherapy insertions in carcinoma cervix and its influence on reporting as per ICRU report 38. En: *Radiotherapy and Oncology* 60 (2001), Nr. 1, p. 15–24

[24] Fogliata, Antonella ; Nicolini, Giorgia ; Vanetti, Eugenio ; Clivio, Alessandro ; Cozzi, Luca: Dosimetric validation of the anisotropic analytical algorithm for photon dose calculation: fundamental characterization in water. En: *Physics in medicine and biology* 51 (2006), Nr. 6, p. 1421

[25] Fraass, Benedick ; Doppke, Karen ; Hunt, Margie ; Kutcher, Gerald ; Starkschall, George ; Stern, Robin ; Van Dyke, Jake: American Association of Physicists in Medicine Radiation Therapy Committee Task Group 53: quality assurance for clinical radiotherapy treatment planning. En: *Medical physics* 25 (1998), Nr. 10, p. 1773–1829

[26] Gagne, Isabelle M. ; Zavgorodni, Sergei: Evaluation of the analytical anisotropic algorithm (AAA) in an extreme water-lung interface phantom using Monte Carlo dose calculations. En: *Journal of Applied Clinical Medical Physics* 8 (2007), Nr. 1

[27] Gifford, Kent A. ; Followill, David S. ; Liu, H H. ; Starkschall, George: Verification of the accuracy of a photon dose-calculation algorithm. En: *Journal of applied clinical medical physics* 3 (2002), Nr. 1, p. 26–45

[28] Hasanzadeh, Hadi ; Abedelahi, Ali: Introducing a simple tissue equivalent anthropomorphic phantom for radiation dosimetry in diagnostic radiology and radiotherapy. En: *Journal of Paramedical Sciences* 2 (2011), Nr. 4

[29] Hodapp, N: The ICRU Report 83: prescribing, recording and reporting photon-beam intensity-modulated radiation therapy (IMRT). En: *Strahlentherapie und Onkologie: Organ der Deutschen Röntgengesellschaft...[et al]* 188 (2012), Nr. 1, p. 97

[30] ICRU, Phantoms: computational models in Therapy, Diagnosis and Protection. En: *International Commission on Radiation Units and Measurements Report* 48 (1992)

[31] Khan, Faiz M. ; Gibbons, John P.: *Khan's the physics of radiation therapy.* Lippincott Williams & Wilkins, 2014

[32] Klein, Eric E. ; Hanley, Joseph ; Bayouth, John ; Yin, Fang-Fang ; Simon, William ; Dresser, Sean ; Serago, Christopher ; Aguirre, Francisco ; Ma, Lijun ; Arjomandy, Bijan [u. a.]: Task Group 142 report: Quality assurance of medical acceleratorsa). En: *Medical physics* 36 (2009), Nr. 9, p. 4197–4212

[33] Mejía Agudelo, Luis A. [u. a.]: *Análisis dosimétrico de las distribuciones de dosis para las técnicas de tratamiento (campos tangenciales con cuñas, campos complementarios e IMRT) en radioterapia de cáncer de mama*, Universidad Nacional de Colombia, Tesis de Grado

[34] Nisbet, A ; Thwaites, DI: Polarity and ion recombination correction factors for ionization chambers employed in electron beam dosimetry. En: *Physics in medicine and biology* 43 (1998), Nr. 2, p. 435

[35] OIEA: *Determinación de la dosis absorbida en radioterapia con haces externos, COLECCION DE INFORMES TECNICOS N° 398.* OIEA en Austria, 2005

[36] Podgorsak, Ervin B. [u. a.]: Radiation oncology physics. En: *a handbook for teachers and students/EB Podgorsak.–Vienna: International Atomic Energy Agency* 657 (2005)

[37] R. K. Fulkerson, Ph.D. ; Holmes, S. M.: User's guide to TG-142. En: *Standard Imaging* (2013)

[38] Reft, Chester S.: Output calibration in solid water for high energy photon beams. En: *Medical physics* 16 (1989), Nr. 2, p. 299–301

[39] Schneider, Wilfried ; Bortfeld, Thomas ; Schlegel, Wolfgang: Correlation between CT numbers and tissue parameters needed for Monte Carlo simulations of clinical dose distributions. En: *Physics in medicine and biology* 45 (2000), Nr. 2, p. 459

[40] Senthilkumar, S: Design of homogeneous and heterogeneous human equivalent thorax phantom for tissue inhomogeneity dose correction using TLD and TPS measurements. En: *INTERNATIONAL JOURNAL OF RADIATION RESEARCH* 12 (2014), Nr. 2, p. 169–178

[41] Sievinen, Janne ; Ulmer, Waldemar ; Kaissl, Wolfgang [u. a.]: AAA photon dose calculation model in Eclipse. En: *Palo Alto (CA): Varian Medical Systems* 118 (2005), p. 2894

[42] System, Varian M.: *Eclipse Algorithms References Guide*. Varian, 2011

[43] Ten Haken, Randall K. ; Lawrence, Theodore S.: The clinical application of intensity-modulated radiation therapy. En: *Seminars in radiation oncology* Vol. 16 Elsevier, 2006, p. 224–231

[44] Webb, Steve: Conformal intensity-modulated radiotherapy (IMRT) delivered by robotic linac-testing IMRT to the limit? En: *Physics in medicine and biology* 44 (1999), Nr. 7, p. 1639

[45] White, DR ; Booz, J ; Griffith, RV ; Spokas, J ; Wilson, IJ: Tissue substitutes in radiation dosimetry and measurement. En: *ICRU Report* 44 (1989)

A. Appendix A: Dosimetric profiles for photon energy spectrum of 15 MeV

The dosimetric profiles of this appendix are related to the tests recommended by TG-53.
- Test 1:

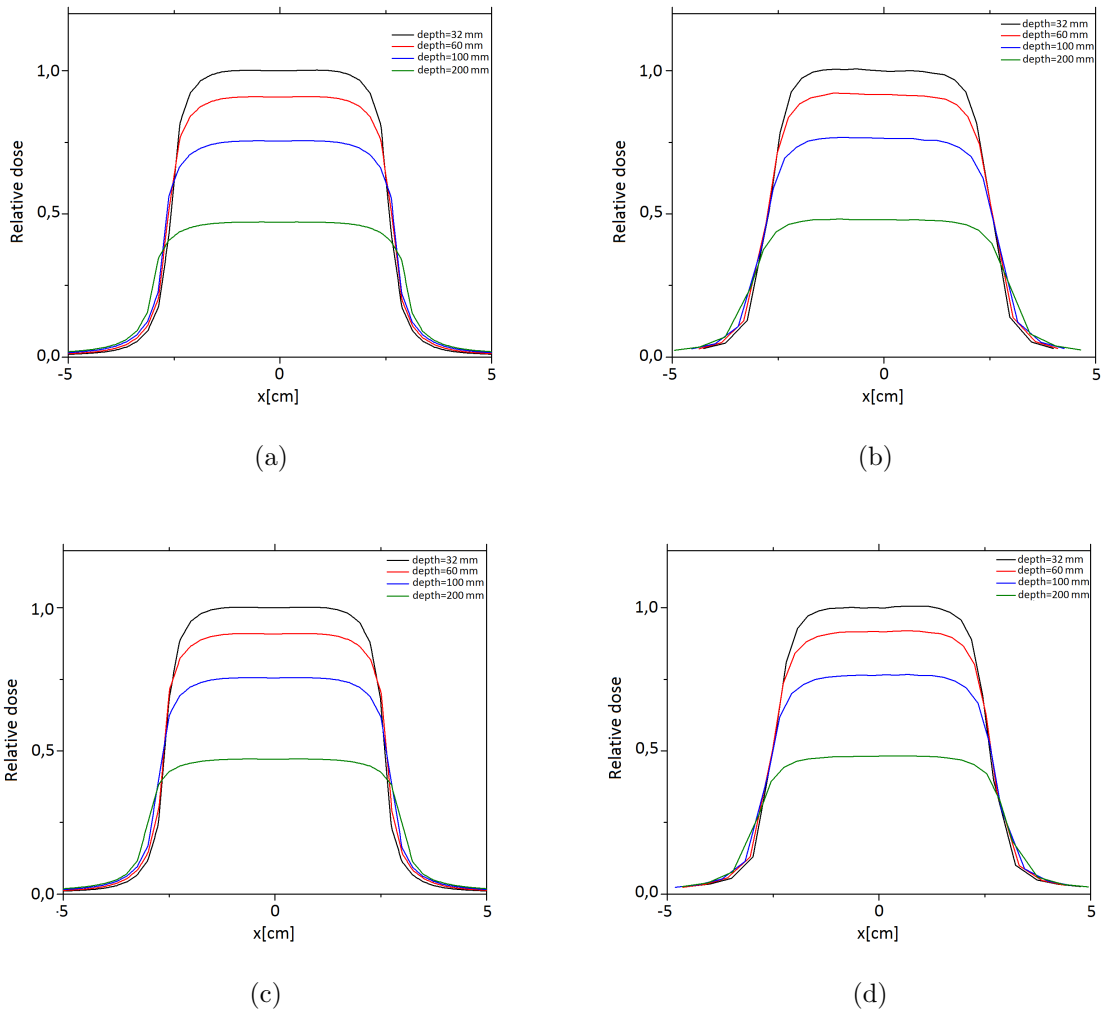

(a) (b)

(c) (d)

Figure A-1.: Radiation profiles of test 1: 5×5 cm^2 a) AAA cross-plane profile, b) measured cross-plane profile, c) AAA in-plane profile and d) measured in-plane profile.

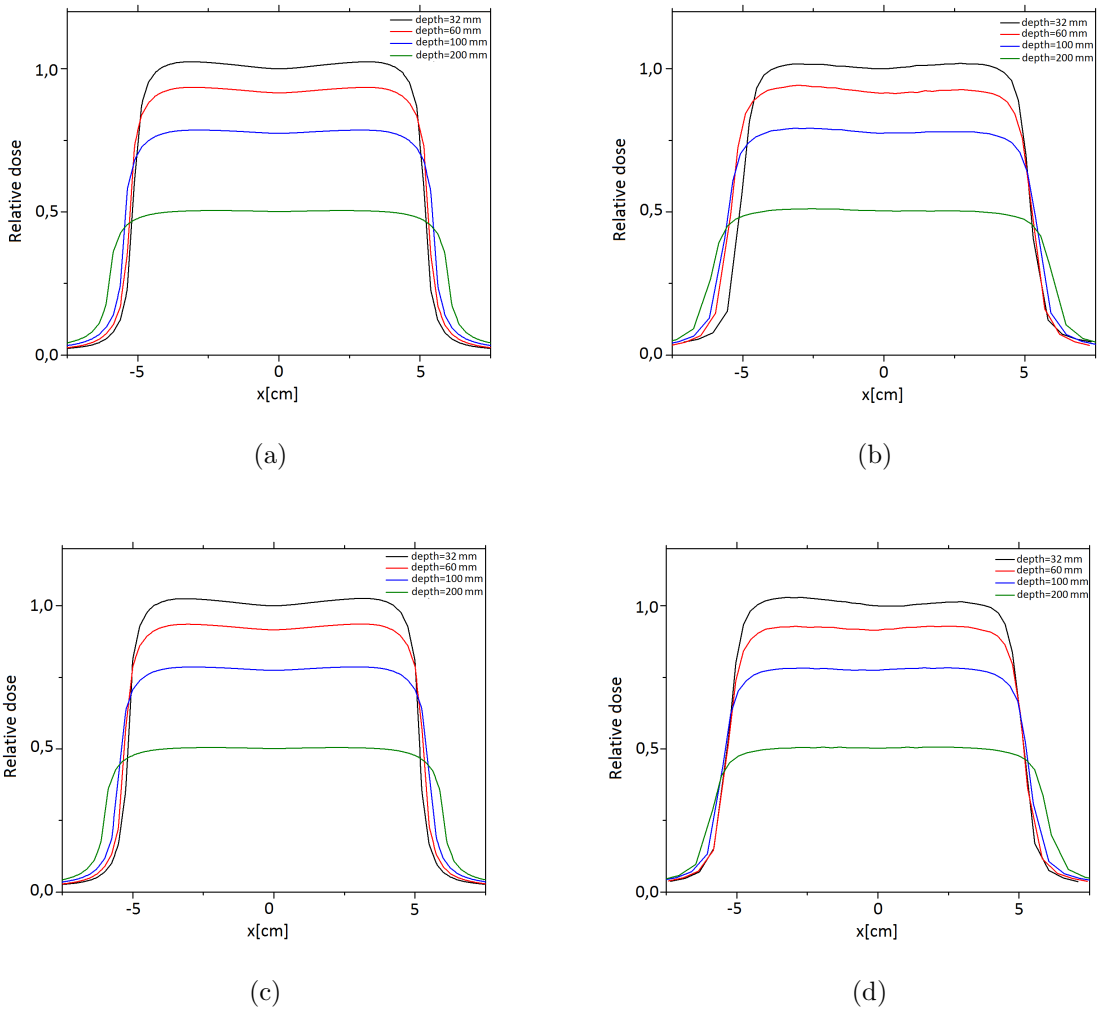

Figure A-2.: Radiation profiles of test 1: 10×10 cm^2 a) AAA cross-plane profile, b) measured cross-plane profile, c) AAA in-plane profile and d) measured in-plane profile.

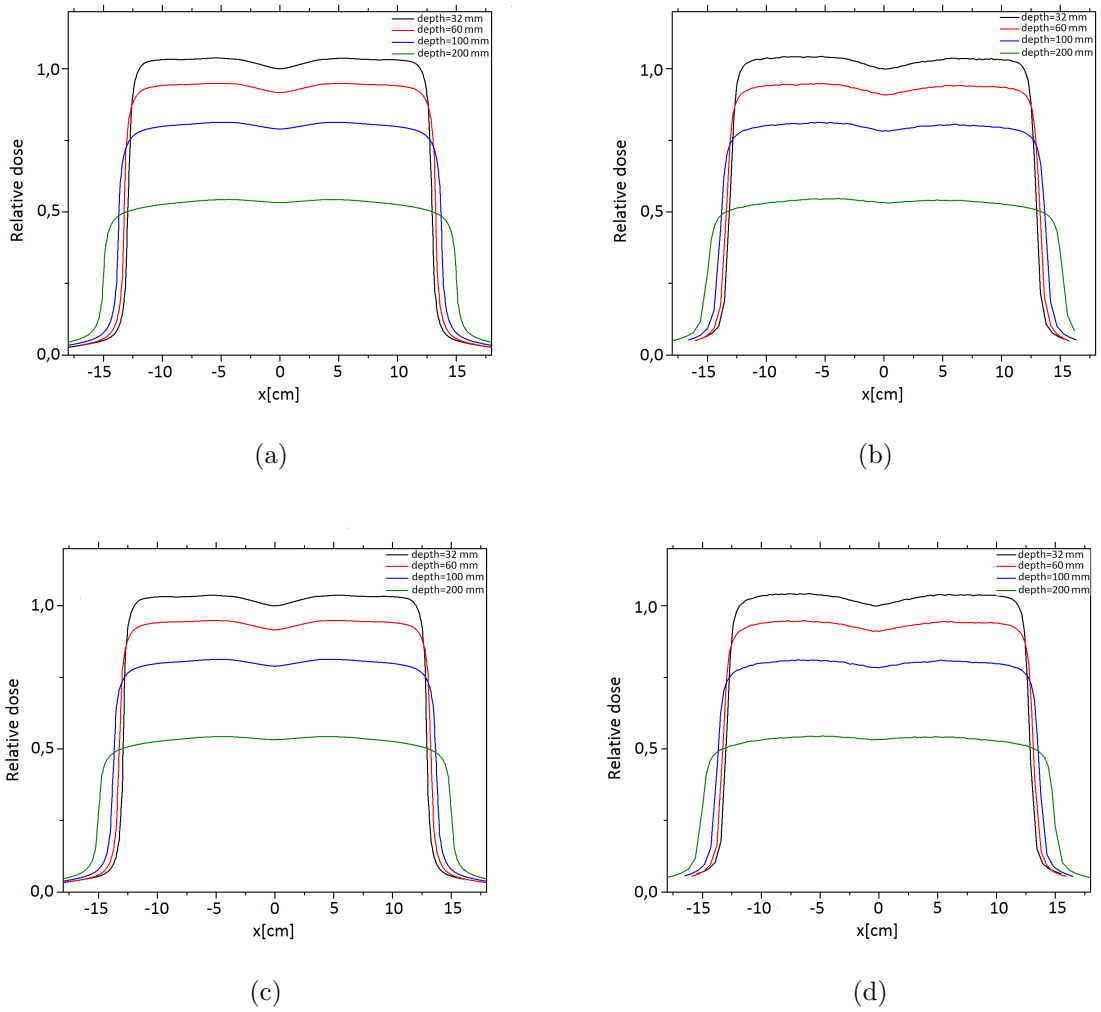

Figure A-3.: Radiation profiles of test 1: 25×25 cm^2 a) AAA cross-plane profile, b) measured cross-plane profile, c) AAA in-plane profile and d) measured in-plane profile.

- Test 2 :

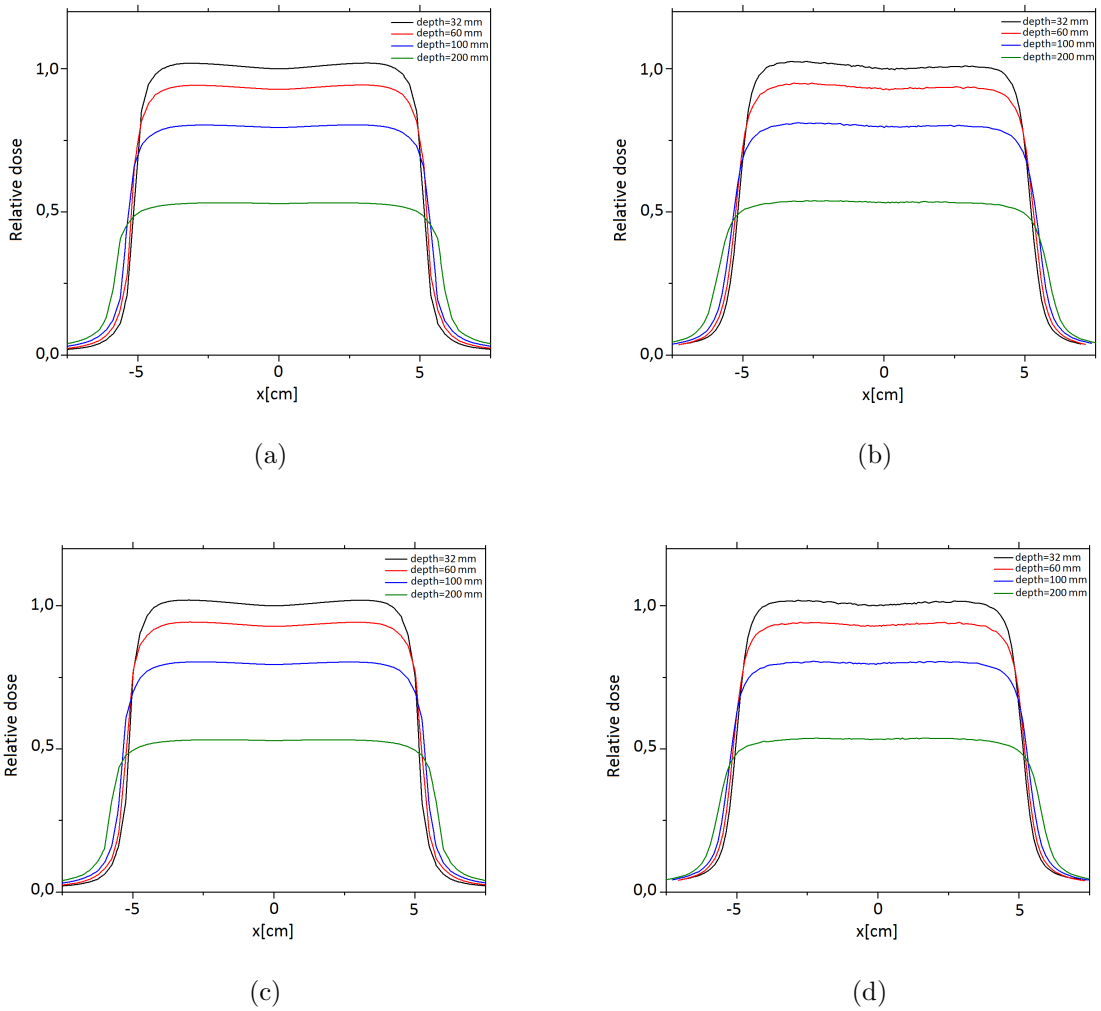

Figure A-4.: Radiation profiles of test 2: 8×8 cm^2 a) AAA cross-plane profile, b) measured cross-plane profile, c) AAA in-plane profile and d) measured in-plane profile.

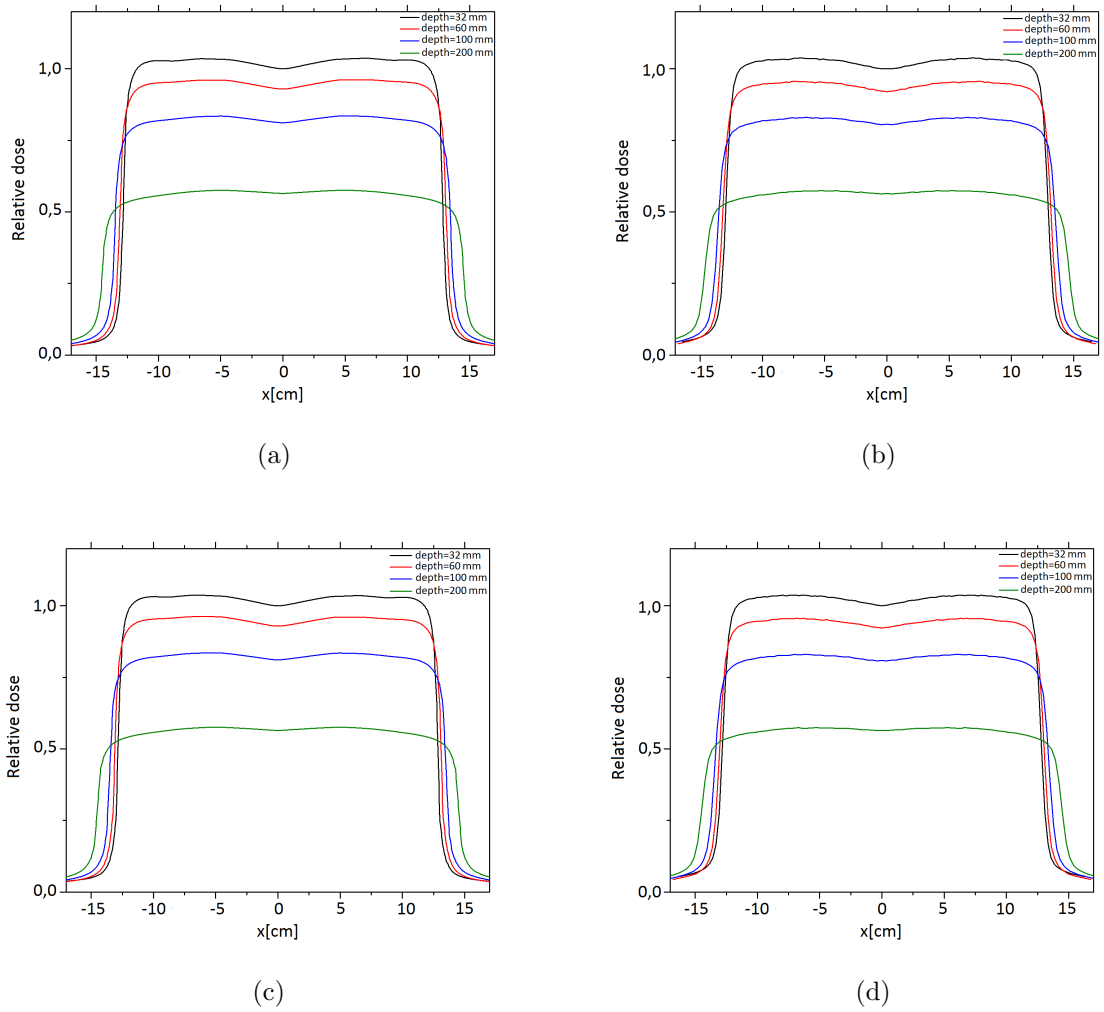

Figure A-5.: Radiation profiles of test 2: 20×20 cm^2 a) AAA cross-plane profile, b) measured cross-plane profile, c) AAA in-plane profile and d) measured in-plane profile.

- Test 3:

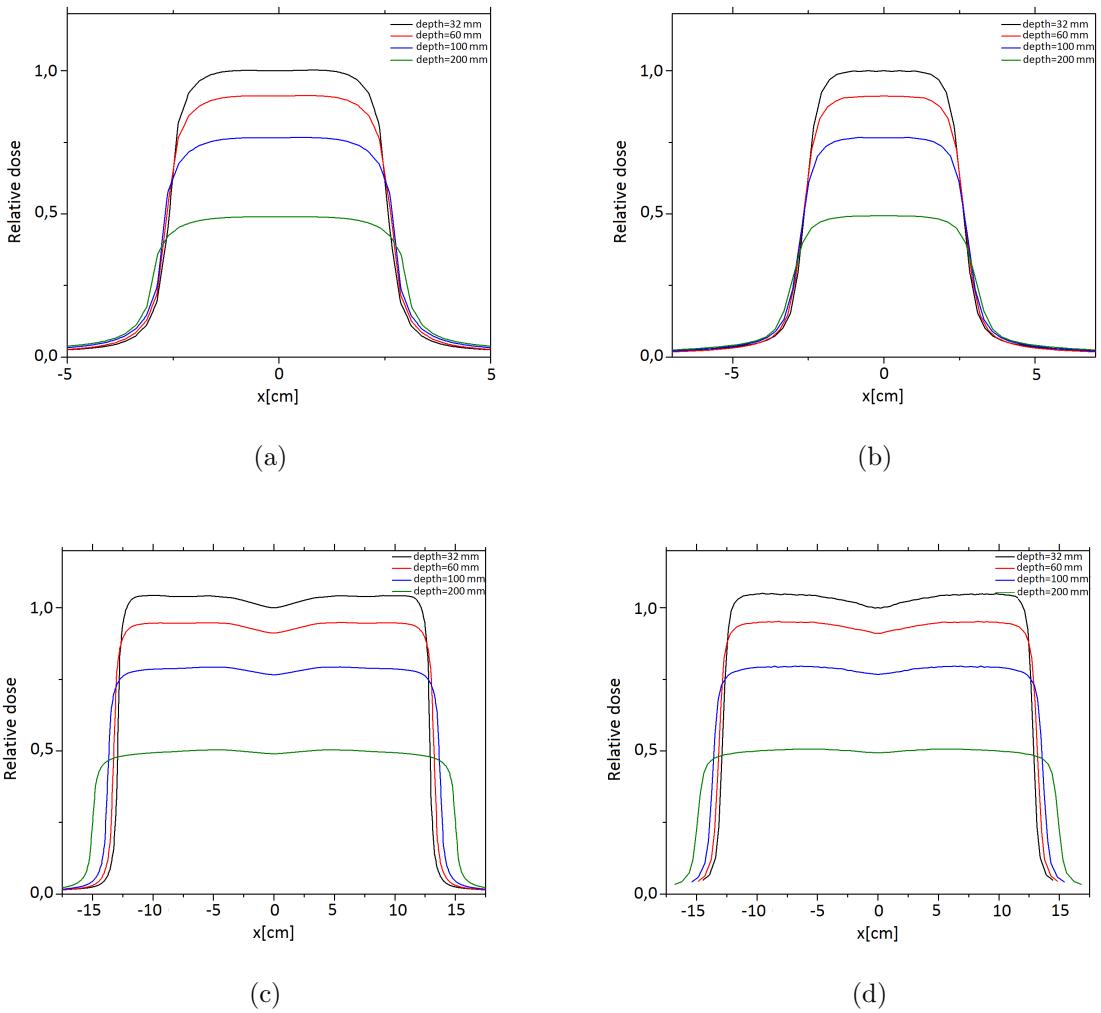

Figure A-6.: Radiation profiles of test 3: 5×25 cm^2 a) AAA cross-plane profile, b) measured cross-plane profile, c) AAA in-plane profile and d) measured in-plane profile.

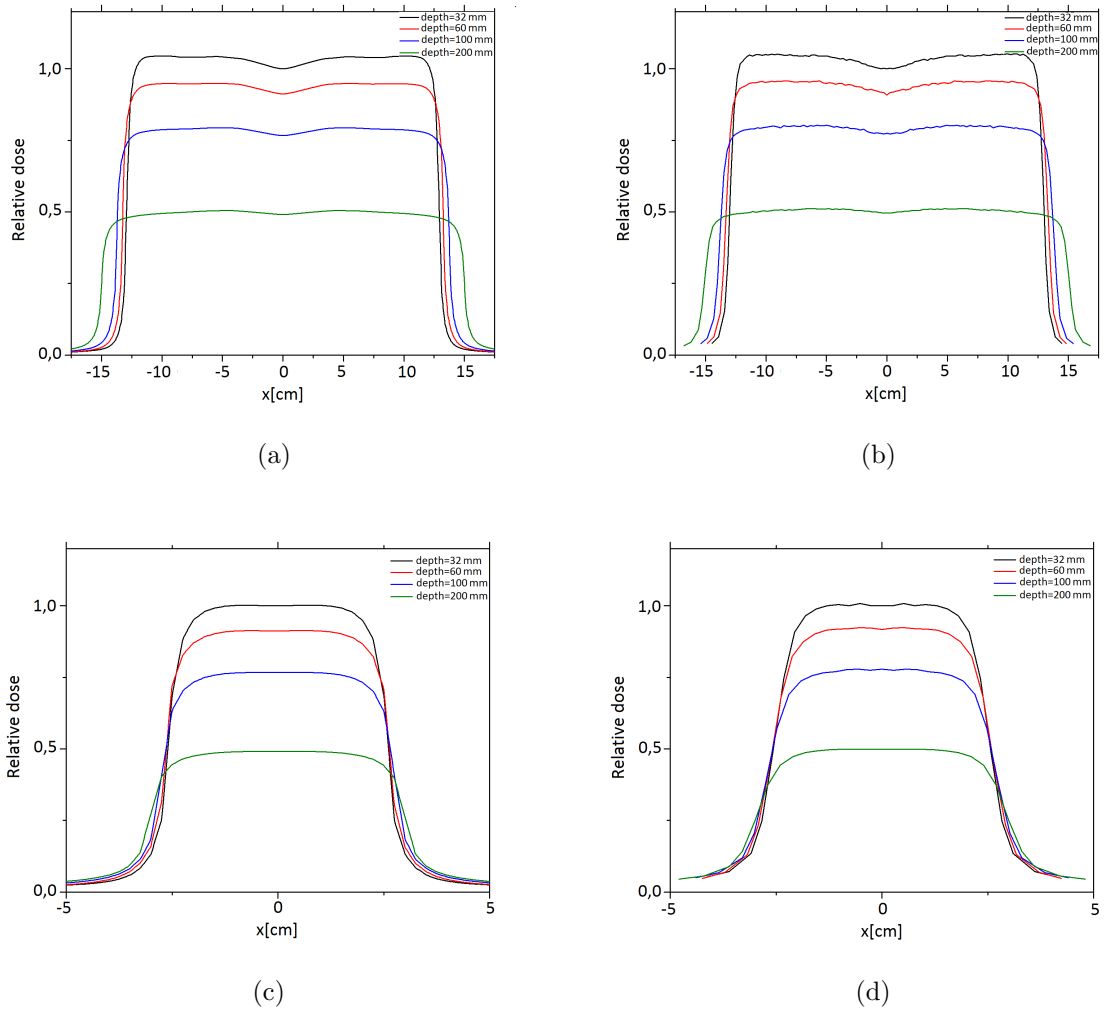

Figure A-7.: Radiation profiles of test 3: 25×5 cm^2 a) AAA cross-plane profile, b) measured cross-plane profile, c) AAA in-plane profile and d) measured in-plane profile.

- Test 4:

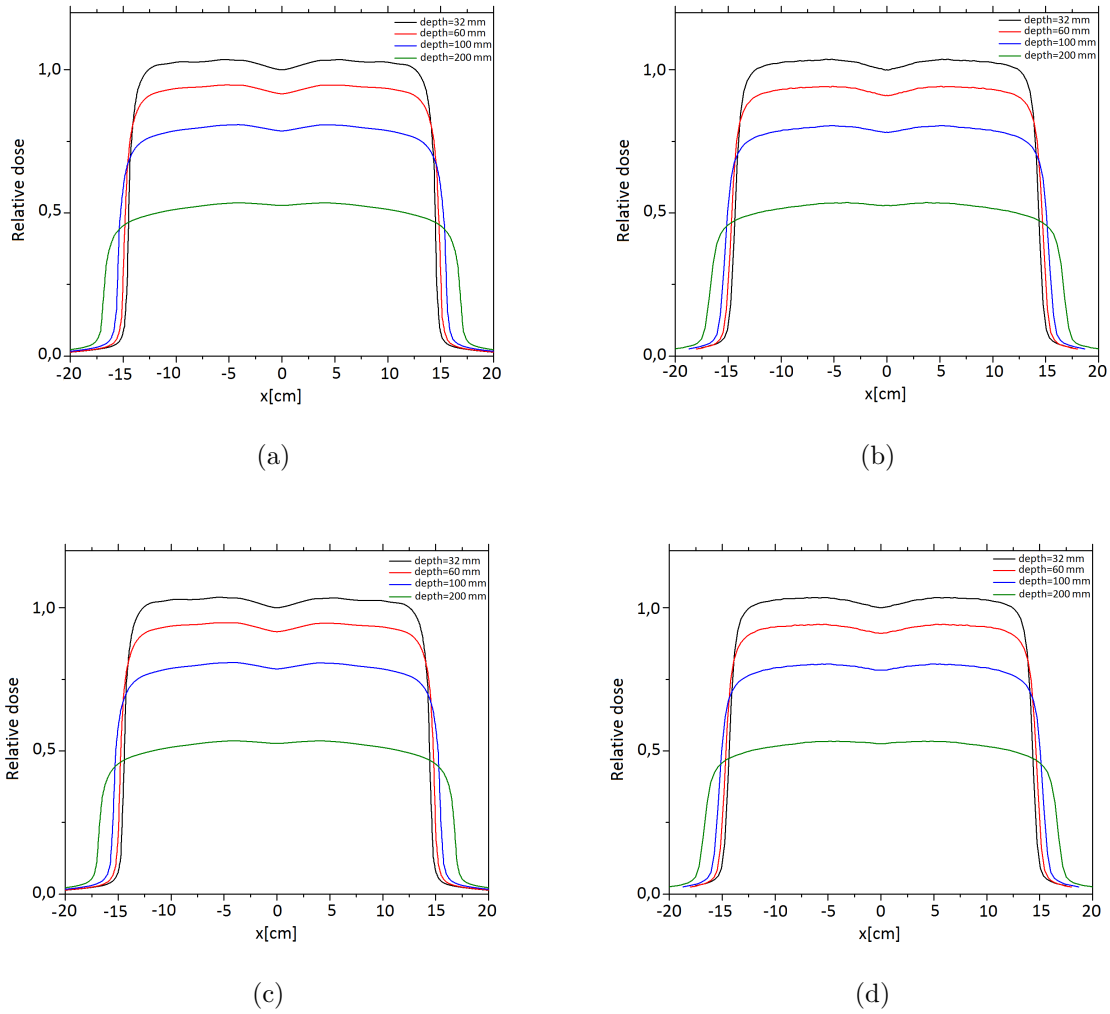

(a) (b)

(c) (d)

Figure A-8.: Radiation profiles of test 4: 20×20 cm^2 and collimator at 45° a) AAA cross-plane profile, b) measured cross-plane profile, c) AAA in-plane profile and d) measured in-plane profile.

- Test 5:

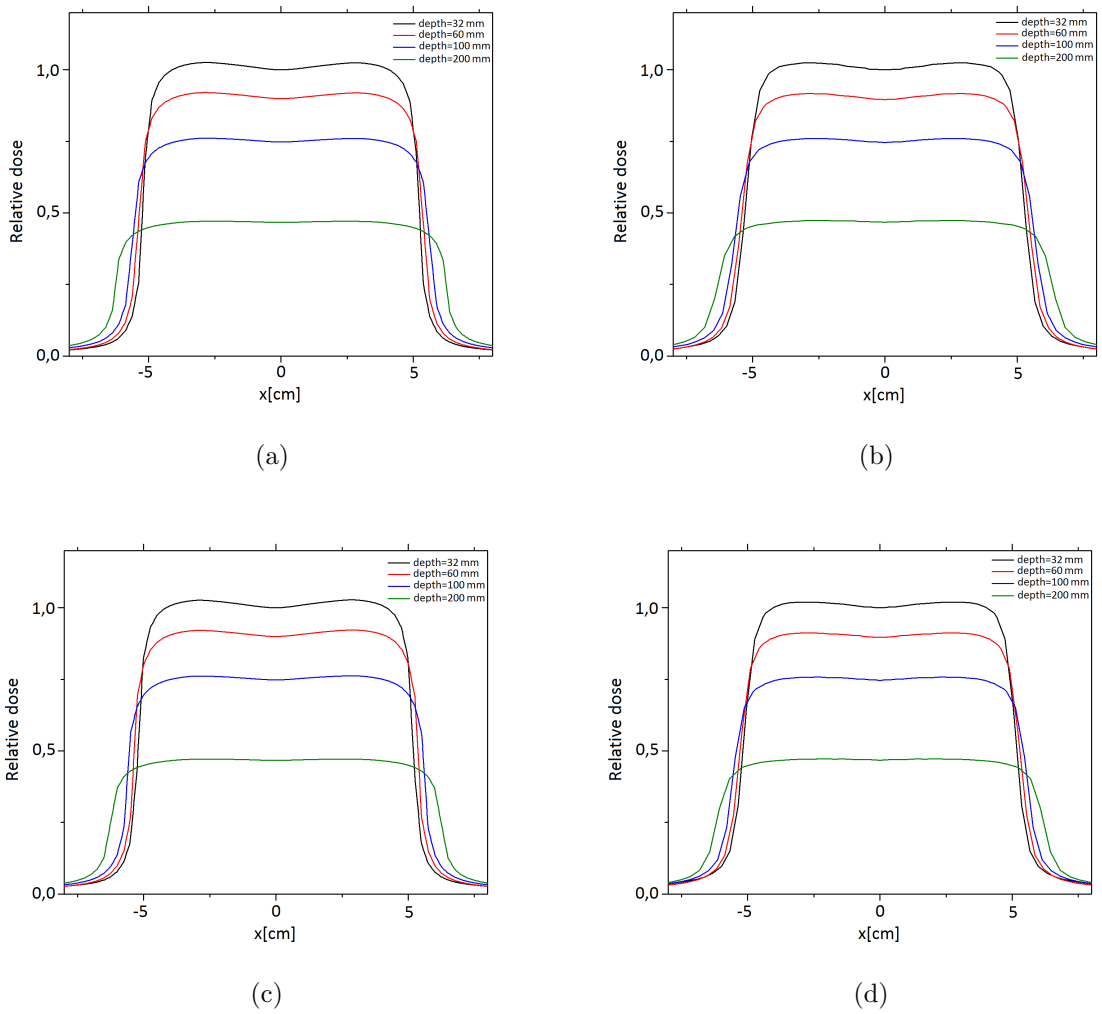

Figure A-9.: Radiation profiles of test 5: 10×10 cm^2 at isocenter a) AAA cross-plane profile, b) measured cross-plane profile, c) AAA in-plane profile and d) measured in-plane profile.

- Test 6:
Incidence oblique at 305°

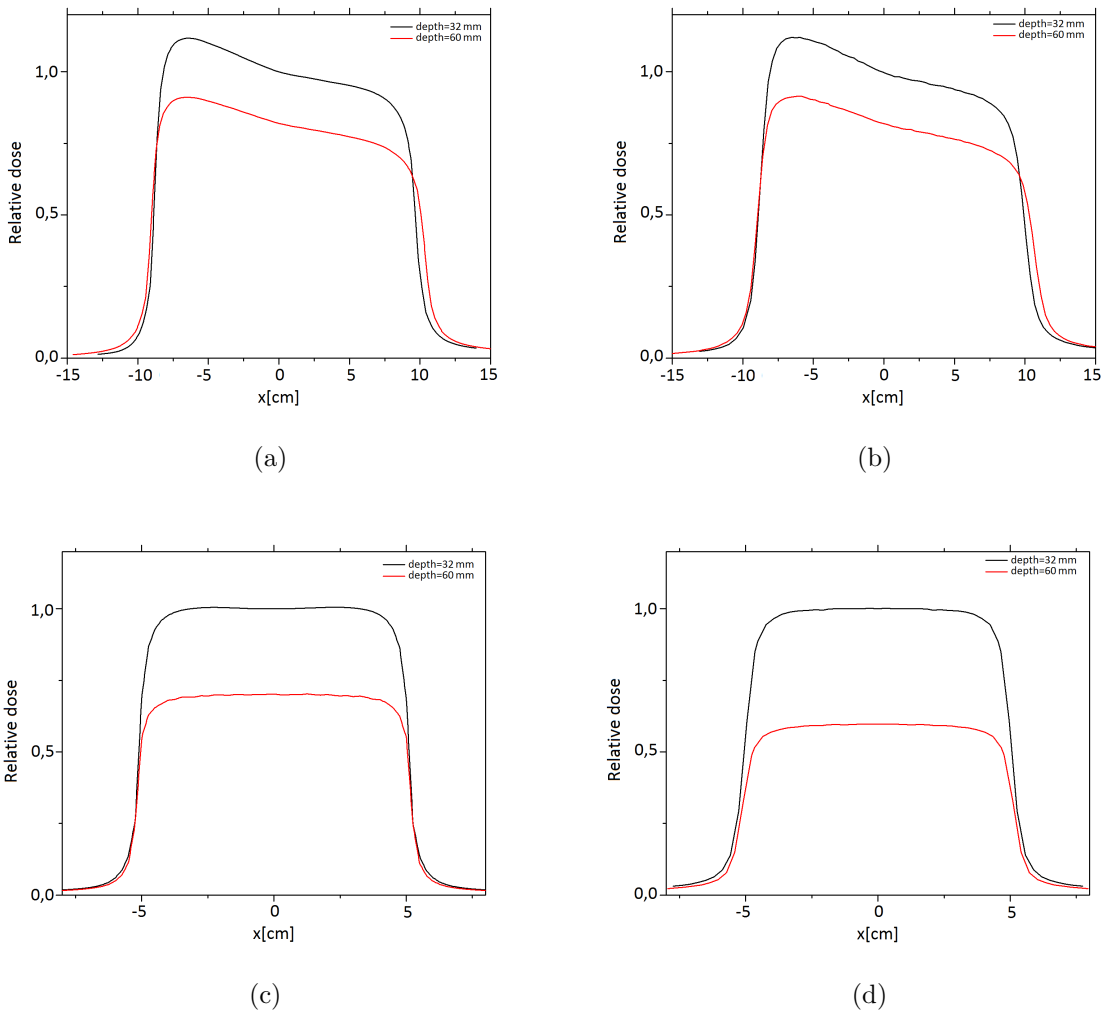

(a) (b)

(c) (d)

Figure A-10.: Radiation profiles of test 6: 10×10 cm^2, gantry at 305° a) AAA cross-plane profile, b) measured cross-plane profile, c) AAA in-plane profile and d) measured in-plane profile.

Incidence oblique at 330°

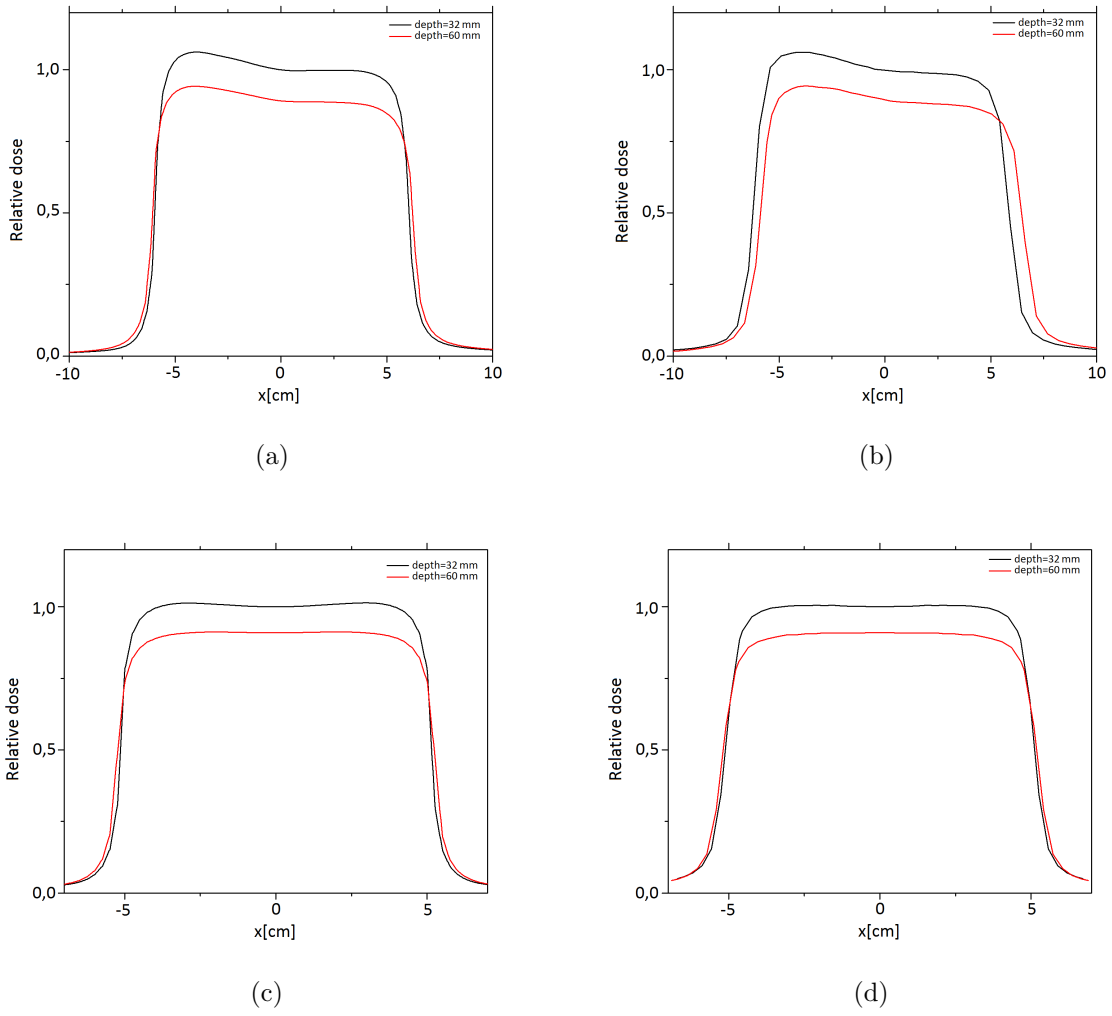

Figure A-11.: Radiation profiles of test 6: 10 × 10 cm^2, gantry at 330° a) AAA cross-plane profile, b) measured cross-plane profile, c) AAA in-plane profile and d) measured in-plane profile.

- Test 7:

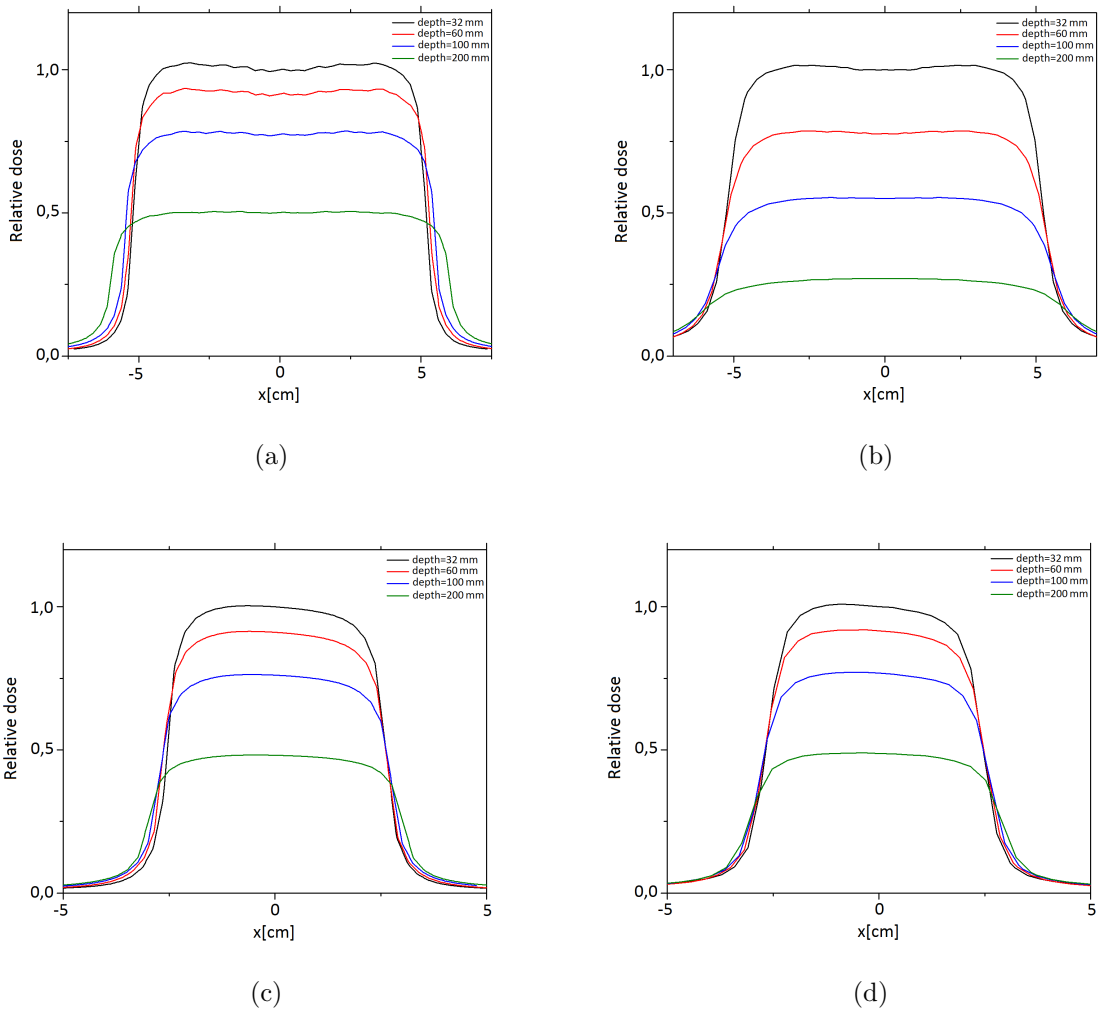

Figure A-12.: Radiation profiles of test 7: 10 : 0 cm^2 a) AAA cross-plane profile, b) measured cross-plane profile, c) AAA in-plane profile and d) measured in-plane profile.

- Test 8:

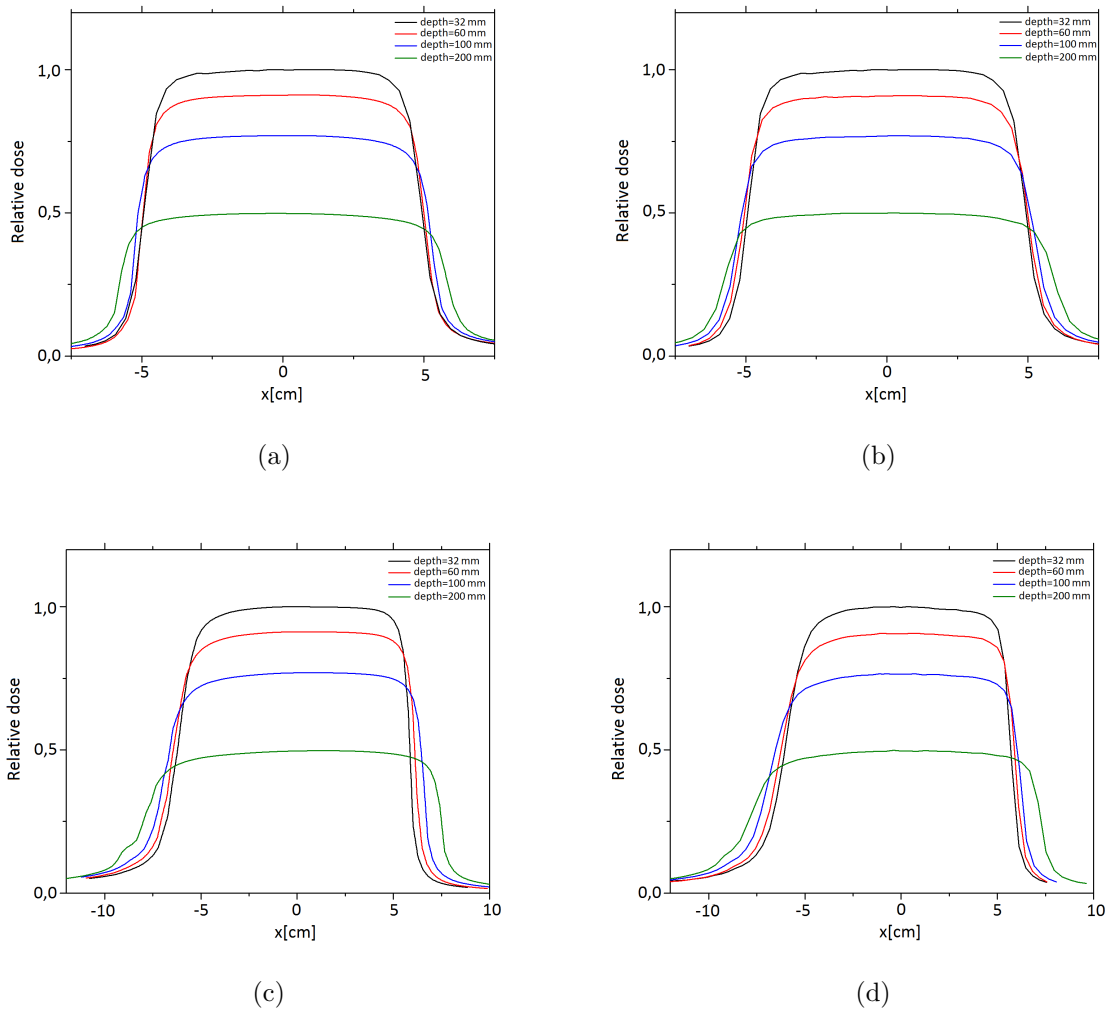

Figure A-13.: Radiation profiles of test 8: Triangle shape a) AAA cross-plane profile, b) measured cross-plane profile, c) AAA in-plane profile and d) measured in-plane profile.